Quantitative Metal Detection by Microwave Assisted Laser Induced Breakdown Imaging and Spectroscopy

By

Adeel Iqbal

A thesis submitted for the degree of Masters of Philosophy in Chemical Engineering

FACULTY OF ENGINEERING, COMPUTER AND MATHEMATICAL SCIENCES

SCHOOL OF CHEMICAL ENGINEERING

THE UNIVERSITY OF ADELAIDE, AUSTRALIA

Declaration

I certify that this work contains no material which has been accepted for the award of any other degree or diploma in my name, in any university or other tertiary institution and, to the best of my knowledge and belief, contains no material previously published or written by another person, except where due reference has been made in the text. In addition, I certify that no part of this work will, in the future, be used in a submission in my name, for any other degree or diploma in any university or other tertiary institution without the prior approval of the University of Adelaide and where applicable, any partner institution responsible for the joint-award of this degree.

I give consent to this copy of my thesis, when deposited in the University Library, being made available for loan and photocopying, subject to the provisions of the Copyright Act 1968.

I also give permission for the digital version of my thesis to be made available on the web, via the University's digital research repository, the Library Search and also through web search engines, unless permission has been granted by the University to restrict access for a period of time.

I acknowledge the support I have received for my research through the provision of an Australian Government Research Training Program Scholarship

Adeel Iqbal

Acknowledgment

I would like to express my sincere gratitude to all who have guided and supported me during past 1.5 years of my research candidature at the University of Adelaide. I would like to take the opportunity of pay special thanks to Associate Prof. Zeyad Alwahabi for his outstanding supervision and thorough guidance throughout my studies, without his guidance and encouragement this thesis could not have been possible. I would also like to thank my co-supervisor Prof. Christophe Fumeaux for his time to time guidance and help.

Furthermore, I shall further extend my gratitude to Dr. Zhiwei Sun, Shengjian Chen and Matthew Wall for their kind suggestions and support in experimental work, data processing and journal publications.

Last but not least, I would like to acknowledge the efforts of Mr. Jeffery Hiorns and Jason Peak from mechanical workshop at the School of Chemical Engineering for their technical support and excellent craftsmanship. In the end, I would like to thank my wife and kids for having faith on me and supporting me throughout this period.

Abstract

Real time, in-situ quantitative detection of the metals is important for many applications such as industrial processes for the quality control, mining for the quick scan of rocks samples, monitoring of the heavy metal contaminations for the pollution control and real-time analysis of the agriculture land for nutrients monitoring and fertilizer selection. Laser Induced Breakdown spectroscopy (LIBS) being able to offer quick response and multi-elemental analysis without sample preparation, can meet these requirements. As most of the mentioned applications involve detections of the trace metallic elements, thus LIBS is desired to deliver quantitative measurements with high sensitivity and improved limit of detection. Despite of inheriting some excellent features, LIBS suffers a few limitations such as low Signal to Noise Ratio (SNR), weak limit of detection and low sensitivity. Several methods have been suggested in literature to improve the performance of conventional LIBS, which are based on the concept of aiding LIBS by a secondary source of energy. Microwave-assisted laser induced breakdown spectroscopy (MW-LIBS) is one of these improvement methods, which has immense potential to be considered as a reliable analytical technique due to high sensitivity, improved SNR and limit of detection. However, further improvement in the performance of MW-LIBS is desired for the reliable quantitative metal detections at low concentration while offering high sensitivity.

This research is amid to investigate the improvement of MW-LIBS using two different approaches. This first is to improve the plasma emission detection by single elemental imaging and the second is to improve the microwave injection by a well-designed near field applicator (NFA).

Indium in solid matrix was used to investigate the improvement in emission detection by single elemental imaging. A narrow bandpass filter was used to select the elemental, indium emission at 451.13 nm. This narrow bandpass filter was attached with an ICCD camera to investigate the response of imaging based detection technique at various, laser

and microwave powers. Variation in image intensity at several concentrations of indium and evolution of plasma at various microwave powers, was also investigated. Spectral detection was carried out simultaneously with narrow-band imaging to study the extent of improvement in sensitivity. Outcomes demonstrated that imaging technique offers 14-fold improvement in sensitivity following enhancement by microwave radiation, as compared to spectral detection in LIBS with no microwave enhancement. Microwave injection devices such as NFA, being the main component to inject the microwave radiation into the laser ablated plasma, is the most important part of MW-LIBS system, hence defines the performance of the entire MW-LIBS setup. Therefore, having an efficient NFA can considerably improve the signal quality and detection capabilities of MW-LIBS. Considering the importance of an efficient NFA, four designs of NFAs were simulated using the characteristics of available setup, simple isolation techniques such as quarter-wave choke and a finite ground plane were used. These designs were fabricated and tested in the MW-LIBS setup for the copper detection in a solid sample. Spectral detections and broadband plasma imaging were carried out simultaneously to investigate the effect of various NFA designs on the signal quality, size of the plasma and improvement in the detection limit for the existing MW-LIBS setup. From the experimental results, it was concluded that the design D having a finite ground plane of 30 mm diameter performed better than the rest, using this design D a signal enhancement of 849 times was achieved. While 79–fold SNR at 2.6 mJ/pulse laser and 1.2 kWatt microwave power, was observed. By using design D of NFA, ore sample having certified copper concentration of 3.38 ppm was detected with the 166 SNR.

The demonstrated high SNR, presents the possibility of detecting sub parts per million in future.

Table of Contents

List of Figures

List of Tables

Chapter 1 Introduction

1.1 Background

In-situ and quick quantitative detection of metals is very important in many applications such as industrial processes, mining and environmental analysis [1-5]. In industrial process, it can be very important to detect the in-line compositions of various metallic elements to maintain the quality or continuous analysis of effluents to comply with the environmental regulations. Similarly, detection of precious metal such as gold in soil, or quick and remote detection of various other metals of interest in ores samples from mines, is also very important. Detection of heavy metals in soil and in water bodies is also another important aspect due to rising health concerns, as heavy metals being one of the major cause of soil and water pollutions are required to be monitored continuously. However, conventional metal detection methods involve sample collection, pre-treatment and laboratory procedure which are often costly and time consuming.

Therefore, to meet these highly versatile analytical demands of quantitative detection of metals, it is highly desirable to use a quick, versatile and remote analytical method such as laser induced breakdown spectroscopy (LIBS). LIBS can meet these requirements due to its proven analytical qualities such as quick response, no sample preparation, multi-elemental detection and ability to analyse gas, liquid and solid samples [6, 7].

LIBS is a branch of atomic emission spectroscopy, which is based on the creation of the plasma on the surface of a target substance, by using a laser source. This laser ablated plasma contains atoms, ions and free electrons in excited state at very high temperature in the range of 1000-15000K [8]. During the cooling process, these excited atoms and ions emit unique characteristic radiations which can be spectrally resolved by a spectrometer and CCD array, for qualitative and quantitative measurements. A typical LIBS set-up can

consist of a laser source and emission detection channel involving spectrometer, fibre optics cable and an ICCD camera. The collected signals are plotted as, intensity as a function of wavelength by the software connected to the spectrometer and CCD detector. As each element in the periodic table emits radiation at a specific wavelength hence constituent element can be identified from the emitted wavelength, following the spectra data base lines such as NIST [9]. The quantitative measurement can be carried out by developing calibration curve from the sample of known concentration using similar matrix. LIBS is being studied from more than 40 years, but prior to 1980's scientists were mostly interested in basic physics of plasma formation [10]. A few instruments based on LIBS were developed but have not found widespread [10], because early LIBS systems were considered to be overly complicated, limited in spectral coverage, bulky and expensive with very specific applications in the laboratory.

Due to advancements in spectroscopic and laser technology, LIBS operation has been simplified. In addition to this, availability of compact high-performance lasers, evolution of high-resolution and sensitive intensified-CCD arrays, development of compact, low-cost, high-resolution spectrometers and analytical software, LIBS systems have become more affordable and versatile [11]. LIBS can outperform conventional analytical techniques due to very promising feature such as quick response, no sample pre-treatment and multi-elemental detection. Which means that it can generate results within fraction of seconds without sample collection and treatment, hence can be very helpful for in-line measurements, in continuous production facilities.

Multi-elemental detection capability is the most interesting feature of the LIBS which enables this method to identify all constituent species of a sample without changing analytical setup. In addition, LIBS can also be used to analyse all sorts of samples, for example gas, liquid and solid, as being a contactless method switching between material is easy and precise without fearing chances of contamination. These feature makes LIBS a strong competitor for many practical applications such as: space and underwater exploration, heavy metal detection and ore identification in mining.

However, some limitations of shorter plasma life, low sensitivity for low elemental concentration, poor limit of detection and weak SNR, make LIBS fall behind from other analysing techniques. Due to these limitation, LIBS is not yet being considered as a mainstream analysing method. However, in recent past various improvement methods, double laser pulse, spark discharge, flame/torch, steady magnetic field, spatial confinement, and MW-LIBS [7], have been proposed basing the concept of aiding conventional LIBS by a secondary source of energy. The first five mentioned improvement techniques, either can make conventional LIBS system costly, difficult to align and control or may not offer significant improvement. While, the MW-LIBS is more convenient and cost-effective improvement technique, which relies on the idea of coupling the microwave radiation in the laser generated plasma.

MW-LIBS offers a noticeable enhancement in the emission signals by a factor 1~1000 [8] depending on sample type however, further work is required to improve sensitivity and limit of detection, so that MW-LIBS can be presented as a reliable analytical technique to carryout qualitative metallic detection for trace concentration with high precision. Till present all studies are based on the concept of enhancing and retaining LIBS signal by adding another energy source in the conventional setup. No improvement technique based on the alternative emission collection method has been proposed. The microwave radiation influences the laser ablated plasma in two ways first, the plasma life time increases second, the spatial dimensions expand. The considerable enhancement in plasma dimensions will make emission out of focus therefore, the coupling of all emission into the fibre optics cable is not possible. While it is also believed that the emission signals are reduced as they travel from plasma to spectrometer through fibre optics bundle and series of other optics. Hence by reducing this signal loss and capturing all plasma emission MW-LIBS performance can be improved.

In addition, NFA being the main component of microwave injection system can affect the performance of MW-LIBS setup in many ways such as, an efficient well-designed NFA can impart considerable improvement through effective transmission of the supplied power while minimising the reflection coefficient and then efficiently radiating this transmitted

power by inducing a concentrated localised electric field. In this project, improvement in MW-LIBS system have been suggested by two separate means: I) proposing an alternative emission collection method such as based on narrow bandwidth imaging technique to minimise the emission loss II) improving microwave injection system by a well-designed NFA.

1.2 Objective and Aim of the Project

Aim of this project is to improve sensitivity and detection limit of the MW-LIBS by overcoming the still present shortfalls. As sensitivity and Limit of detection are the two maintain concern in LIBS, which are required to be addressed, to develop MW-LIBS as a reliable analytical method. Hence, the improvement in sensitivity has been suggested by improving the emission collection and microwave injection systems. An alternative collection method i.e. single elemental imaging has been suggested, which consists of a narrow band customised filter and an ICCD camera. This elemental imaging system, due to its large field of view offers more sensitivity and temporal elaboration, by presenting plasma images. This novel technique is simple, relatively cheap and compact, as its comprises off less optical instruments.

Microwave injection system has been improved by designing and then testing five designs of microwave near field applicators, keeping the first design as reference. Spectral detection and broad plasma imaging was also carried out simultaneously to study the extent of improvement.

Aims of the thesis are as follows:

- To improve sensitivity and signal quality of MW-LIBS by a novel emission collection method i.e. elemental imaging.
- To improve the sensitivity and limit of detection of MW-LIBS by developing an efficient near field applicator for the efficient microwave injection in LIBS.

1.3 Thesis Outline

This thesis has been written in conventional narrative form.

Chapter 1: Introduction: it contains introduction of the thesis containing background, research gaps, aim, objectives and outline of the thesis.

Chapter 2: Literature review: This chapter contains work done so far, research gaps and prospects of this project.

Chapter 3: Quantitative Metal Detections by Elemental imaging: it is the technical chapter which demonstrates improvement in MW-LIBS by elemental imaging of indium in solid samples. This chapter contains background, experimental setup, results and discussion and summary.

Chapter 4: LIBS Enhancement by Efficient Microwave coupling: This chapter contains background, experimental setup, results and discussion and summary.

Chapter 5: Conclusion: it contains conclusion of thesis, prospects and recommendations.

Chapter 2 Literature Review

Analytical detection of elemental metals has very wide range of applications in industrial processes, mining, agriculture and environmental monitoring. Fast inline continuous monitoring of production process is a matter of major concern in many industrial applications to control and optimize the process, where a quick, versatile and contact less detection method such as LIBS can improve the performance of system while saving time and cost. Similarly, fast detection and identification of minerals from rock surface and drill core samples is highly desirable, LIBS being able to offer quick scan of samples for all constituent elements makes conventional, time consuming and costly laboratory based methods, a second choice in rapid decision making [2]. In addition, detection of metals (nutrients and heavy metals) for agriculture and environmental monitoring is very important, for example identification of nutrients in soil for agriculture sites is very important for the selection of type and strength of fertilizers. The most common process of soil analysis, involves sample collection by farmers, submission of those samples in specialized soil analysis laboratories and collection of results after 2-3 weeks. This lengthy, time consuming and costly procedure cannot offer real time monitoring of nutrients and hence optimization of fertilizer patterns is not possible, therefore application of portable LIBS can be very useful in this field [1]. Heavy metals on the other side are considered as a major cause of land and water pollution, these heavy metals also include metalloids such as arsenic which can cause toxicity even at very low level of exposure.

Recently, due to increased use of these toxic metal in industrial, agriculture, domestic and technological applications, environmental and health concerns have increased as these heavy metals are ending up as contaminants in land and water bodies [5]. Pollution by these elemental is at elevated levels in the surroundings of mining, foundries, smelters and other metal processing industries. These metals also occur naturally in the earth crust

however most of the exposure and environmental contamination are caused by the aforementioned sources, therefore requires a compact, fast analysing method for better monitoring and control. LIBS because of, having the inherent desired qualities can be a potentials solution to this problem.

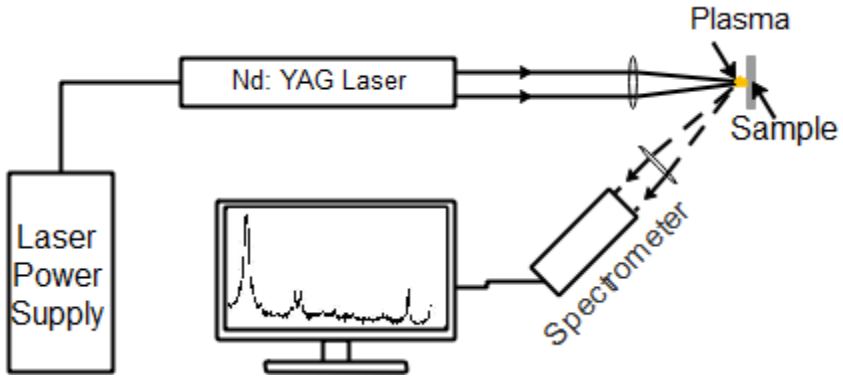

Figure 1: Laser Induced Breakdown Spectroscopy Setup

2.1 Laser Induced Breakdown Spectroscopy

Laser induced breakdown spectroscopy utilizes laser pulse as a source of excitation and creation of a tiny plasma on the surface of the analyte. The plasma contains atoms and ions of the whole matrix of the target element at very high temperature. When these elements cool down each of these elements, emits characteristic radiation. The radiation can be resolved spectrally for quantitative detections. Figure 1 presents a typical LIBS setup where a focussed pulsed, Nd: YAG laser beam creates plasma on the solid surface, the plasma is then resolved by a spectrometer and CCD detector, which is synchronized with the laser pulse. The captured emission intensity is plotted as a function of wavelength by the

software connected to the CCD detector. Atomic emission data base such as NIST [9] can be used to identify the elements from the wavelengths of captured spectra.

The emission from plasma consists of many spatial regimes as shown in fig. 2, which has the plasma emission lifetime plotted against optical emission intensity. The plasma emission just after the laser are dominated by continuum/white light and doesn't contain much information about the species, as the variation in intensity with wavelength is very small, during this time emissions from atoms and ions also exist but small concentrations and trace elements are suppressed by strong continuum light. Therefore, it is necessary to have a gated detector such as ICCD camera with spectrometer to avoid strong light by delaying the detection time. The very fast gating function of the detector is also very important due to the short plasma life-span, which varies from a few to hundreds of micro-seconds depending on the experimental conditions, such as laser power and nature of target sample [7].

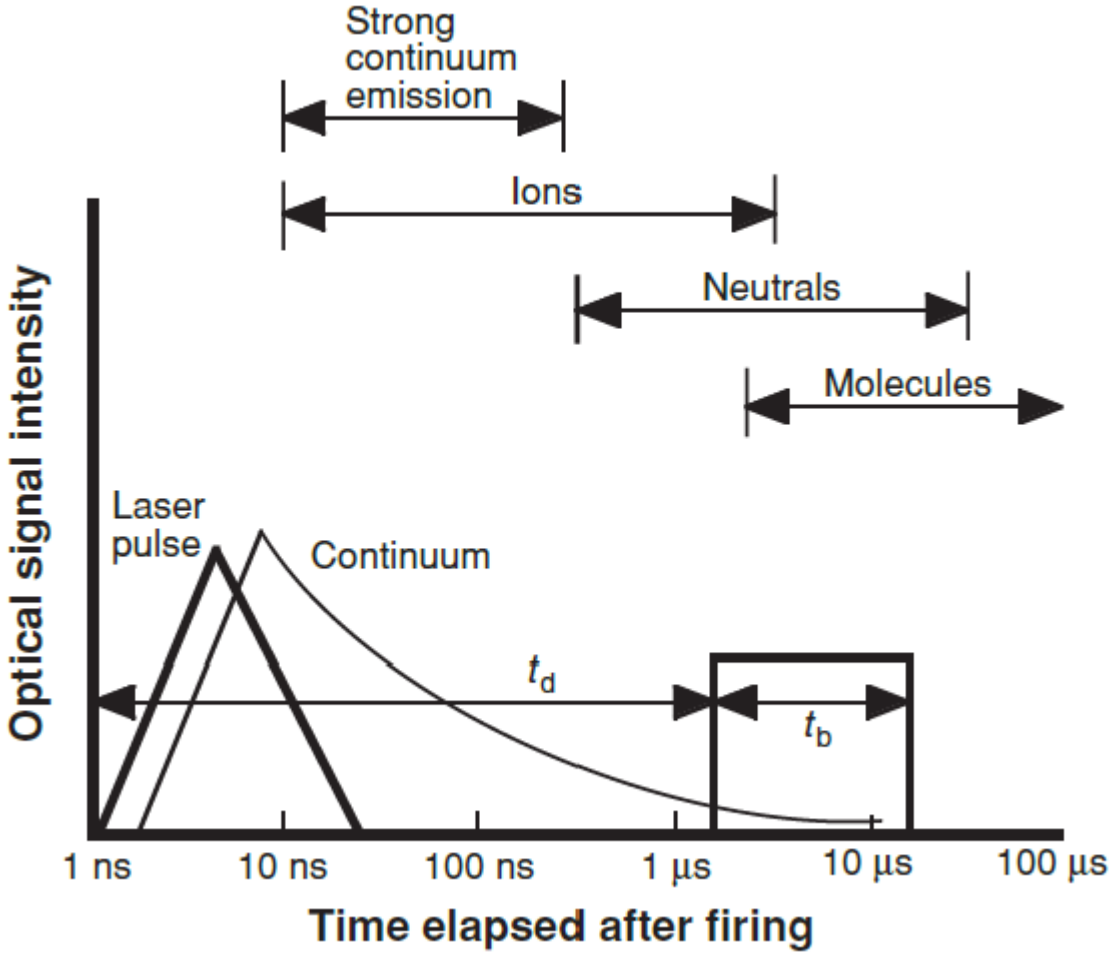

Figure 2: Time lapse after laser firing vs optical signal intensity [10].t_d is the delay time and t_b gate pulse width.

2.2 Instruments and Optical Components

Performance of LIBS is very dependent on the optical components and instruments involved in a typical LIBS setup. For example, several diverse types of lasers with different properties are commercially available which can be used in LIBS, hence can affect analytical characteristics of LIBS, due to different laser-material interactions. In general laser power should be higher than the ablation threshold of the material, being tested in serval order of magnitude to record reasonably strong signal, since the mass of the ablated plasma is very important factor in this respect. As ablation threshold varies with the material being tested therefore, trial and error may be required in conventional LIBS to find out optimum laser power for a material, usually for conventional LIBS setups laser power requirement are high such as tens of mJ/pulse for a properly focused beam (focal diameter 1-200 μm) [12].

Generally, Q-switch controlled laser beam having ns-pulse duration is considered the optimum selection for LIBS in terms of achieving better limit of detections(LoD). Studies of various laser pulses reveal that ultra-short (femto-second) laser pulse generate more sample ablation in stochiometric term, which consequently results in better spatial resolution and thus more accurate analysis [11]. The femto-second pulse can have an impact on the analytical capabilities of LIBS in future however, currently it is a matter of discussion that whether to replace the compact robust ns-laser source with heavier and costly fs-lasers or not as because, one of the LIBS's development aim is to make compact LIBS device for in-field and remote measurements.

Variation in laser wavelength can affect performance of LIBS therefore selection should be made considering the material being tested [13] for example UV is good for ceramics, metals and stones while for water analysis, due to strong absorption in UV and IR region, selection of visible wavelength would be favorable. Spectrometer being the only analytical component of the whole LIBS setup, outlines the measuring capabilities of the whole setup, hence should be robust with fast synchronizing ability. Spectrometer for LIBS should have a good spectral coverage for example from UV to visible section and resolution for atomic

spectroscopic standard. The detector in the spectrometer should be sensitive with fast gating function to provide good signal-to-noise (SNR) and should be able to offer analysis at low limit of detection. These requirements are usually closely met by charge-coupled detector array (CCD) spectrometer or gated intensified CCD camera(ICCD) spectrometers. CCD array based spectrometers are more robust, sensitive and offer better SNR but have poor resolution and cannot go in nano-second gating, while Echelle ICCD camera spectrometers are bulky with moderate SNR but offer excellent time and resolution.

Usually ICCD camera spectrometers are used in laboratory setups for research, while CCD spectrometers are mostly used for remote application or for routine analysis. Other optical components of the LIBS setup can consist of diversion mirrors, focusing lenses, fiber optics bundle which make the laser focusing and signal collection channels and can be found in various geometric configurations in various LIBS setups, however in recent years introduction of fiber optical bundle in LIBS setup have become common which has increased the flexibility of the LIBS system [9].

2.3 Quantitative Detections by LIBS

LIBS's use for analytical purpose was started in 1980[10] to analyze hazardous aerosols and for diagnostic in nuclear power industry, in 1992 portable units were developed for surface analysis in remote conditions, in 2000 LIBS was used by NASA on MARS [10]. In terms of analytical measurements LIBS has some excellent features such as no sample preparation, versatility, quick response, multi-element detection. LIBS offer impressive results in qualitative or comparative detections however its quantitative abilities are considered to be moderate and needs to be improved in various aspects which will be discussed later in this chapter. Quantitative detections by LIBS can be carried out by calibrating the system with the standard calibration curve from same material matrix. LIBS can response differently for different matrix due to, non-linear laser material interactions and variation in the ablation threshold, during ablation and vaporization process. This phenomenon is also called as matrix effect, which means LIBS can response differently for same elemental

concentration if surrounded by varied materials. Matrix effect is also a limitation for quantitative detections as most of the time standard calibration curves are not available for many practical applications, in that case calibration curve needs to be developed [14], by recording spectra of known concentration of elements keeping the matrix same. Intensities from these spectra are then plotted as a function of concentration for the elements of interest, to develop a calibration curve for future quantitative detections. This often leads to complex analytical procedure and sample preparation but once the calibration curve is developed for a specific application, detection becomes fast and easy.

Various other calibration methods to minimize the matrix effect have also been proposed, for example C. Chaleard [15], has reduced matrix effect by normalizing the emission signals by vaporization mass and plasma excitation temperature. Electron density and excitation temperature has been used to introduce a calibration model [16]. Some other calibration methods like emission lines of internal reference elements [17], powder surface densities [18], statistical methods based on artificial neural network [19], partial least square and wavelet-transform hybrid model[20] and principal component analysis [21], have been used significantly to reduce matrix effect. Calibration free laser induced breakdown spectroscopy has also been proposed (CF-LIBS) [22, 23]. Recently Lijuan Zheng [24] has demonstrated absence of matrix effect in conventional LIBS for analysis, with the surface-assisted solution analysis configuration.

LIBS offers decent limit of detection in pico-femtogram range which can further be improved by various means, Which means that LIBS these days can offer similar performance as that of bulk sampling technique such as sampling (AAS, ICP-OES, XRF, and ICP-MS [25, 26]) or solid micro sampling (μ-XRF, LA-ICP-MS [27, 28]) techniques while having the added benefits of quick results and no sample pretreatment. LIBS being a nondestructive, contactless technique can be very beneficial for in-line measurements in process industry such as for quality control, where one laser generated spark can be examined for all constituent elements. Being compact LIBS can be used for unconventional remote measurements such as space and undersea explorations. Prominent applications

of LIBS are in many important fields such as biomedical, environmental, agriculture, industrial processes and nanoparticle technologies.

For instance, LIBS is being used widely in bio-medical and biological applications, this branch of LIBS is also known as bio-LIBS [7]. The reason of this increased use in this field is generally because LIBS is contactless, non-destructive, reagent-less technique, which can also be easily coupled with microscope making it feasible and convenient to incorporate into medical equipment. In addition, LIBS can generate localized or mapping type analysis, in this field performance of LIBS is excellent as most of the analysis in biomedical field are of qualitative in nature. The most studied application of bio-LIBS is the identification of pathogens using multivariate chemometric methods. Bio-LIBS is being applied to soft tissue for various studies from more than 7 years, for identification of bacteria, viruses, spores, tissue classification, human bones, teeth and various stones in human body such as gallstones, cholesterol stones and kidney stones [7, 29, 30]. Bio-LIBS is also being used for kidney diagnostics, blood, urine, hair, fingernails and teeth analysis.

For environmental and geological analysis, the major attraction is that the LIBS setup can be developed as a portable device, which can be flexible in term of sample presentation and can generate quick results, remotely, making LIBS a very convenient tool for rapid decision making. In many studies, LIBS has been employed for analysis of soil, minerals, aerosol and water [31].

Most of the soil analysis involving LIBS are based on carbon detection, which presents heath and activity in soil and considered as one of the major factor affecting the global climate. Hence in this field, most important aspect of research is to develop a compact mobile technique such as compact LIBS, to measure total: organic and inorganic carbon and degree of humidification in soil. LIBS can also be very useful to study the toxic elements (heavy metal) and nutrients in soil which can be very important for farming. However, at present soil analysis results from LIBS indicate that due to the highly heterogeneous nature of soil, quantitative results often are affected by matrix effect for instance many soil samples are rich with iron (Fe) and aluminum (Al) hence spectral interference from these

components prevent use of intense carbon lines at 247.86nm and 193.03nm specially in case of low resolution portable spectrometers.

LIBS is also very useful in geochemical fingerprinting, quantitative and qualitative studies on rock types are also available in LIBS literature. Analysis of aerosol is an important field in LIBS applications and is one of the oldest application, yet the complete understanding of the process involved was developed only in the past decade. A few important studies in this field are based on the development of methods for more efficient particle collection on a substrate [32], differentiation between gas-phase and particulate analytes [33], and a comparative study of heavy-metal concentrations in Asian dust and local pollution events [34].

Water analysis by LIBS for environmental purpose is also an important field however, it is difficult to apply LIBS on liquid samples due to presence of free surface, micro air bubbles and suspended particles within the liquid which cause focusing problem and emitted light collection is obstacle by the liquid, as plasma being within the liquid layers. In addition, extra quenching on plasma results in lower plasma temperature, week emission signals, short plasma life time and small plasma size[35]. These problems can be overcome by soaking water in sorbents such as paper or wood to create a solid matrix however detection limits are week 0.1-1mm [7], which prevent LIBS to be used for monitoring of water quality. However, LIBS can be used for waste water or industrial effluent analysis such as for continuous monitoring. Use of LIBS in industrial processes is attractive but the LIBS setups are required to be specialized with customized instrumentation to meet the harsh fast phased highly automated environment. Most of the industrial applications of the LIBS include analysis of alloys, plastics, waste, ceramics, glasses and detection in nuclear plants. Analysis of coal and fly-ash by LIBS in also an important application for coal based power plants. LIBS appears to be an excellent match for steal industry, where continuous monitoring of the constituent elements at various stages of production process, give vital information about the quality of the product and raw materials. An analytical system based on LIBS for the on-line analysis of iron ore for pelletizing plants was developed. This LIBS based instrument successfully performed measurements of Si, Ca, Mg, Al, and graphitic

carbon contents, in different iron ore slurries prior to filtration and pelletizing [36]. A automated computer system for fixed interval analysis was also developed and connected with LIBS based equipment which offered analysis in less than five minutes for each sample [37]. Performance of coal fired boilers is highly dependent on the properties of coal and combustion parameters, for optimal performance, continuous analysis of coal samples is required to optimize the combustion parameters. LIBS technique has been used widely for the compositional analysis of coal [38, 39]. A nonlinearized multivariate dominant-factor-based partial least-squares (PLS) model was applied to coal elemental concentration measurement using LIBS [40]. Analysis of fly ash for the determination of unburned carbon is also an important application of LIBS, for the estimation of combustion efficiency. Software controlled system based on LIBS, has also been used in power plants for combustion control, by continuous monitoring of coal samples and fly ash [36, 41]. Automated LIBS system has also been applied in boiler control system for power plants, to achieve efficient and stable combustion [42].

The nuclear power plants are a source of clean and cheap energy however, safe process is very important as radioactive contamination can be a very serious threat to the surrounding environment and human resource working, in these facilities. Radioactive waste from nuclear power plants, nuclear weapon testing and waste of radioactive substances used in research can be a serious concern, in terms of soil, water and atmosphere contamination [36, 43]. LIBS has been studied as a potential analytical tool to improve the operations and safeguards for electro refiners such as those used in processing spent nuclear fuel [44]. LIBS has been employed for the investigation of spatial and temporal evolution of uranium and other nuclear materials is laser ablated plasma.

Optimum operating conditions for the detection of small concentration of uranium has also been investigated for LIBS [59]. In mining detection of rock and drill core samples for quick identification of elements helps rapid decision making, hence a potential application of LIBS can be, analysis by a compact remote LIBS system to, generate quick in-situ results. Navid et. al. [2] proposed a simple statistical analytical technique for mineral identification from the elemental results of LIBS.LIBS was used for calibration and to generate complimentary

information for the other, fast scanning method such as Laser Induced Fluorescence Imaging. In this study suitability of detecting multiple elements in one spectrum was presented and application of LIBS was discussed for sorting purposes. M.Gaft et. al. [45] developed a machine based on LIBS and performed on belt evolution of phosphate measuring Mg, Fe, Al, Bone Phosphate Lime, insoluble phase, the metal impurity ratio and coal analysis for ash measurement. The LIBS results, when compared with control analysis, a good correlation was observed. The frequent analysis data was generated by LIBS system, which proved to be very helpful for the optimization of processes such as, minerals blending, separation of materials and quality control for mineral processing. Olli et. al. [46] applied LIBS for on line analysis of drill core samples, drill core samples of a gold mine from Finland were used for analytical purpose.

Heavy metals are considered as a potential source of soil and water pollution. The waste of industrial and mining process, shipping activities can cause ocean and river contamination, resulting negative impact on the biological life. The contamination of soil is a serious threat for human life and agriculture activities [3]. Continuous monitoring of heavy metal contamination is soil and water has many potential applications, which are as versatile in nature as other application involving LIBS. Anna et. al. [3] has applied LIBS for detection of heavy metals such as chromium, zinc, lead, and copper in sand matrix.

LIBS is also being implemented in healthcare, food and other consumer based industries for quality control purposes. For example, wheat, milk powder, gelatin, breakfast-cereals, bakery products, hair dyes, telcum, coffee, toys and tobacco were analyzed to estimate the presence of toxic elements and heavy metals. Food such as rice, spinach, olive oil, apple was successfully tested for organic contaminations such as pesticides or salmonella [7]. A decent amount of publications in literature are available on the use of LIBS in nanoparticle monitoring, in various applications such as detection of nanoparticles in gas phase [47].Some portable instruments for field based detections of nanoparticles in aqueous solution have also been developed[48]. Even the enhancement in LIBS by nanoparticle has also been reported by De Giacomo et. al. [49]. The nanoparticle enhancement LIBS (NELIBS) is based on the concept of deposition of a nanoparticles on the surface of the solid sample

for analysis [49]. In this study, the signal enhancement of 1-2 orders of magnitude, in LIBS signals was observed by depositing sliver nanoparticles on the surface of metal samples. Authors purposed this technique as suitable for metal detections as concentration and size of nanoparticles do not affect LIBS emission signals, if within the range of around 1nm for diameter and 1 order of magnitude for concentration. However, no considerable enhancement in signal was observed for semiconductors and insulators.

2.4 Qualities and Limitation of LIBS

In-spite of having excellent features such as quick response, multi-element detection, information richness and no sample preparation. LIBS is not yet being considered as a mainstream analytical technique for sensitive quantitative measurements due to a few drawbacks such as, poor detection limit, week signal to noise ratio, low signal quality for low concentrations, matrix effect and loss of information due to short plasma life [6, 7, 11]. As most of the quantitative detections specially those involving metals, require detection of trace or very low concentrations in complex matrix conditions. Hence it is very important to improve performance and quantitative detection capabilities of LIBS by various mean, for the development of reliable detection equipment based on LIBS. Literature has many studies suggesting various methods for the improvement of conventional LIBS system, which are mainly based on the concept of coupling another energy source into the laser ablated plasma for the improvement in sensitivity and signal quality.

2.5 LIBS Improvement methods

Limitations of conventional LIBS can be eliminated or reduced by adopting following improvement techniques.

- Double laser pulse LIBS
- Spark Discharge assisted LIBS
- Flame /Torch assisted LIBS

- Spatial Confinement assisted LIBS
- Magnetic Confinement assisted LIBS
- Microwave assisted LIBS

2.5.1 Double Laser Pulse LIBS

One of the proposed methods, is to improve performance of LIBS by using double laser pulse approach as shown in fig. 3. In this technique one pulse ablates the plasma on the sample surface while the second pulse enhances and retains the plasma. The purpose of the double pulse approach is to increase performance of conventional LIBS by achieving better coupling of the laser energy to the target and ablated material, leading to better production of the analyte atoms in an excited state. It was expected that the improvement in analytical capabilities of LIBS could be achieved by the double pulse laser configuration without any loss of reliability. The double pulse approach was first suggested by Piepmeier and Malmstadt in 1969 [50] and Scott and Stroheim in 1970 [51] (aluminium alloy samples in air). They suggested that, because a large portion of laser energy is absorbed by the plasma plume, the second laser pulse could lead to further excitation of species in the plasma. In 1984, Cremers et. al. [52] performed a detailed study of the possible applications of the laser double pulse technique for analytical purposes. In this study, the authors demonstrated the greatly increased emission intensities of elements during the bulk analysis of transparent liquids. The double pulse technique has been found in several configurations: various geometries (fig. 4) of laser beams, different collection geometries, different laser wavelengths and pulse durations, various pulse energies. In some studies, the double pulse configuration was realized with a single laser, while other studies used a two-laser configuration. The two-pulse technique offers more flexibility in the configuration arrangement, the choice of pulse energy, and the delay between pulses.

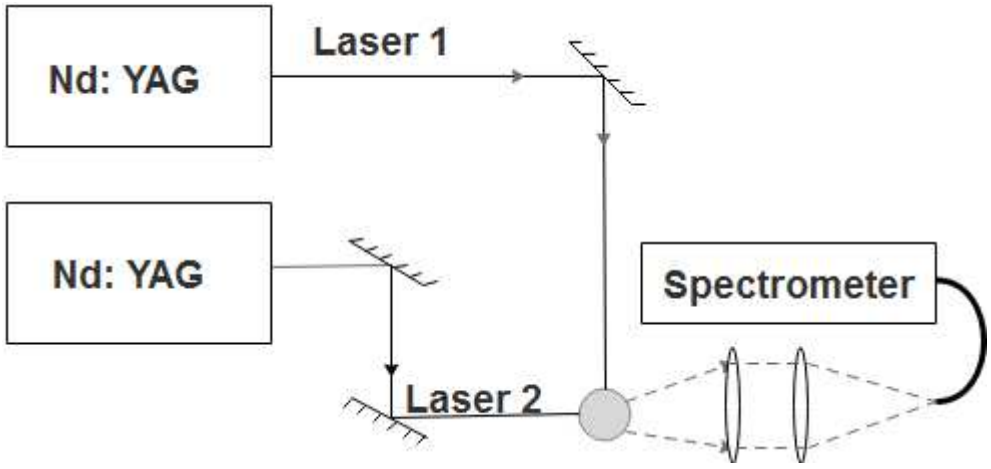

Figure 3: Double laser pulse LIBS setup with two laser configuration

Single laser based double pulse LIBS systems are simple and easy to align but offer very limited variation of pulse energies and the delay between laser pulses [53]. Various double pulse configurations are presented in fig. 4. Two main suggested beam configurations, for the double pulse LIBS system are collinear and orthogonal. In the collinear case (a) both pulses have the same axis of propagation and are directed at right angle to the sample surface. The orthogonal configuration has 2 further sub classifications such as orthogonal re-heating (b) and orthogonal pre-ablation (c). In the case of the orthogonal re-heating mode, the first pulse irradiates the sample and the second re-heating pulse propagates parallel to the target surface. For the orthogonal pre-ablation configuration, the first laser

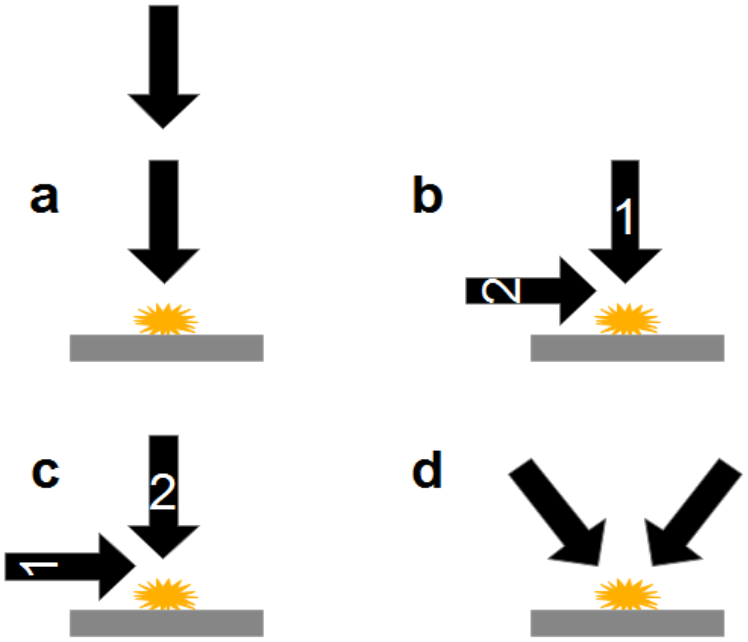

Figure 4: a) Collinear. b) Orthogonal re-heating. C) Orthogonal pre-ablation. d) Crossed beam, laser configurations.

pulse irradiates parallel to the target surface generating a laser induced plasma above the target, and the second ablative pulse is directed orthogonal to the target surface. From the practical point of view, the collinear configuration is the simplest approach for the

realization of the double pulse technique. Currently, it represents the only geometric configuration for stand-off double pulse LIBS applications [53].

The combination of femtosecond (fs) and nanosecond (ns) laser pulses in orthogonal configurations was also investigated by Scaffidi et. al. [54] and possible configurations were studied, fs-pulse parallel to the sample surface in pre-pulse mode or in re-heating mode, and ns-pulse parallel to the surface in pre-pulse or re-heating mode. For the studied wavelengths and pulse energies, it was found that the ns-pulse is much more effective in the re-heating mode. Later, Scaffidi et. al. [55] reported the enhancement of both material removal and emission intensity in the double pulse orthogonal configuration with a femtosecond pre-spark pulse and a nanosecond ablation pulse. This orthogonal combination yields eight-fold and ten-fold increases of material removal for brass and aluminium, respectively. The observed increase in the emission enhancement factor was 3–4-fold [50].

Double Pulse (DP)-LIBS have been used in many applications such as, reheating DP configuration was applied by Hai et. al. [56] for the laser cleaning process of mirror(HL-2A tokamak). The first laser pulse with low energy removed the surface impurities while second pulse was used for the analysis. Oba et. al. [57] analysed gadolinium oxide (Gd_2O_3) pallets by two orthogonal configurations of DP-LIBS. The reheating laser configuration demonstrated 25-fold enhancement while no enhancement was observed for pre-ablation configuration. Labutin et. al. [58] analyzed chlorine, sulfur and carbon in concretes with two collinear DP- LIBS configuration. Many environmental studies based on DP-LIBS, are also available in literature such as monitoring of pollutant [59], analysis of polluted soils samples, lead determination of soil samples and estimation of sulfur in coal samples [59] by collinear double pulse configuration, are some of the important environmental applications of DP-LIBS. Collinear DP-LIBS have also been used to improve the discrimination of explosives by diminishing the contribution of atmospheric oxygen and nitrogen to the LIBS signal[60]. Quantitative detection of Copper as impurity in silver jewellery has also been performed by DP-LIBS [61].

The existence of the various proposed geometrical configurations of lasers beam, collection geometries, laser wavelength, pulse durations and various pulse energies, have made this method overly complex and difficult to synchronize in comparison with the achieved signal enhancements and improved detection limits. In addition, selection of laser wavelengths, energies and delay time for single or double pulses to achieve optimum performance for every single species needs repetitions and adjustments in experimental setup, which eventually makes LIBS to lose its characteristic of quickness. Furthermore, adding another laser source makes the experimental setup difficult to align and increases the cost of the LIBS setup.

2.5.2 Spark Discharge Assisted LIBS

The enhancement of LIBS signals by a high voltage fast discharge is a relatively cheap improvement approach, which is based on the concept of creating a spark discharge, in the close vicinity of the laser ablated plasma by using two electrodes, simple capacitor and high voltage power supply [62]. This improvement method creates less sample surface damage due to the significant reduction of the required laser pulse energy. Nassef et. al. [63] applied the spark discharge on the laser ablated plasmas of Copper (Cu) and Aluminium (Al) . Two tungsten cylindrical rods were used as electrodes and high voltage between these two electrodes was delivered by a high voltage dc power supply. One electrode was attached to a 0.25 mF capacitor through a 500 kV current-limiting resistor, while the other electrode was grounded. By applying spark discharge an enhancement of 6-fold in signal to noise ratio was achieved for the investigated emission lines, as compared to that obtained from LIBS without spark discharge. Alexander et. al. [64] applied spark discharge for chemical analysis by LIBS and Laser Ablation Molecular Isotopic Spectrometry (LAMIS). By applying electric pulse, the enhancement in the emission intensity of atomic Calcium and Sodium for LIBS and molecular OH, AlO, CaF for LAMIS was demonstrated respectively. In other studies of soil and Silicon analysis by Zhou et. al. [65-67] a relatively different experimental approach was used. In these studies, small capacitance and higher discharge voltage were used with another difference that capacitor was directly connected to the

two electrodes without any resistor in circuit [65]. Enhancement of soil plasma with a nano-second discharge was studied [66], high capacitance and circuit voltage, increased signal intensity and noise level. The limit of detections of various elements such as Pb, Mg, Sn in soil sample with 6 nf capacitor and 11kV voltage, were 1.5 mg/g, 34 mg/g and 0.16 mg/g, respectively. Eschlböck-Fuchs et. al. [68] applied spark discharge on laser ablated plasmas of solid samples of slag, pressed Fe_2O_3 powder and gypsum with PTFE polymer surface layer.

2.5.3 Flame/Torch Assisted LIBS

In Flame/torch assisted LIBS, laser ablated plasma is generated in the blue outer envelope of a flame or in a commercial butane micro torch to improve the LIBS sensitivity [69, 70]. L. Liu et al. [69] used commercial butane torch and laser plasma was generated in the blue flame of the torch. Fast imaging and spectroscopic analysis was carried out by LIBS with and without micro torch. The emission intensity and signal-to-noise ratio was studied as a function of delay time. The experimental results showed an improvement of 3 times, in signal intensity of Mn and V. By the use of micro torch, the limit of detection of Mn and V were reduced from 425 ppm and 42 ppm to 139 ppm and 20 ppm respectively.

In another study L.Liu et. al. [70] created laser plasma in outer blue flame of neutral oxy-acetylene flame. An enhancement of 4 times in signal intensity was observed. Electron temperature and density was also calculated which showed that elevated temperature and low plasma electron density was achieved before 4 μs in flame environment. Use of a commercial torch or flame for enhancement of LIBS, makes system cheap portable and compact, but this flame assisted LIBS does not offer temporal control and may need sample preparation for many applications. In addition, enhancement in LIBS signals and sensitivity may not be very impressive. By applying electric arc fluorine and sulphur was detected easily while these elements could not be detection by conventional LIBS.

2.5.4 Spatial Confinement Assisted LIBS

Spatial confinement was first reported approximately a decade ago, in this technique plasma is created inside a confined space having a few millimetre dimensions. After the creation of the plasma the expanding shockwave is being reflected on plasma by cavity walls and transfers energy to compress plasma which increases plasma temperature and hence emission intensities. Confined spaces were made of varied materials such as quartz, metals and PTFE having various shapes such as rectangular, hemisphere, cylindrical and various other shapes. These confined spaces of various shapes were generally polished to reduce absorption by walls and were studied to see the effect. The size of cavity is also a vital factor in this improvement method. Li et. al. [71] studied the effect on wall distance on the Copper plasma. An enhancement of 5.2 times was observed for the delay time of 11.7 ms at laser energy of 180mj and wall distance of 9 mm. Wang et. al. [72] used seven groups of cylindrical cavities having various diameters and depths.It was observed that persistence of the Cu (I) line was longer compared with that obtained by using the cavities with smaller diameters, with persistence longer than 30 ms. For the same diameter of cylindrical cavity, the depth of the cavity did not significantly influence the persistence of the Cu (I) line.

Yeates et. al. [73] studied plasma volumes ablated, in the aluminum rectangular cavities of fixed depth of 6 mm and varying heights of 2.0, 1.5 and 1.0 mm, which were compared with freely expanded plasma. The influence of aspect ratio (depth/diameter) on the plasma parameters was investigated [67, 74]. Fused silica glass was used as the sample and silicon emission lines to measure temperature and electron number density. The plasma temperature and the electron density were the highest for the largest aspect ratio cavity. While with the decrease in aspect ratio, the plasma temperature and electron number density in the cavity approached the flat surface results [67].

This method is relatively cheap however, the cavity walls needs to be cleaned before each experiment to avoid contamination and to maintain reflection by the cavity walls. This drawback makes this technique somewhat unrealistic for practical applications.

2.5.5 Magnetic Confinement Assisted LIBS

LIBS assisted by magnetic confinement is based on the concept that when a strong external magnetic field either steady or pulsed is applied to laser ablated plasma in LIBS then the free movement of electrons and ions will be affected by Lorentz force which slows down the plasma expansion. This slow plasma expansion causes reduced plasma volume, increased electron concentration, higher collision frequency, higher plasma temperature resulting in stronger plasma emissions. This technique was first reported by Mason and Colgberg in 1991. Rai et. al. [75] studied the effect of a steady magnetic field generated by two rare earth (neodymium and samarium cobalt) permanent magnets on the optical characteristics of the laser-ablated plasma in air. When the plasma interacted with steady magnetic field of about 0.5 T, the enhancement factors of 2 and 1.5 for solid and liquid samples were achieved, respectively.

Li et. al. [76] investigated the influence of a magnetic trap fabricated from two permanent magnets (NdFeB) on the laser-induced copper plasma. The temporal- and spectral-resolved emission spectroscopy was performed and an enhancement of spectral lines for all neutral, single and dual ionized species was noted in the presence of nonuniform magnetic field. Harilal et. al. [77] studied the dynamics and confinement of laser-produced aluminum plasma expanding across a 0.64 T transverse magnetic field (two neodymium magnets) by using fast imaging, emission spectroscopy and time of- flight spectroscopy. Changes in plume appearance and dynamics, enhancement in emission and ionization, and enhancement in velocity were observed in the presence of the magnetic field. A recent study, which combines spatial and magnetic confinement to analyze vanadium (V) and manganese (Mn) in steel [78] demonstrates 11 and 30 ppm limit of detection for V and Mn respectively.

2.5.6 Microwaves Assisted LIBS

Microwave assisted laser induced breakdown spectroscopy (MW-LIBS) is based on the concept of enhancing and retaining laser ablated plasma by induced microwave radiations. Laser assisted microwave plasma spectroscopy (LAMPS) was initially developed by Ocean Optics and its partner company Envimetrics. A microwave cavity was used in the LAMPS setup and an improvement in detection sensitivity by a factor of 10 to 1000, depending on

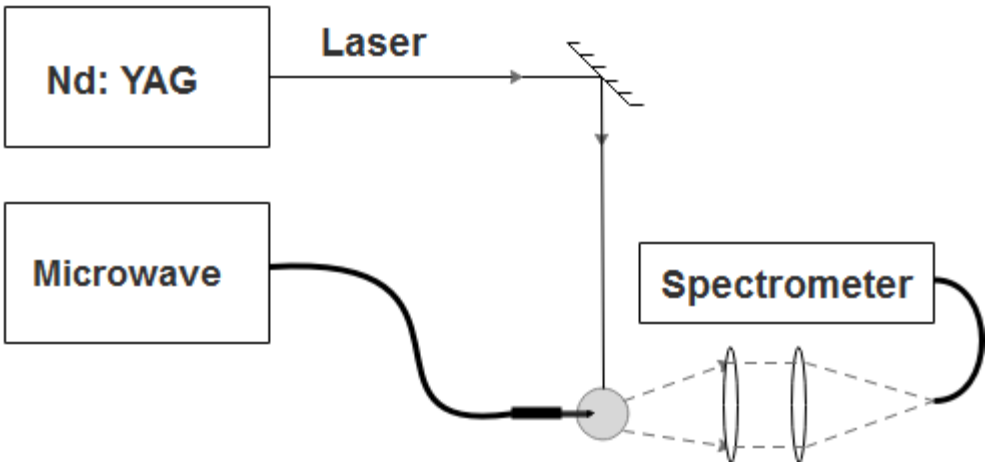

Figure 5: MW-LIBS setup using an antenna to induce microwave radiation at ambient condition.

the sample type, was claimed and visual enhancement in the plasma size was also observed [8]. Liu et. al. applied a microwave cavity for copper detection in soil sample [79] and reported 23 times enhancement in copper signal as compared to conventional LIBS, this study also demonstrated a detection limit of 30 mg/kg of copper and 23mg/kg of silver in soil samples while these concentrations could not be detected by conventional LIBS, same group also applied microwave cavity for elemental analysis in alumina ceramic sample [80] and reported upto 33-times enhancement for various elements. In this study, it was claimed that enhancement was maximum when laser ablation was induced at low irradiance on large area and was stronger for transitions with low excitation energy. The authors in this work also demonstrated that enhancement is dependent of the type of element. In gaseous samples, Ikeda et. al. [81] studied the enhancement of laser- and spark-induced plasmas in air by microwave radiation induced by an antenna, while a mesh chamber was also introduced around the sample which acted as microwave resonator and shield. This study reported that by microwave, 15 times enhancement in lead (Pb) spectra generated by laser, was achieved while spark generated plasma was enhanced by 880 times at 2KWatt microwave power, as microwave radiations were accepted by both plasmas. Authors also declared that this technique is suitable for detection of molecules in gaseous samples.

Khumaeni et. al. [82] demonstrated antenna-coupled microwave enhanced LIBS using solid Gd_2O_3 sample at lower pressure in enclosed cavity environment, where a loop antenna having 3mm diameter was used to deliver the microwave radiation close to the laser ignited plasma. This study demonstrated an enhancement of upto 32 times in Gd line due to the absorption of microwave radiation by laser plasma. The authors in this study also made a linear calibration curve of Ca contained in Gd_2O_3 sample and claimed 2mg/kg detection limit of Ca in this solid sample. In another study, Khumaeni et. al. [83] investigated the effect of microwave on the enhancement of the laser plasma, Nd:YAG laser was used to generate plasma on the surface of calcium oxide pellet, in a reduced pressure argon surrounding gas. A 400 watt microwave radiation was delivered by a loop antenna. The

results confirmed that in the presence of the electromagnetic field, induced by microwave radiation, the plasma lifetime was extended from 50 to 500μs, which was similar to the microwave pulse duration. Plasma temperature, electron density was also increased following microwave injection and plasma emission diameter was increased to 15mm. A 200 times enhancement in calcium (Ca) lines was also observed following microwave injection [83]. Tampo et. al. [84] applied a wire antenna induced microwave assisted LIBS for the analysis of nuclear fuel, a 50-fold enhancement in the emission signal of gadolinium ions, with a 250 watt (2.45 GHz) microwave radiation was achieved. The concentration of europium per gadolinium ranging from 5% to 100 ppm was measured following the enhancement by microwave radiation and on the basis of extrapolation of the calibration curve, the detection limit for microwave assisted LIBS was estimated to be 40 ppm. Alwahabi et. al. [85] applied antenna induced microwave radiations at ambient conditions for the detection of low and high concentrations. Viljanen et. al. applied microwave radiation in ambient conditions without any cavity by using an antenna which was called near field applicator (NFA). This NFA was installed at a distance of 0.5 mm from laser beam and 1 mm from sample surface. Authors studied the effect of microwave radiation for copper (Cu) detection in Cu/Al_2O_3 solid sample, they achieved 93-fold signal improvement as compared to conventional LIBS and also demonstrated a detection limit of 8.1 parts per million (ppm) limit for copper Cu [86]. Wall et. al. applied microwave radiations through NFA at ambient conditions for detection of indium in aqueous solution. In this work liquid sample was continuously circulated, while MW-LIBS and conventional LIBS were applied on the liquid jet. Limit of detection of indium in water solution was demonstrated as 10.1 ppm for MW-LIBS and 124 ppm for conventional LIBS, hence an enhancement of 11.5-fold was claimed to be achieved [87]. Hu HQ e.t al. [88] applied microwave assisted LIBS to study Cd in rice. Being a heavy metal Cd element is a cause of pollution hence, study of rice contaminated by this element is important for environmental and health concerns. Blank and laboratory polluted rice samples were used for analytical purpose. Emission line Cd I 228.802 nm was used for the detection while actual concentration of Cd was measured by anodic stripping voltammetry. Detection limit of Cd in rice sample with conventional LIBS

was 13.69 μg/g while with microwave enhancement 2.16 μg/g Cd in rice sample was detected successfully. Compared with conventional LIBS, plasma emission intensity was enhanced from 9 to 27 times following microwave enhancement.

Microwave radiation can be injected into the conventional LIBS system either by a microwave cavity or through a microwave antenna, such as NFA. A typical antenna based MW-LIBS setup is shown in fig. 5, this enhancement method is based on the use of microwave radiation as a secondary source of energy to enhance and re-excite the laser ablated plasma [79-83, 86, 87]. The microwave radiation interacts with the low electron density region of the laser plasma, while the enhancement happens due to free electron, atom and ions collision. The plasma electron density at which absorption of microwave radiation starts, is termed as critical electron density. Initially the laser ablated plasma has higher electron density about 10^{17}–10^{19} cm^{-3} which decreases during the de-excitation or relaxation process and around 10^{11} cm^{-3} (7.10^{10} cm^{-3} for a microwave radiation at 2.45 GHz) [80], plasma tends to accept microwave radiation and it no longer remains mirror for microwave radiations. At this stage, further rapid decay of the electron density stops because the microwave can then drive the motion of the free electrons by inducing concentrated electric field in the close vicinity of plasma. While the kinetic energy is induced by multiple electron-atom/ion collision, as a result excitation of de-excited atoms and ions, happens. Since excited atoms and ions in the plasma are useful emitters which give characteristic line emission of the constituent elements, hence more emissions, contributing to the stronger signal, are expected to be collected. As long as the microwave remains coupled, energy can be transferred to the plasma, and the emission lifetime of the plasma could potentially be the duration of microwave pulse. Microwave assisted LIBS can be very useful technique for practical applications because it doesn't require high laser power, which actually is a draw back in MW-LIBS as microwave radiations cannot effectively couple with the plasma having high electron density, generated by the high energy laser pulse. Therefore, in MW-LIBS laser energy in only required to be slightly higher than the ablation threshold as compared to conventional LIBS, where power of laser required to be the 10s of the times higher than the ablation threshold. As in MW-LIBS once

the plasma starts absorbing the microwave, the further decay of the electron density stops which can supress the need of more ablation mass and electron density as required in case of LIBS. This low laser requirement of MW-LIBS can actually be very useful for development of compact light weight equipment, which is an ultimate objective of the development of LIBS. The low laser power requirement of MW-LIBS even further strengthens the claim of LIBS as being a non-destructive analytical technique. Furthermore MW-LIBS can also be very useful for aqueous detection by reducing the splash effect, as being able to use of low laser power for plasma ablation. Another advantage of the MW-LIBS technique is that the microwave pulse duration can be extended to 100 of millisecond which can make MW-LIBS very suitable for sensitive detection of molecules and isotopes [80].

As the synchronization of the microwave radiation with laser beam is very important for the efficient and exact coupling of microwave radiations at the critical density of plasma. Therefore, usually in a typical microwave setup, microwave radiations, are induced a few hundred micro-second before laser pulse and are turned off after the end of gate-width of the detector. The experimental setup of MW-LIBS is relatively simple in terms of synchronizing microwave radiations with laser pulse and to control microwave power itself. MW-LIBS presents significant improvement in sensitivity as compared to other cost effect methods. Being simple and sensitive MW-LIBS can be applied to many practical applications for sensitive detection, however further improvement is required in limit of detection and sensitivity, because from the review of the publications related to MW-LIBS, it can be concluded that the lowest detection limit achieved with MW-LIBS was 2 ppm for Ca as presented in table 1, which demonstrates the limit of detection achieved in various studies, presenting a clear need of improvement in

Element	**Matrix**	**Detection limit (ppm)**	**Reference**	**Microwave Injection By**
Europium (Eu)	(Eu)/Gadolinium (Gd)	40	Tampo *et al* [84]	Antenna
Calcium (Ca)	Gd_2O_3	2	Khumaeni *et al* [82]	Antenna
Copper (Cu)	Soil	30	Liu *et al* [79]	Cavity
Silver (Ag)	Soil	23.3	Liu *et al* [79]	Cavity
Copper (Cu)	Al_2O_3	8.1	Viljanen *et al* [86]	NFA
Indium (In)	Aqueous solution of In_2Cl_3	10.1	Wall *et al* [87]	NFA

Table 1: Limit of detection of various elements in MW-LIBS

the performance of MW-LIBS for the application in elemental metallic detections, as most of the analytical applications involving metal such as, heavy metal detection for environmental monitoring, require detections in sub part per million with good sensitivity.

Chapter 3 Quantitative Detections by Elemental Imaging

3.1 Background

By the review of the literature of LIBS, it can be concluded that till present, all LIBS's improvement works have focused to enhance the plasma life and intensity. No improvement method based on the improvement of the signal collection channel has been reported. While it is believed that in MW-LIBS enhancement tends to drops after a certain microwave power, when the effect of microwave power on the signal enhancement is studied [86], this can happen due to increased plasma volume, as emissions can become out of focus, resulting an inefficient detection by the conventional spectrometric detection channel when fibre optics is used. It is also believed that the plasma signals are reduced during their endeavour from plasma to spectrometer and ICCD camera, through series of optical components. Hence, it can be possible to further improve the sensitivity of MW-LIBS by efficient detection of all plasma emission while reducing the signal loss. Therefore, it can be very attractive to develop an alternative relatively simple yet efficient signal collection channel, involving less optical components such as elemental imaging. This imaging method is based on the concept of using narrow band filter to allow only a specific wavelength light to pass through for the detection by an ICCD or even a simple camera. This alternative detection channel can be more efficient due to involvement of less optical components. While offering more sensitivity towards plasma enlargement in MW-LIBS due to its large field of view.

This concept of broad plasma imaging, for the temporal investigation of the evolution of plasma, is not new in the literature of LIBS. Fast imaging of whole plasma has been carried out in parallel to spectroscopy for example, L. Liu et. al. [70] applied fast imaging for the

temporal investigation of the laser generated aluminum plasma and studied the flame effect on plasma evolution. In another study, L. Liu et. al. [69] applied the imaging on the plasma from steel sample, to study the effect of micro torch on plasma evolution. Harilal et. al. [77] recorded plasma images to study the effect of magnetic field on plasma evolution and compared these with the images of plasma, recorded without magnetic field. Eschlböck-Fuchs et. al. [68] used an ICCD camera to record the temporal images of the laser plasma, which was enhanced by electric arc discharge. Bob Kearton and Yvette Mattley [8], captured images of laser plasma in conventional LIBS and in laser assisted microwave plasma spectroscopy (LAMPS), to compare the results. However, till present broad imaging of plasma was applied for temporal investigation of plasma evolution, the concept of narrow bandwidth imaging using a narrow bandpass filter, for quantitative detection is novel in nature.

Recently, with to advancement in manufacturing of novel filters, it has become possible to achieve signal elemental imaging by using filter and camera combination for example, replacing the spectrometer with a filter (or a filter system) in LIBS. Novel filters with an ultra-narrow band pass (BP) up to 0.1 nm are commercially accessible now, e.g. filters manufactured by Alluxa [89]. This level of spectral resolution is comparable to small compact spectrometers typically used in portable applications of LIBS. Besides, both high transmission throughout (T_S) and high optical density (OD) are unique for these new narrow bandpass filters. Therefore, it is possible to replace the spectrometer in LIBS with a simple filter, leading to a more compact and efficient setup, but potentially also of lower cost. In contract to spectrometer system, this alternative detection channel may not be able to offer multiple elemental detections as many filters could be needed and replacement of the filter followed by need of focus and alignment would be required while switching between elements. However, this problem can be resolved by using a low-resolution cheap spectrometer to identify the matrix and major elements of interest can be detected by imaging with high sensitivity, alternatively a filtering system can also be used with the camera to resolve the issue. In this chapter, an efficient alternative spectrometer-free detection channel has been reported by using narrow band filter and ICCD camera system.

This novel concept of elemental detection in MW-LIBS based on imaging has been demonstrated by using two narrow band filters. These filters are combined, to spectrally select the target element emission, which is then recorded using an ICCD camera. The demonstrated technique is named as microwave-assisted laser-induced breakdown elemental imaging (MW-LIBEI). Quantitative detection of indium in solid sample, using elemental imaging was carried out in conjunction with conventional spectrometric detections in order to compare the both detection method and report the extent of enhancement achieved. This detection technique seems to possess several advantages, such as high sensitivity and large field of view (FoV), as will be outlined in detailed in this chapter.

3.2 Experimental Setup and Sample Material

Figure 6a shows the schematic diagram of MW-LIBS setup presenting the entire system with both detection channels. While Fig. 6b presents relative position of NFA, Laser pulse, solid sample and imaging camera in 3-dimesions.

3.2.1 Laser and Microwave

The second harmonic output (532 nm, 6 ns pulse duration) from an Nd: YAG laser (Brilliant B) was used as light source to generate initial plasma as does in conventional LIBS. The laser pulse was focused on the solid sample by a bi-convex UV fused silica lens L1 (f = 100 mm, D = 50.8 mm) to generate plasma, while the energy of Laser was controlled by a Half wave plate and Glan-laser polarizer and was measured in milli-joules (mJ) by ES220C Pyroelectric Sensor. The pulsed microwave radiation, operated at 2.45 GHz, was delivered and coupled into the laser-induced plasma. The microwave pulse was generated with a water-cooled 3 kW Sairem microwave system which is available commercially. The microwave radiation was delivered with a 1 m flexible coaxial cable (50 ohms NN cable) with 0.14 dB@2.45 GHz,

connected with semi rigid cable (RG402/U) at the end. The other end of the semi rigid cable was attached to the NFA through SMA (SubMiniature version A) connector. Other end of the NFA was stripped off to expose the inner silver-plated copper steel core by ~ 25 mm to form a conductor.

The end of NFA conductor was tapered with a double included angle of ~ 45° to form a pointed tip which was located ~ 0.5 mm horizontally and vertically away from the interaction point of the focused laser beam (~ 100 µm in diameter) and the solid sample surface. The NFA and Coaxial cable connection was supported by a three-dimensional adjustment system to facilitate the alignment of NFA with respect to solid sample and laser beam.

In a MW-LIBS, laser is usually fired a few hundred micro-second after the microwave and spectrometric detection is triggered shortly after the laser pulse. However, the gate width of the detector is closed just before the decay of microwave pulse otherwise decay of microwave can be easily confused with that of plasma. Figure 7 describes the gate-width of both detectors (Spectrometer and imaging), microwave and laser pulse durations and operation of controllers which happen in real time for every laser and microwave pulse during an experiment. In the current setup, controller 1 acts as a primary controller while controller 2 operates as secondary as shown in fig. 6a. Controller 1 executes the process by triggering the flash lamp of laser and secondary controller. The secondary controller generates microwave pulse. While after 200 micro-seconds Q-switch of laser gets activated and laser pulse is fired. Both detection channels i.e. spectral and imagining, are synchronized with laser pulse and with each other in a way that just after the triggering of laser pulse, both detection channels are operated simultaneously with the same opening time/gate-width of 800 micro-seconds for a 1 milli-second microwave pulse.

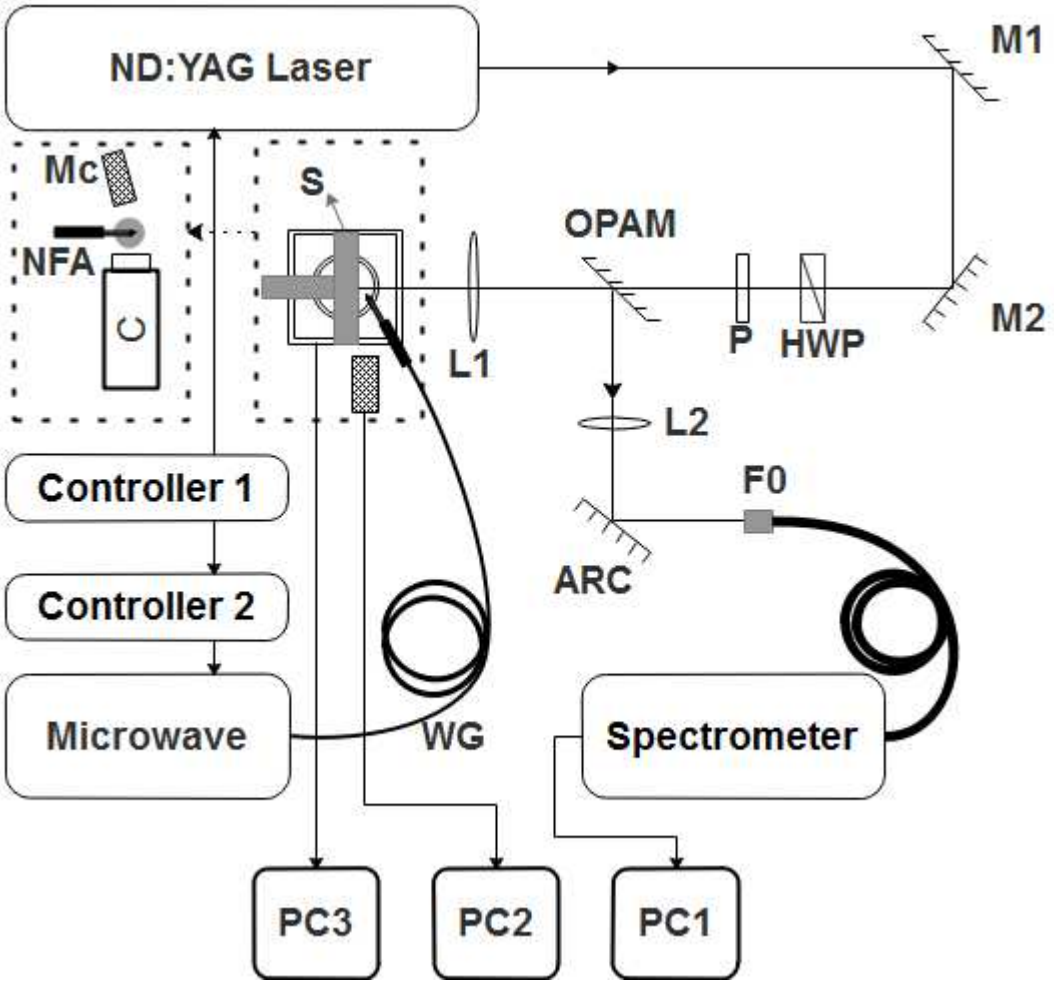

Figure 6a: Experimental setup of MW-LIBS including spectroscopic and imagining detection channel. M1&M2: mirrors, L1&L2: lenses, P: polarizer, HWP: half wave plate, OPAM: off-axis parabolic mirror, ARC: aromatic reflective coupler, S: sample, C: imaging camera, Mc: microscope, NFA: Near Field Applicator.

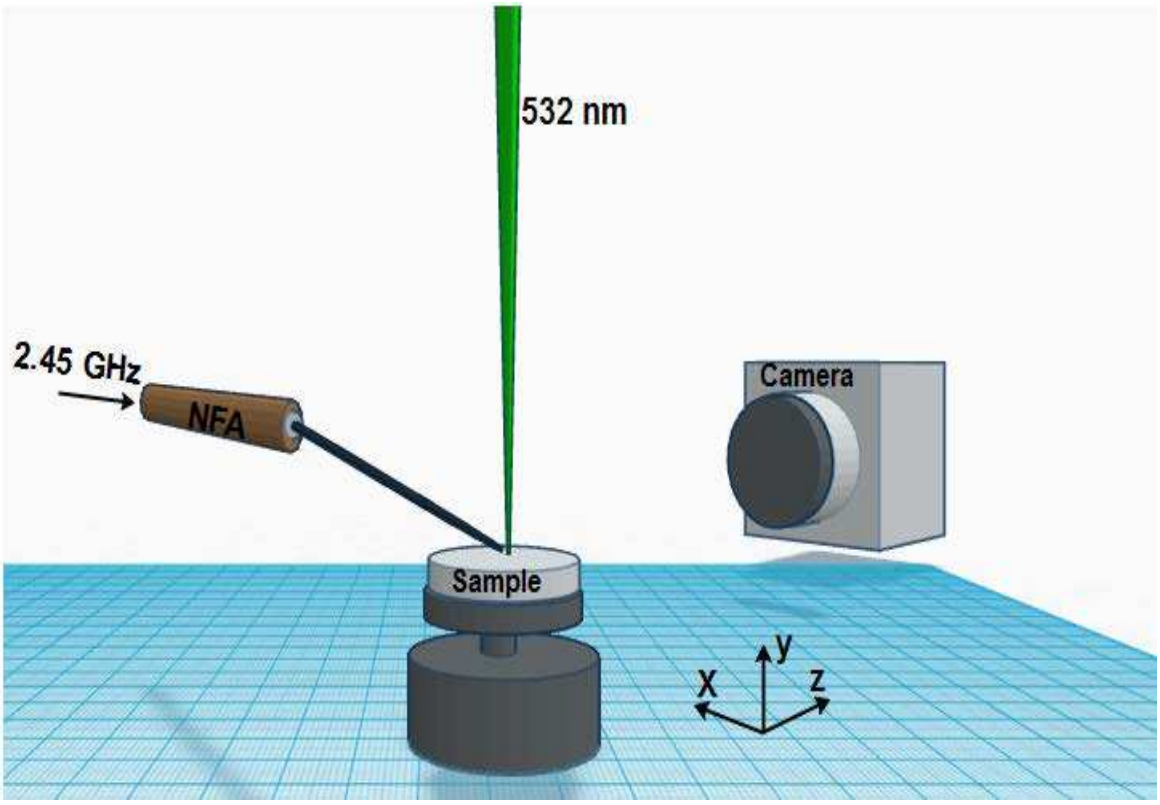

Figure 6b: A close look (3D) showing the setup of NFA, sample and imaging camera.

3.2.2 Imaging and Spectroscopy

The plasma emission was simultaneously recorded through two detection channels. The first is a backward collection scheme that is often used in conventional LIBS set-ups. As shown in Fig. 6a, after the first focusing/ collimating lens (f = 100 mm) the emission was focused by a perforated parabolic mirror and directed by a combination of a focusing lens into another parabolic and then into a fiber bundle (Thorlabs, BFL200HS02). The emitted radiation was then channeled into a spectrometer (f = 500 mm) installed with a 2400 lines/mm grating and an ICCD camera (iStar, Andor). The second detection channel is used for demonstrating the proof-of-concept of the MW-LIBEI technique. The plasma emission was directly filtered by a combination of two BP filters, both 50.8 mm in diameter. This is to select only the 451.13 nm Indium emission line following the transmission from the second (24,372.957 cm-1) to the first excited levels (2212.599 cm-1).

The first filter is a standard filter with a full-width at half-maximum (FWHM) of 10 nm (450FS10-50, Andover), while the second is a custom-made filter with a narrower BP (FWHM = 1.28 nm, Alluxa) [89], centered exactly at 451.4 nm. The two filters have transmission of 54% and 95%, respectively, resulting in a combined transmission of 51% at 451.13 nm. The combined Optical Density (OD) is ~ 5.6 out of the range of 450.12 – 452.68 nm and is ~ 8 below 440 nm and above 460 nm. These high OD values are critical in (MW-) LIBEI to block not only strong emissions from other elements, e.g. excited atomic nitrogen and Oxygen from buffering air, but also the background emission integrated over the full spectral region.

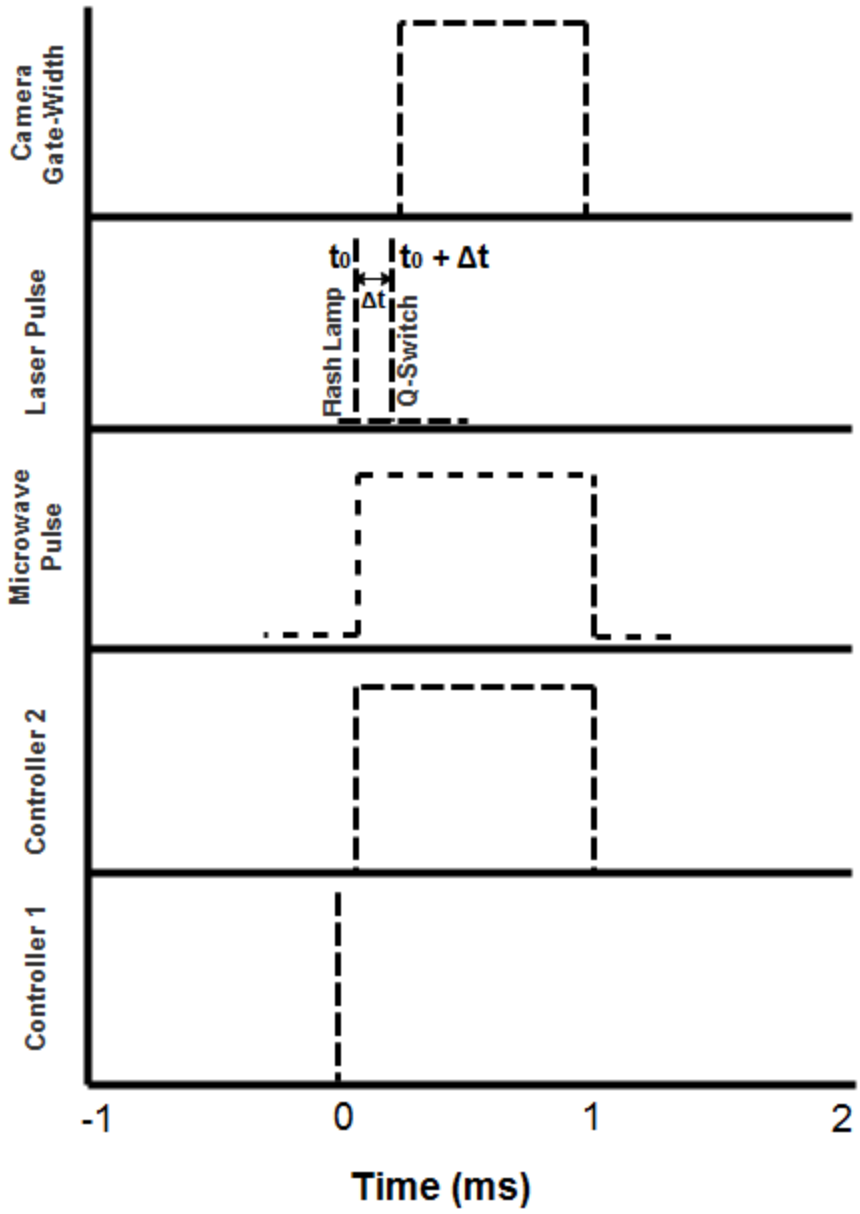

Figure 7: Microwave pulse, laser pulse, gate-width of cameras and controllers operation

The combined filters were installed in front of a Nikon focusing lens (f = 50 mm and f-number = 1.8), located at about 300 mm away from the detection volume. The emission signals passing the filters were recorded by a second ICCD camera (iStar, Andor), whose gating time and width were synchronized with those of the ICCD used in the spectroscopic detection channel. While it is possible to use a normal camera with a basic gate function to capture emission, an ICCD was used in this work to facilitate comparisons of the MW-LIBEI signals with those from the spectrometer-based MW-LIBS. The intensifier gain was set at 20 and 200, respectively, for the MW-LIBEI and MW-LIBS cameras. These values correspond to ~ 8% and 78% of the full available gain (255), respectively.

3.2.3 Solid Sample Preparation

To test the quantitative nature and the response linearity of the MW-LIBEI technique, solid samples containing a range of indium concentration from 50 to 1400 ppm (by weight) were prepared. Indium chloride ($InCl_3$) and Sodium Chloride (NaCl) salts were selected to prepare the solid matrix. Due to the hygroscopic nature of $InCl_3$ solid-solid mixing was not possible, in addition it is very difficult to achieve homogeneous mixture in solid-solid mixing. As homogeneous solid sample is very important in LIBS analysis because, LIBS is a point based analytical technique, hence non-uniform analyte concentration within the sample can generate unreliable results. To achieve the homogeneity of solid samples and to overcome the hygroscopic nature of $InCl_3$, both salts were dissolved in distilled water at ambient condition to make 1% solution of indium chloride ($InCl_3$) and 14.25 % solution of sodium chloride. These solutions were mixed (Liquid-liquid mixing) under uniform well-stirred arrangement (by using the magnetic stirrer), to achieve uniform liquid solution. Various concentrations of Indium in solution were achieved by varying the stoichiometric composition of the solution. These solutions were dried in an oven at 250 °C under well-stirred arrangement to evaporate the water.

The next step was to transform these solid mixtures into discs having identical depth and uniform surface. As antenna induced MW-LIBS setup is based on the creation of the strong electric field near the laser ablated plasma, for that purpose the antenna (NFA) has to be placed closer (~0.5mm) to the solid sample and laser pulse. To achieve reliable consistent results NFA should be exactly at the same position for each sample. After switching the solid sample, the enhancement can still be achieved in case of minor variation in distance of NFA from the surface of the solid sample and laser pulse. However, the resulting intensity of the MW-LIBS signal will vary drastically, making the experimental results unpredictable. This intolerant behavior of MW-LIBS towards minute variation of NFA position can make analytical detection by MW-LIBS, very unreliable. Therefore, to cope this problem the solid samples were transformed in round plastic discs having identical 3.5 mm thickness and 21 mm diameter as presented in fig. 8. To evaporate the traces of water, these discs were heated slowly at 51°C for approximately 15 minutes. Alignment of the NFA at the identical position after swtiching the sample for the analtyical purpose can be very challagning as slight variation can effect the signal strength, to overcome this isuue a microscope and computer arrangement was used. After the intial alignment of NFA with the laser pulse and solid sample for the maximum ehmancement, microscope was use to mark the position of solid sample and the NFA , after that all other sample were placed

Figure 8: Indium solid samples transformed into uniform round discs

extactly at the same position using this arrangment. In order to overcome point dependence of LIBS these samaples were placed on a continously rotating based. In this way, the whole sample surface was analysed in a small radius which can also be noted in some tested samples in fig. 8. Feed stock samples from the lead processing plant were also trasnformed into uniform discs following the sample procedure however, no prior chemical treatment was peroformed.

3.3 Results and discussion

To demonstrate the analytical abilities of LIBEI, several following concerns must be assessed. The first is to evaluate the blocking ability of the filtering system. As in LIBS the emission is spectrally resolved, hence the background interference if present, can often be

satisfactorily evaluated and then subtracted from the spectrally resolved signal, recorded by spectrometric detection. However, this approach may not be applicable in case of analytical detection by imaging channel, because all photons at multiple wavelengths, transmitting through the filters and detectable by the camera, can contribute to the image intensity of the element being analyzed for example, interference from the emissions of atomic nitrogen (N) and Oxygen (O), when the sample is being tested at ambient condition. Figure 9 shows the MW-LIBEI signals for indium at three concentrations of 0, 50 and 200 ppm, respectively, averaged from 200 laser shots. The gate width

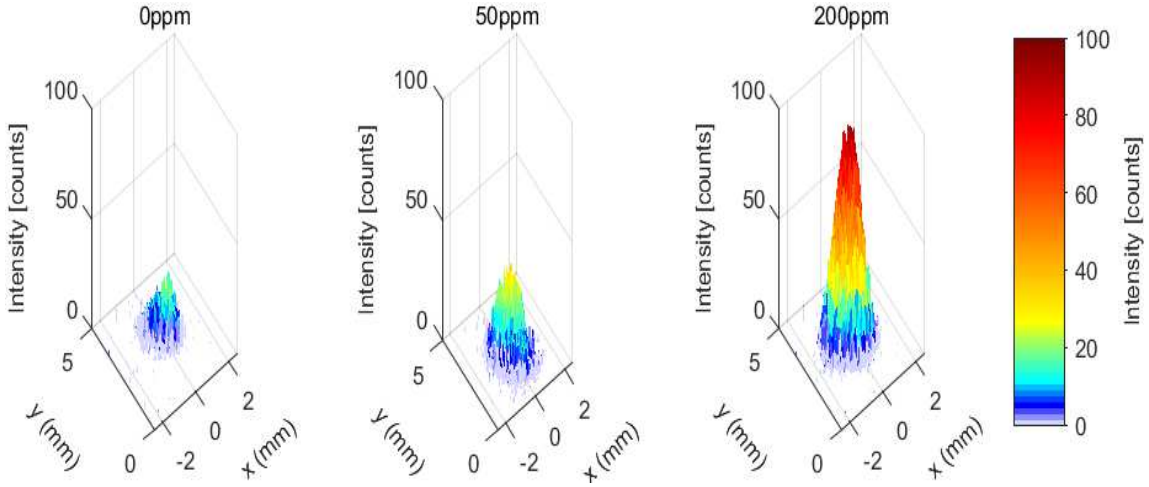

Figure 9: MW-LIBEI emission image plotted in three dimensions for samples with indium concentrations of 0, 50 and 200 ppm respectively, while laser and microwave was 2mJ/pulse and 900 Watts.

of the camera was 800 μs, the laser and the MW pulse was 2 mJ/pulse and 0.9 kW. As shown in Fig. 9, the image intensity for the sample having no indium (0 ppm) is still detectable, but the signal strength is weak, less than 20 counts. The image peak intensity significantly increases to 30 and 100 counts for the samples having an indium concentration of 50 and 200 ppm respectively. While the leaking background influences the LoD of MW-LIBEI, Fig. 9 evidently shows the good sensitivity of MW-LIBEI, for which a further discussion is given below.

The second concern to be assessed in developing MW-LIBEI is the corresponding relationship between MW-LIBEI and MW-LIBS signal intensities, given that the latter holds quite good linear relations with the elemental concentrations. Figure 10 shows simultaneous results of the MW-LIBEI and MW-LIBS intensities measured in samples with different indium concentration (0-1400 ppm). In this measurement, all experimental settings were kept the same as stated in Fig. 9. The intensities of the MW-LIBEI are calculated by integrating area over the plasma image, while those of the MW-LIBS are spectrally integrated over the indium line at 451 nm, both with background subtractions. Figure 10a shows an excellent linear relationship between MW-LIBEI and MW-LIBS with a square correlation coefficient (R^2) value better than 98%. Furthermore, the linearity holds in a large dynamical range, indicating the feasibility of using MW-LIBEI for element quantifications, as quantitative element measurements using MW-LIBS has already been demonstrated [82, 84, 86, 87]. Figure 10b shows MW-LIBEI and MW-LIBS signals against the indium concentration. A general good linear relationship exists in both measurements, noting that there can also be potential uncertainties in concentrations of the samples. The relatively large standard deviations, for both type of signals in Fig. 10b, are attributed to the fluctuation of the coupling efficiency of the microwave to plasma.

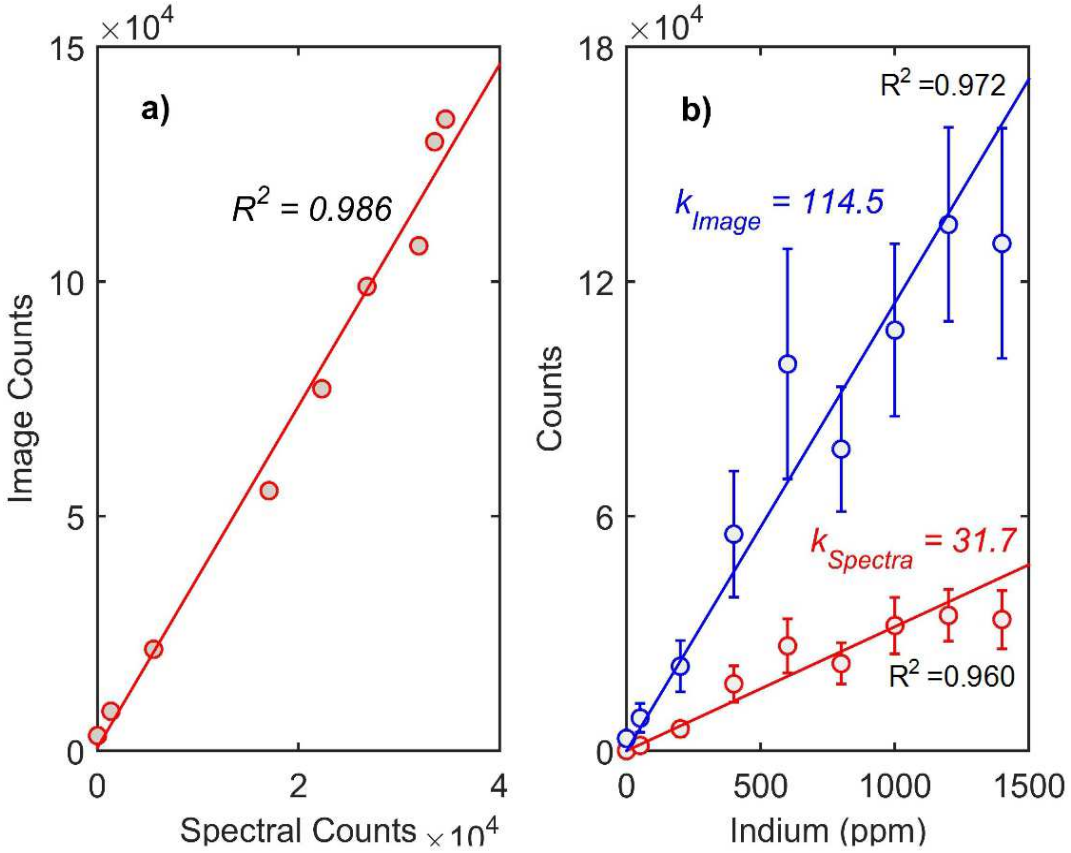

Figure 10: (a) Represents relationship between spectral counts (MW-LIBS) and image intensities (MW-LIBEI) simultaneously recorded by spectrometer and imaging camera. (b) The intensities of MW-LIBS and MW-LIBEI signals as a function of indium concentration.

An important finding is that the slope of the MW-LIBEI signal curve is approximately 3.6 times higher than that of MW-LIBS, indicating an improvement of 3 folds in signal intensity for the present setup using MW-LIBEI. The signal intensity of MW-LIBS may be improved using a low-resolution grating with higher reflection efficiency, such as that of 300 lines/mm. However, noting the gains used for both cameras, the present work clearly demonstrates that the simple MW-LIBEI based on a low-cost camera can achieve higher signals than the MW-LIBS.

This enhancement is particularly attractive because MW-LIBS is already more sensitive than conventional LIBS by a factor of ~ 1-100. Figure 11 presents the indium plasma images at various concentrations. This indium plasma image for each concentration is the average of 200 single images, which were recorded for each concentration in parallel to spectroscopic detections. From the fig. 11, it can be noted that with the increase in indium concentration in solid sample, the plasma intensity tends to increase, which proves the sensitivity of the imaging method for variation in elemental concentration, as demonstrated in fig. 10 (b). A few exceptions can also be observed which corresponds to the uneven variation of indium intensity from imaging and spectroscopy, shown in indium intensity plots of fig. 10 (b).

The potential reasons of this uneven variation are already explained above. The image intensities presented in fig. 10 (b) are calculated from the average indium images of fig. 11 by subtracting the background noise in MatLab. After the subtraction of background noise, all pixel intensities in the indium plasma image were integrated to calculate the total intensity of the indium plasma against each concentration. It is further added that the images in fig. 11 are only representing the indium concentration within the plasma, which means that the size of whole plasma could be larger than the presented images. In fig. 11, the (0,0) presents the approximate position of the laser pulse while NFA being on the right side, this configuration will be explained later in fig. 15, considering the categorized axis as presented in fig. 6(b). The LoDs of MW-LIBS and MW-LIBEI are estimated to be 16 ppm and

50 ppm, respectively. The LoD of MW-LIBS was estimated based on the signal-to-noise method. The LoD of MW-LIBEI was estimated from fig. 9 using visual evaluation method [90]. Considering the leakage through the filter in the absence of the indium (0 ppm) as shown in fig. 9, for a safe detection the acceptable signal value was assumed three times of this leakage, in terms of intensity counts. At this stage MW-LIBEI demonstrates poor LoD because even in sample without presence of indium there was still emission intensity acting as background interference, as shown in fig. 9.

This leakage through filter limits the quantitative detections beyond 50 ppm, however, Fig. 10b demonstrates that MW-LIBEI offers higher sensitivity for the smaller variation in concentration as compared to MW-LIBS. The background interference can potentially be reduced to improve LoD of MW-LIBEI. In principle, a filter with a narrower BP (i.e. that is less than 1.28 nm) and a higher OD can be employed since atomic emission is typically much narrower in spectra. Such a filter, e.g. which has a FWHM of 0.12 nm around 396 nm, indeed had already applied in astronomy study [91]. Another potential method is to introduce a second narrow BP filter that is slightly off-resonant to the target spectral line, installed with the resonant filter in a stereoscopic lens configuration, allowing the recording of the background signal simultaneously.

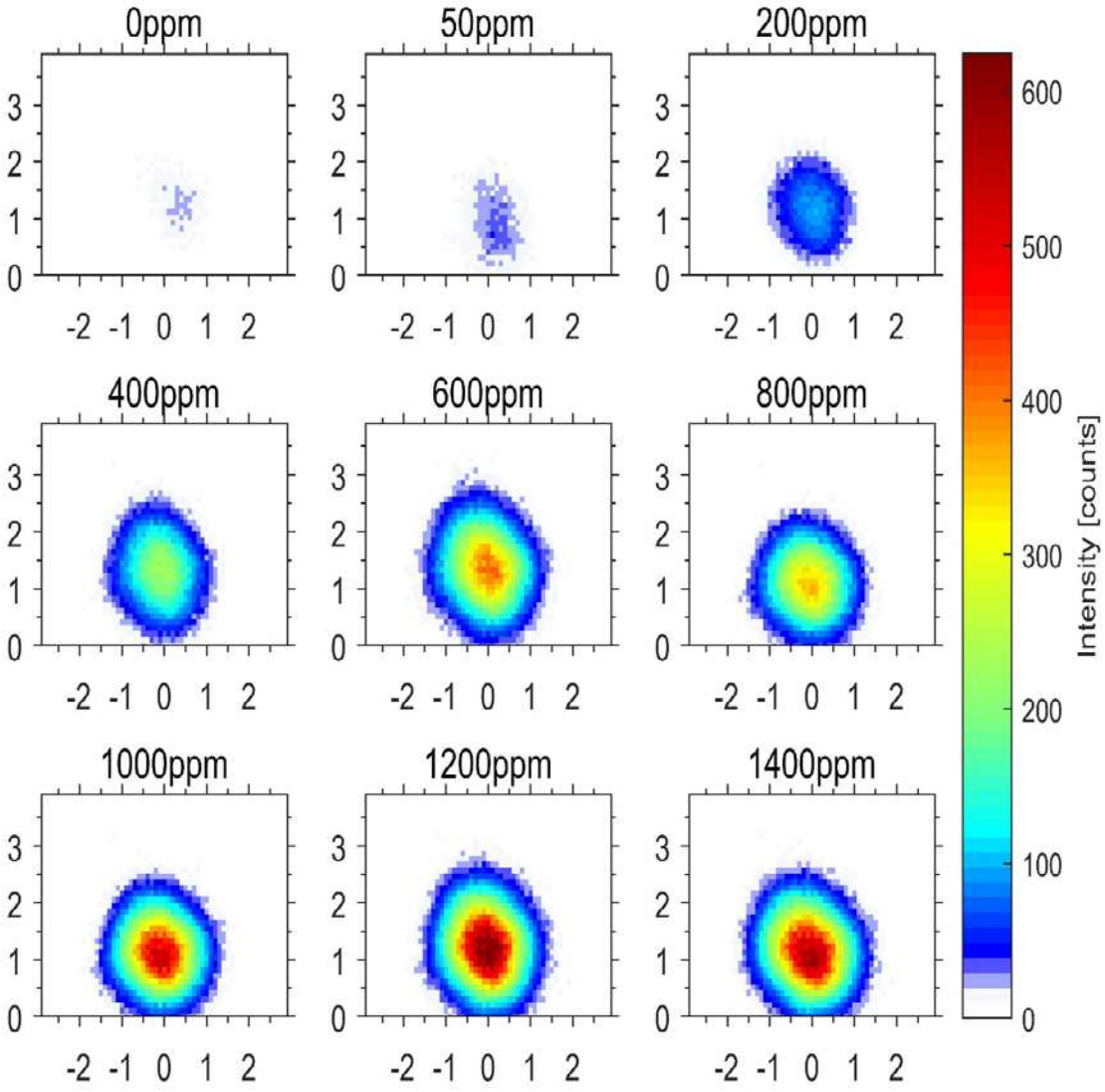

Figure 11: Indium plasma images for selected indium concentration, as indicated, recorded by MW-LIBEI at laser power of 2mj/pulse and microwave power of 900 watts

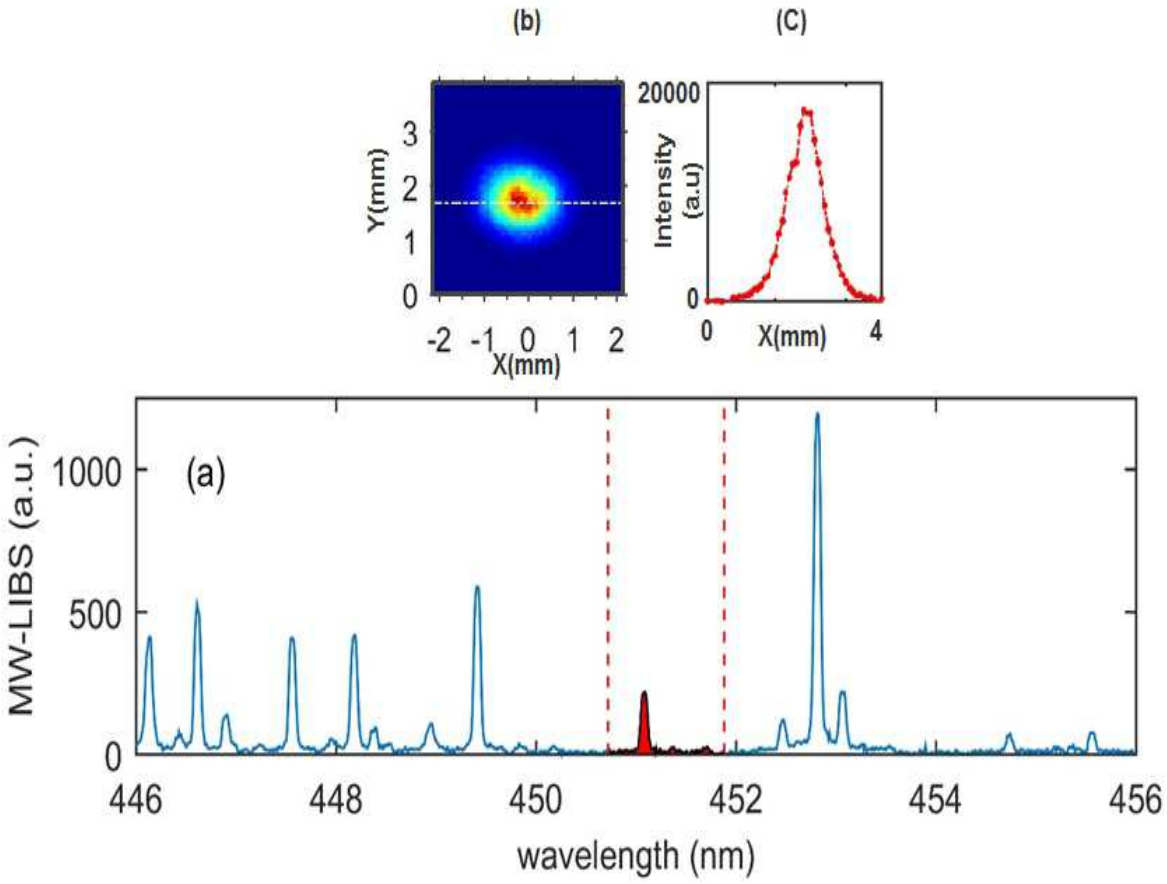

Figure 12: Typical spectrum of MW-LIBS and (b) emission imaging of MW-LIBEI recorded simultaneously in a feedstock sample from a lead processing plant using 2.5 mJ/pulse laser and 900 watts microwave. In (a) the transmission band of the filters is indicted by the two red dashes lines. The cross section of the MW-LIBEI image (b) along the dash-dot line is shown in (c).

The third concern in developing MW-LIBEI may be the neighboring spectral interference from other elements. Figure 12 shows a typical MW-LIBS and MW-LIBEI recorded in a feedstock sample from an industrial lead processing plant. The sample contains many other elements including indium and, therefore, several spectral lines appear within this 10-nm spectral range in the MW-LIBS. However, it is still feasible to select indium signals in the MW-LIBEI with a quite good SNR. Also, the cross section along one-pixel array of the MW-LIBEI image demonstrates both high intensity and great SNR ratio in the MW-LIBEI. The limited capability of detecting multiple elements of MW-LIBS can potentially be resolved by applying a cheap low-resolution spectrometer for multi-elemental identifications.

The necessary role of the microwave source in MW-LIBEI has also been emphasized in fig. 13. The fig. 13 presents the imaging signals recorded with and without the assistance of external microwave source, as well as the corresponding MW-LIBS intensities as comparison. Figure 13a and 13b presents single shot image intensities without and with microwave. Figure 13c and 13d presents averaged image intensities without and with microwave respectively. While Figs. 13e and 13f present a comparison of spectral and image intensities captured by both detection channels, i.e. LIBS and LIBEI without and with microwave, while operated simultaneously. All measurement settings were held the same as shown in Figs. 9 and 10, while without microwave the camera gate-width was only delayed 200 nanoseconds from the laser pulse to capture more indium signal.

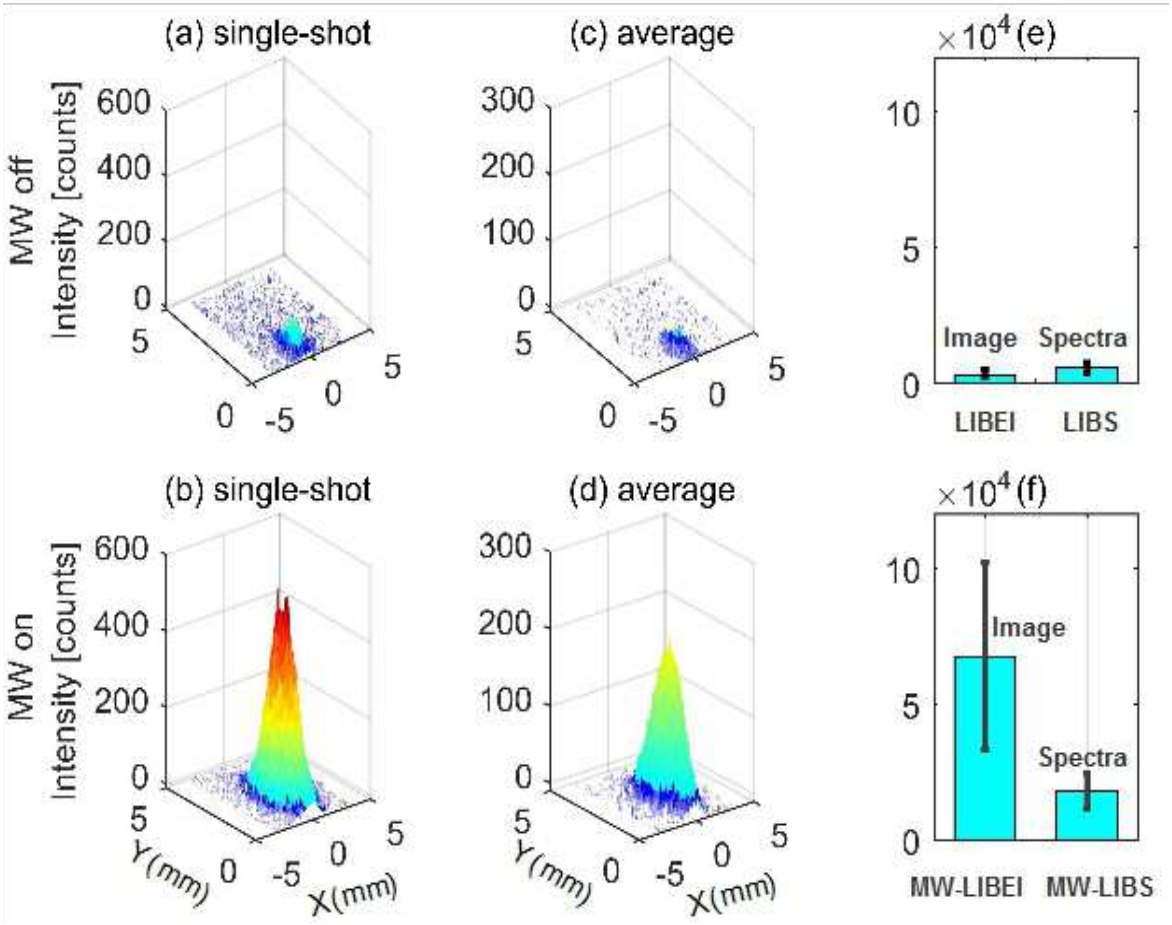

Figure 13: Indium emission images plotted in three dimensions for snapshot signals (a) without and (b) with microwave assistance, and signals averaged over 100 laser shots (c) without and (d) with microwave assistance. The corresponding image and spectral intensities of MW-LIBEI and MW-LIBS are shown in (e) and (f). 400 ppm indium sample, 3 mJ/pulse laser, 0 and 900 watts of microwave powers were used.

Also, a higher laser power (3 mJ/pulse) than in Figs. 9 and 10 was applied to ensure detectable signal in the microwave off testing. Firstly, it can be seen that the signals have been significantly enhanced following the microwave injection, both in spectra and in imaging, revealing the crucial role of microwave. Secondly, the enhancement of LIBEI signal is clearly larger than that of LIBS (Figs. 13e and 13f). This is another advantage of MW-LIBEI, i.e. its large FoV ensures that all emission signals are being captured and makes MW-LIBS more tolerant to the fluctuation of the plasma volume. This tolerance against the change of plasma volume is difficult to achieve in both microwave assisted and conventional LIBS. Comparison of the signal in MW-LIBEI (in Fig. 13f) with that in conventional LIBS (in Fig. 13e), reveals a total signal enhancement of ~ 14-fold for the present MW-LIBEI setup.

Additionally, MW-LIBEI signal can be further enhanced by increasing the microwave power. In Fig. 14a, both normalized MW-LIBS and MW-LIBEI signals are shown against the microwave power, intensities have been normalized using the signal recorded without microwave (MW=0) in both detection techniques. A linear relationship is found in the MW-LIBEI curve for the microwave power up to 1.6 kW, which potentially holds for higher microwave power. Contrastively, the MW-LIBS signal responses nonlinearly to the microwave power above ~ 1.0 kW and appears to be saturated. This non-linear response is attributed to the increase of the plasma volume, as illustrated in Fig. 14b showing that the plasma volume increases linearly with the microwave power when it is effective (> 0.4 kW) on the plasma. In MW-LIBEI, the enlargement of the plasma volume and the enhancement in signals are well detectable because of its large FoV. However, the volume enlargement is not detectable in MW- LIBS beyond 1.2 kW MW power, since the plasma volume becomes too large to be effectively coupled into the fiber optical cable, as clearly illustrated in Fig. 14a. It should be noted that the plasma volume was calculated based on an effective radius.

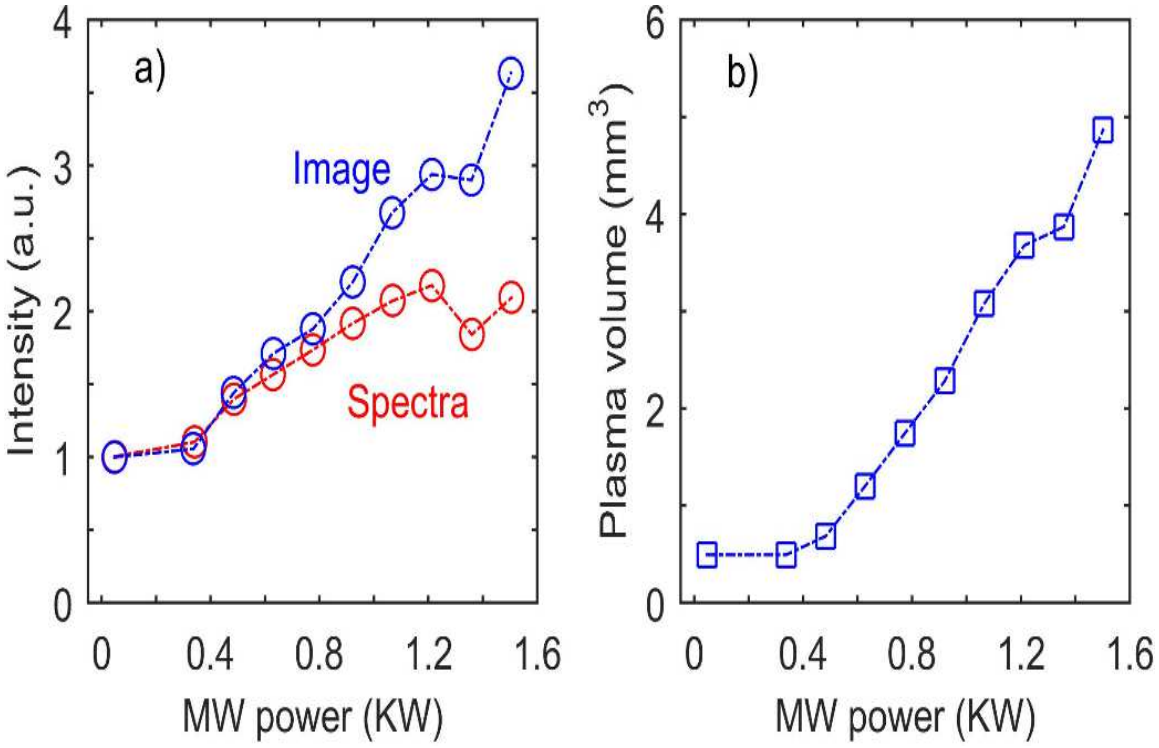

Figure 14: (a) Normalized intensities of MW-LIBEI and MW-LIBS, as a function of the microwave power, and (b) the corresponding plasma volume recorded in MW-LIBEI using 2.5mJ/pulse of laser.

A process of image binary was applied firstly to the recorded image based on the $1/e^2$ value of the maximum intensity to get the projected area of the plasma, from which an effective radius was calculated by assuming that the plasma is spherical in shape. This process was acceptable because that, as shown in Fig. 12b, the plasma images are reasonable approximated as round in the present work. In addition, it is also significant to demonstrate the change in physical appearance of the plasma following the microwave injection at various powers, to strengthen the claim of MW-LIBEI benefiting from FoV.

Figure 15 presents the change in the appearance and intensity of indium plasma images, captured at various microwave powers keeping the laser power constant. 200 single shots were recorded at each microwave power and plotted as an average image. X-axis in these figures represents the position of the sample holder. NFA is placed 1 mm from sample and 0.5 mm from laser beam, while laser beam is propagating at 10^o towards solid sample. Y-axis represents vertical distance from the sample holder and is at right angle to the axis of imaging camera (Z-axis) as shown in Fig. 6b. Axis values have been presented in millimeter (mm) by calculating the pixels/mm from recorded image of a sample, having known length and width. Zero mm on the X-axis is the approximate position of the laser beam while NFA applicator is located on the right as shown in Fig. 15. Form this figure it can be seen that with the increase of microwave power, physical appearance and intensity of plasmas tend to increase substantially, which proves the concept of FoV in MW-LIBEI. While a few exceptions can also be observed at 0.9, 1.1 and 1.2 kW which are assumed to be, because of damaged surface of solid sample, resulted as irregular microwave coupling. In contrast to LIBS, MW-LIBEI is suitable for a single elemental detection. It is worth noting that a stereoscope in front of the camera lens can offer a second elemental detection channel, if needed. A low-cost spectrometer can also be used for elemental identification and or, for larger scans to identify the whole matrix, whereas major species of interest can be analyzed by elemental imagining.

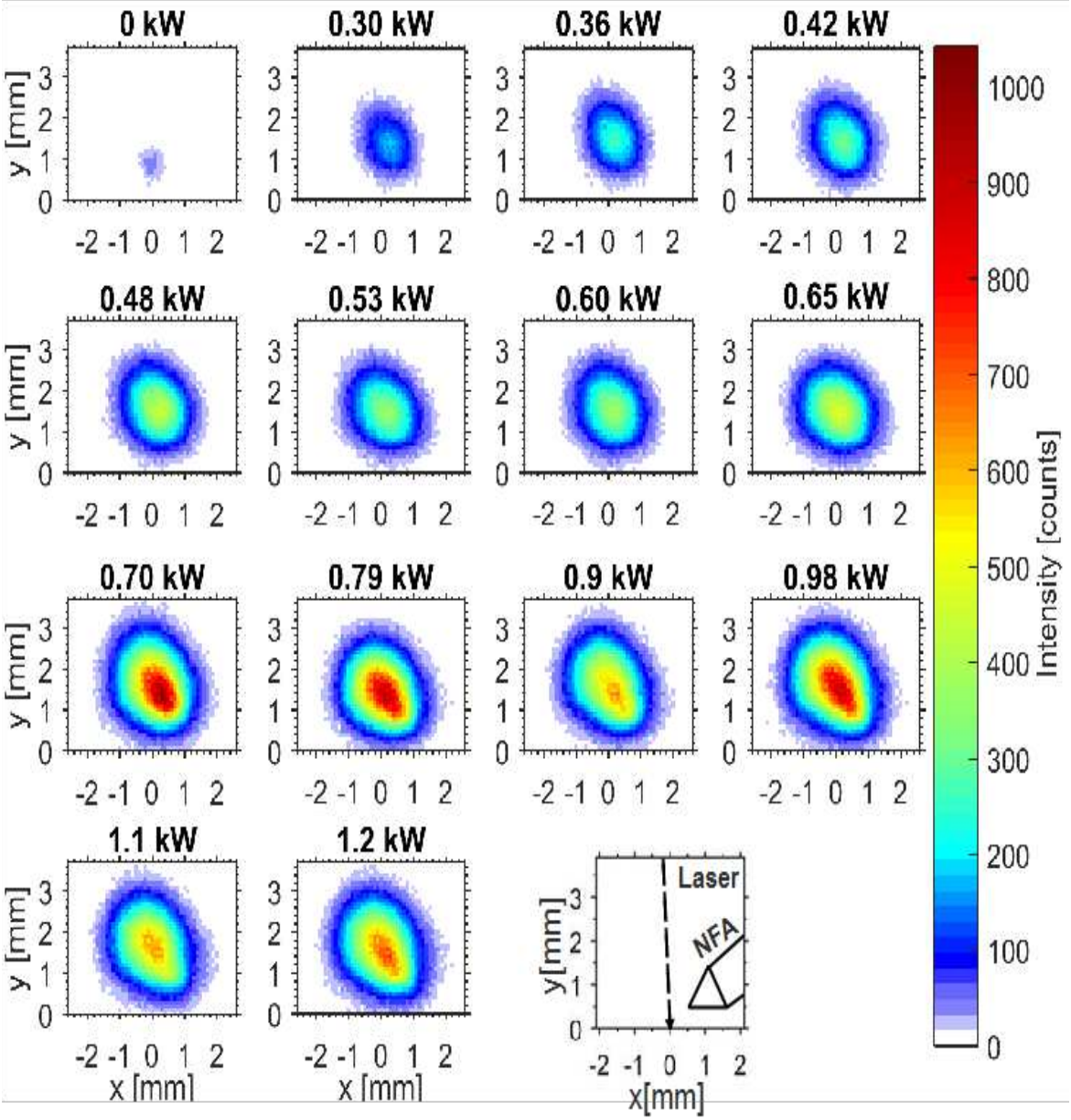

Figure 15: Plasma images from a 1200 ppm sample at various microwave powers, 2.5 mJ/pulse laser was used. Axis are presented in mm with the point (0,0) approximating the incident location of the laser beam on the sample.

3.4 Summary

The objective behind the use of single elemental imaging for quantitative detection was to collect the maximum plasma emission following the enhancement by microwave, as the conventional spectroscopic detection loses emission signals, due to increased plasma volumes in MW-LIBS. In addition, no LIBS enhancement method based on alternative yet improved collection channel was reported while it is believed that vital signals are lost in spectroscopic detection. Hence, microwave-assisted laser-induced breakdown elemental imaging as a new elemental detection method has been demonstrated. MW-LIBEI offers a desirable high-level of intensity because of the large FoV and a negligible flight-out-of-view. An improvement of 14 folds in the detection intensity as compared to conventional LIBS was demonstrated for indium in solid samples. The demonstrated improvement in the intensity is because of the large FoV of the MW-LIBEI technique, which is not available in MW-LIBS. From the experimental results, it can be concluded that MW-LIBEI offers more than 3-fold enhancement in signal intensity as compared to MW-LIBS. The detection intensity can be further improved by increasing the power and the pulse-duration of the microwave radiation.

However, signal quality and consistency in microwave assisted LIBEI and LIBS, is highly dependent on the alignment of microwave antenna with laser pulse and solid sample, slight variation can produce unpredictable results. Hence minor sample preparation and an efficient arrangement to place NFA exactly at the same position for each sample (after switching) is desirable. The limit of detection of the MW-LIBEI technique is higher than that of the MW-LIBS, 16 ppm versus 50 ppm, at this stage due to unresolved background interference especially for the detection at ambient conditions, but it can be potentially improved by using a filter (or a filtering system) with a narrower BP or higher OD. Furthermore, the MW-LIBEI is a spectrometer-free technique, in which only a relatively simple camera, with neither fast gating nor an intensifier, can be used to achieve similar detection capability as that of conventional MW-LIBS. The spectrometer-free MW-LIBEI

technique responds well to the demand for cost-effective, reliable, sensitive and real-time detection in remote and harsh environments including, space, defense, environment, chemical processing and mining industries.

Chapter 4 LIBS Enhancement by Efficient Microwave coupling

4.1 Background

Efficient coupling of the supplied microwave power, into the laser generated plasma is a key factor to achieve the desired enhancement in the performance of the proposed MW-LIBS setup. Performance of the antenna based microwave assisted LIBS system depends majorly on the performance factors of the antenna (also known as near field applicators NFA) such as, efficient transmission of the supplied microwave power and then radiation of that transmitted power in the form of concentrated localised electric field. A NFA being the central component of the microwave system, can considerably improve the coupling efficiency and plasma enhancement for the same supplied microwave power by two means i) improving the transmission of power by reducing the refraction/return power ii) efficient radiation of supplied microwave in terms of localised electric field distribution and strength.

Therefore, design and optimisation of a NFA, by considering the features of the microwave and LIBS system in the available setup, is very crucial to achieve desired improvement. However, by the review of the literature it can be concluded that no performance enhancement study based on the improvement in design of NFA, has yet been reported in the literature of MW-LIBS. The development of an efficient NFA can be very attractive because it is already evident from the studies that MW-LIBS needs less Laser power as compared to conventional LIBS systems, meanwhile a well-designed NFA can also further reduce the microwave power requirement, suppressing the need of bulky microwave power sources. Hence use of cheap, robust microwave sources without compromising the improvement in the performance, can take MW-LIBS a step ahead towards the development of the compact portable commercial devices.

In this chapter the improvement in the performance of the MW-LIBS system have been investigated, following the use of 4 new designs of NFA. This development process has two parts 1) design of 4 NFA based on the full wave electromagnetic simulations performed with CST Microwave Studio (CST) [92], while considering the factors such as the influence of the electromagnetic environment, reflection coefficient to maximize the electric field strength at the location of the laser ablated plasma. These designs have minor geometrical variations, fifth design is considered as base design for comparison 2) Testing of these design in MW-LIBS setup for the evaluation of coupling, efficiency and overall improvement in the performance of the system.

Using these new NFA designs, MW-LIBS was applied for copper (Cu) detection in solid sample, while simultaneous imaging of whole plasma was also performed. Microwave dependence and spatial evaluation was investigated for each design to study the final effect on the plasma size and emission intensity.

4.2 Design of NFA

The NFAs in a typical microwave-assisted LIBS setup for ambient conditions, such as demonstrated in chapter 3 are affixed with adjustable posts and connected to the microwave generator through a series of equipment and coaxial cables in a relatively open space. Therefore, these NFAs are more sensitive to the exterior environment compared with the microwave launching devices, in a relatively confined environment since the objects electrically connected or in proximity to them can have an impact on their performance and repeatability owing to electromagnetic coupling.

This is especially critical for metallic objects such as the NFA holder and the adjustable posts, whose positions might change for different measurements. In order to develop the NFAs with a predictable performance, this type of impact must be mitigated through appropriate electromagnetic design. Hence, different applicator designs involving some well-known techniques such as a quarter-wave choke or a finite ground plane [93] are

proposed to strongly limit the return currents along the outside of the coaxial cable feeding the NFA. This will consequently limit the direct coupling to the outside objects in the system. Such an undesired coupling can drastically alter the efficiency of a NFA, and in the presence of a typically complicated environment, can reduce the performance parameters. Four designs variations of NFAs, namely designs B, C, D and E, are designed, fabricated and investigated in this paper by comparing them to a reference design A.

The general schematic diagrams of the NFA designs are shown in Fig. 16, where (a) refers to the reference design A, while (b) shows the design B and (c) the generic geometry of designs C, D and E. Their dimensions are given in Table 2, as designed for operation at a microwave frequency of 2.45 GHz. All considered NFAs consist of a rod-shaped conductor fed by a standard SMA (subminiature version A) connector for radio-frequency (RF) connection. The rod of the applicator conductor is made of silver plated copper clad steel and has a radius of 0.45 mm, and is formed by stripping the inner conductor of a 50 Ω rigid coaxial cable, and sharpening its tip to an angle of α. In this study, design A is considered as a reference NFA and does not have any electromagnetic isolation to the environment.

In contrast, the other four NFAs employ some simple but effective isolation techniques such as choke and ground plane to render their performance more robust and predictable. The main aim of those techniques is to suppress the return RF currents on the outside of the coaxial cable. To this end, a quarter-wave choke is soldered on the outer conductor for design B whereas for the other three NFAs a finite-size circular ground plane is added to the design. The SMA connector at the other end of the cable is connected to the waveguide output from the microwave generation apparatus. When excited with microwave power at the system frequency of 2.45 GHz, designs D and E are working at their fundamental resonant mode while designs B and C operate at higher-order modes, as shown in Fig. 17. In principle, the resulting NFAs are variations of monopole antennas but the main

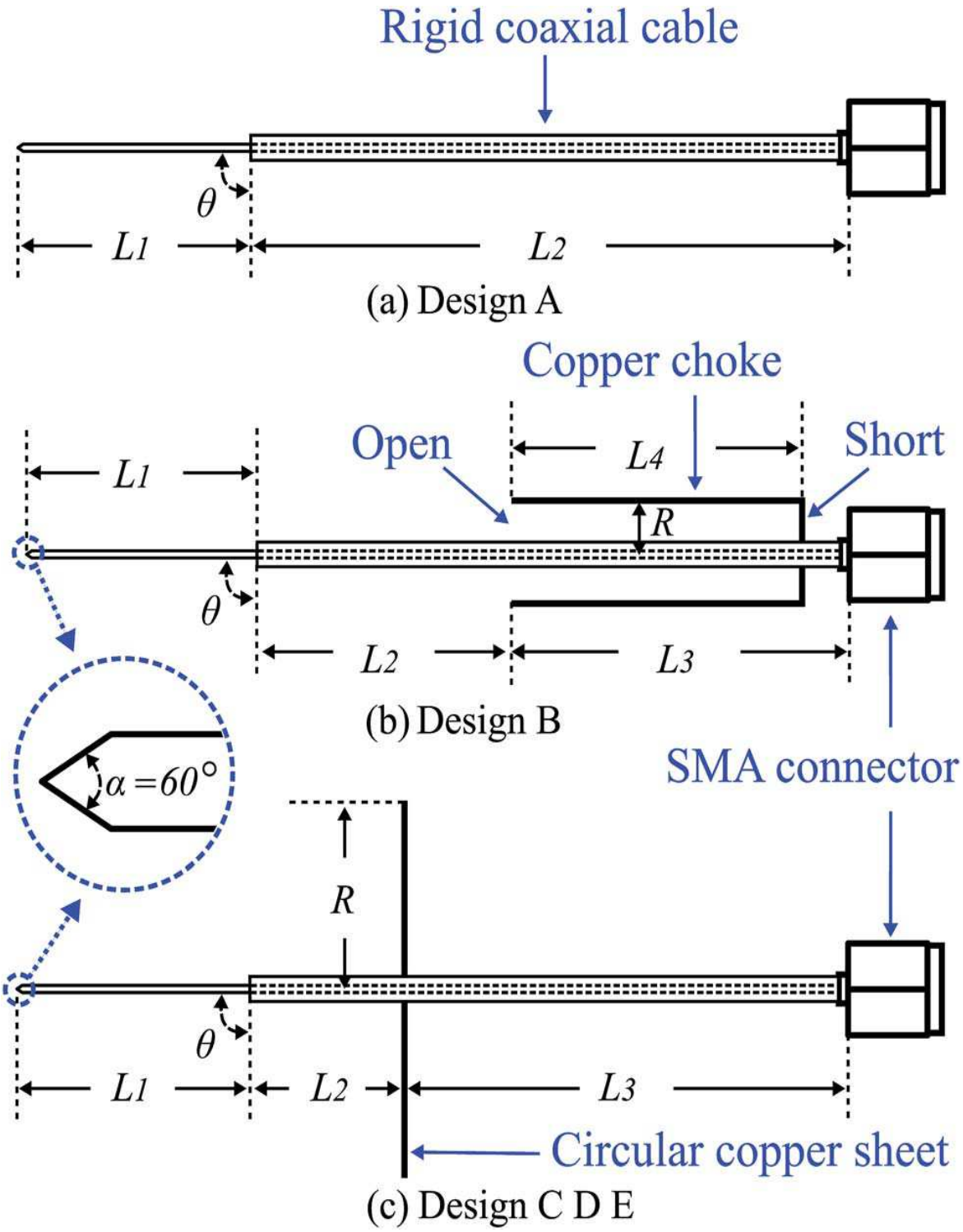

Figure 16: NFA configurations: (a) reference NFA design A (b) NFA with quarter-wave choke (design B) and (c) NFAs with ground plane (designs C, D and E).

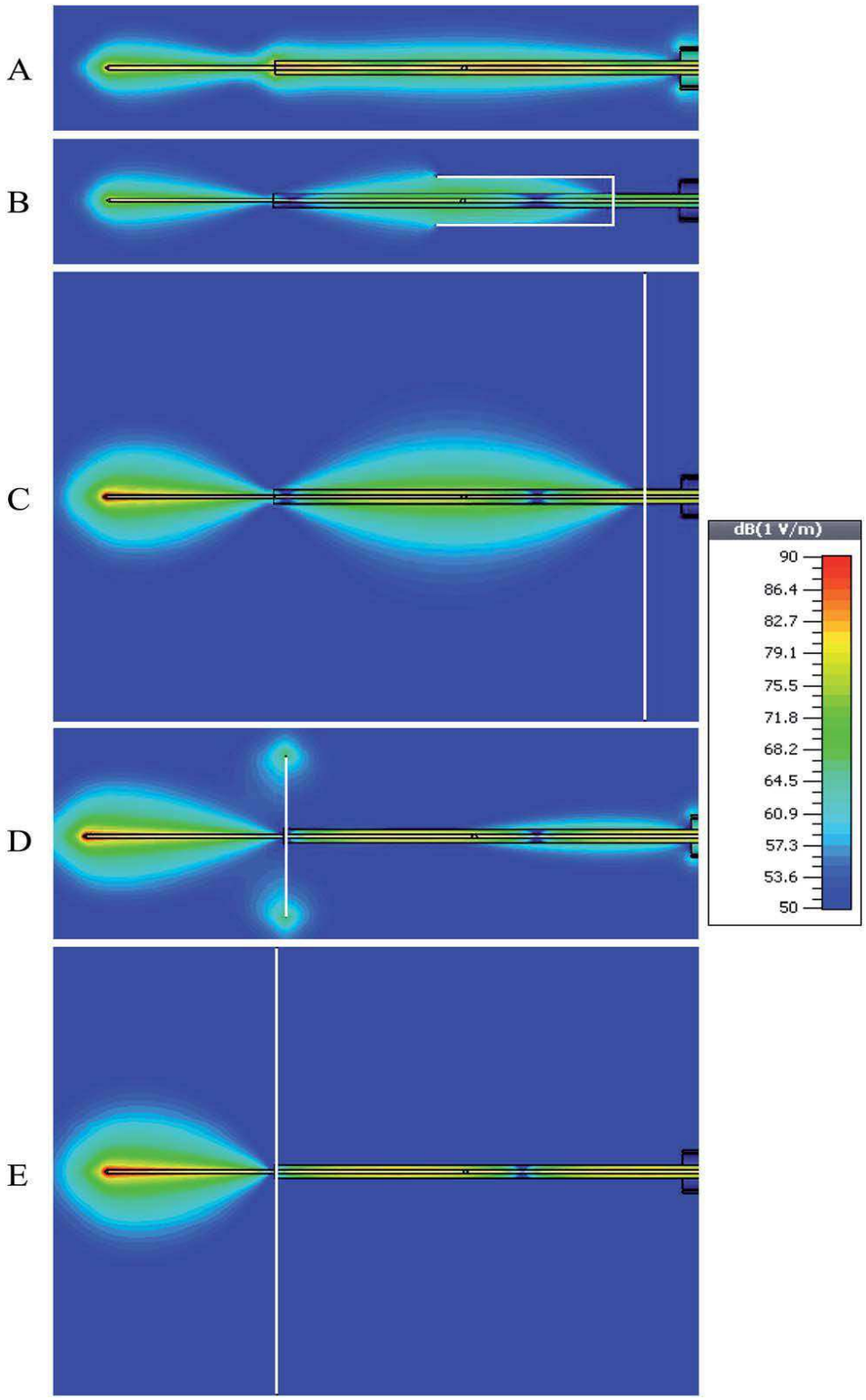

Figure 17: NFA electric field magnitude distribution at 2.45 GHz: (A) reference NFA A, (B) NFA B with a quarter-wave choke, (C) NFA C with a large ground plane (R ¼ 42.5 mm) close to the SMA connector, (D) NFA D with a small ground plane (R ¼ 15 mm) and (E) NFA E with a large ground plane (R ¼ 42.5 mm) close to the start of the rod conductor.

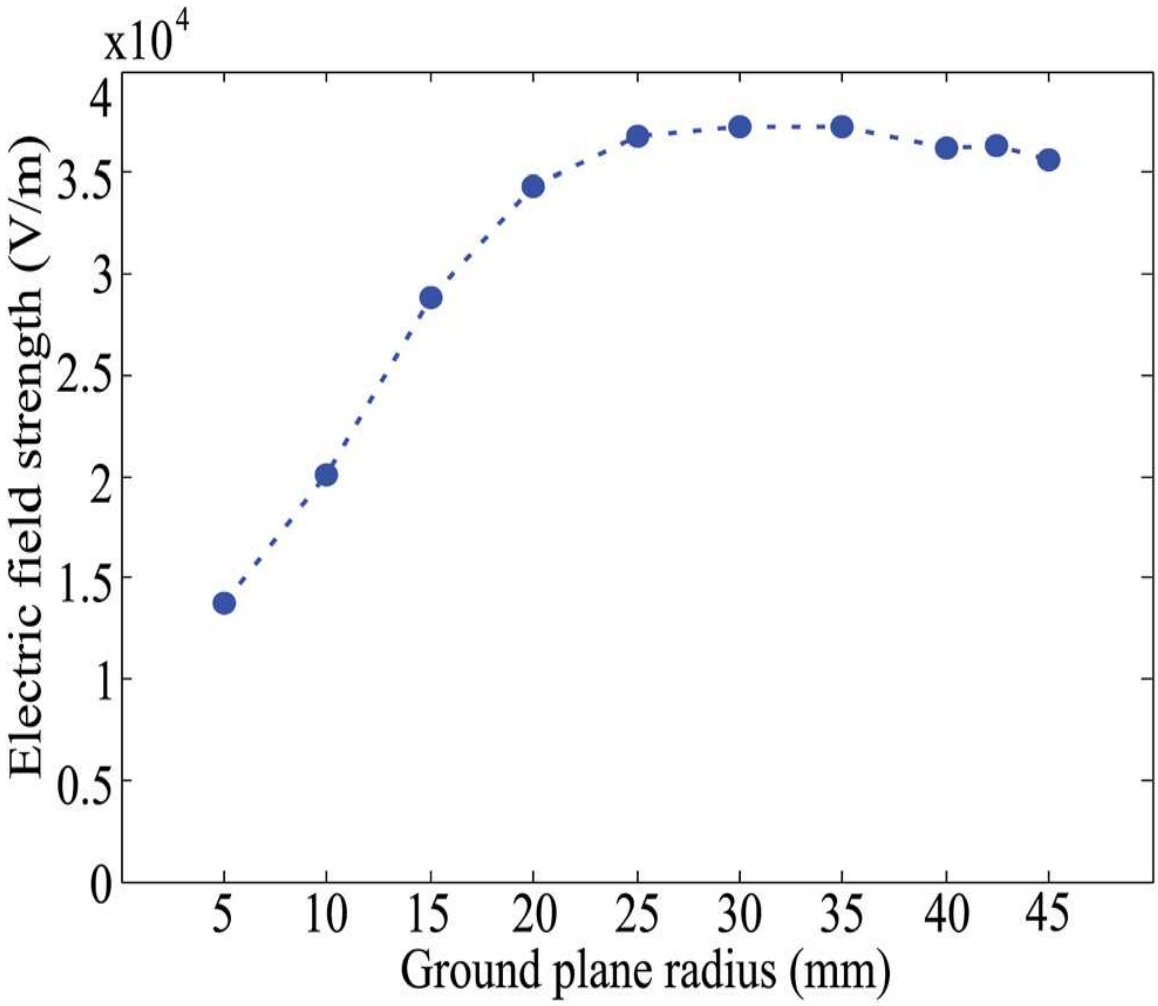

Figure 18: Simulated electric field strength near the tip of the NFA as a function of the ground plane radius.

NFA Design	L_1(mm)	L_2(mm)	L_3(mm)	L_4(mm)	R (mm)
A	28	68.5	----	---	---
B	27.5	30.5	38	30	1.6
C	28	61	7.5	---	42.5
D	33	0	68.5	---	15
E	28	0	68.5	---	42.5

Table 2: Dimensions of the NFA designs under investigation. The configuration of reference A is shown in Fig. 16 (a), whereas design B refers to Fig. 16 (b), and the parametrized geometry of designs C, D and E is shown in Fig. 16 (c).

difference is that they are designed for operation in the near-field through maximization of field strength at the end of the tip. Compared with a NFA such as design A without an added choke or ground structure, these devices offer higher predictability in design as well as enhanced system performance and stability, as it will be seen in the later sections of this chapter. On the one hand, the choke and ground plane enhance performance predictability as they act as an electrical isolation between the antenna and the physical objects behind it, thus suppressing return RF currents on the outside of the coaxial cable.

More importantly, on the other hand, the electric field strength near the tip of the applicator increases owing to the ground plane, according to the image theory[94]. Due to the importance of the ground plane size, NFAs D and E are designed to have different ground plane sizes while varying the position of the ground plane between NFAs C and E provides additional information in the investigation. The proposed NFAs are designed and simulated using CST where the time-domain full-wave solver based on a finite integration of Maxwell's equations is used [92]. A 3D NFA model with realistic electrical characteristics for the materials involved was constructed, and a finite free-space computational domain truncated by perfectly-matched absorbers was considered.

The behavior of the structure under microwave excitation of the coaxial cable was then calculated, and the device characteristics including a reflection coefficient, electric field strength, efficiency and radiation patterns can be obtained from the simulation results. For the present application, the critical parameters under investigation are the surface current density on the coaxial outside conductor behind the ground plane, reflection coefficient and electric field strength around the NFA tip. The length of the NFA conductor L1, as shown in Fig. 16, determines the resonance/operation frequency and is approximately a quarter of the wavelength at the operation frequency of the microwave source. For design B, L4 and L2 are also nearly a quarter of the wavelength which forms a very high impedance on the coaxial outer conductor near the choke open end, thus suppressing return RF currents. The longitudinal position L2 of the circular ground plane for designs D and E is zero since both resonate at the fundamental mode. For C, L2 is approximately twice the length L1, as it operates in its third order resonant mode in which its stripped conductor

and coaxial cable outer shell act together as an additional radiator. The length L3 is not a critical parameter, since it is behind the ground plane and thus does not affect markedly the NFA performance. In all cases, the conductor tip was tapered with an angle $\alpha=60^{o}$ which offers a compromise between high electric field strength and acceptable durability of the tip during operation. The conductor bending angle Θ in all the NFAs is set to be 90^{o} as this allows simple design and an easier comparison. However, it is noted that the designs can be adapted to other angles to fit specific system configurations and requirements.

From theoretical expectations, to minimize return currents and radiation towards the back of the ground plane, the ground plane radius R should be made as large as possible. This is confirmed by a parametric study of applicators with different ground plane sizes. As shown in Fig. 18, the simulated electrical field strength at a point 0.2 mm away from the NFA tip rises when the ground plane size increases, and it stabilizes (with minor variations) with a ground plane radius of around 30 mm. Nevertheless, the feasible size is limited by the available system space. For present system, R = 42.5 mm is the maximum feasible ground plane radius.

From the simulation results, as expected, it is found that the surface current density on the coaxial outer conductor behind the choke or the ground plane is very small for NFAs B to E. This indicates that exterior electromagnetic coupling to objects in this region will not be insignificantly altering the operation of the devices. This also confirms that in these cases, removing the objects behind the ground plane, even if electrically connected or close to the coaxial cable, is a valid modeling simplification. In contrast, to achieve a more accurate simulation result, influence of the objects in proximity to the NFA tip such as the sample under test, should be included in the simulation. This issue will be discussed in the following section in conjunction with the considerations on the rejection coefficient.

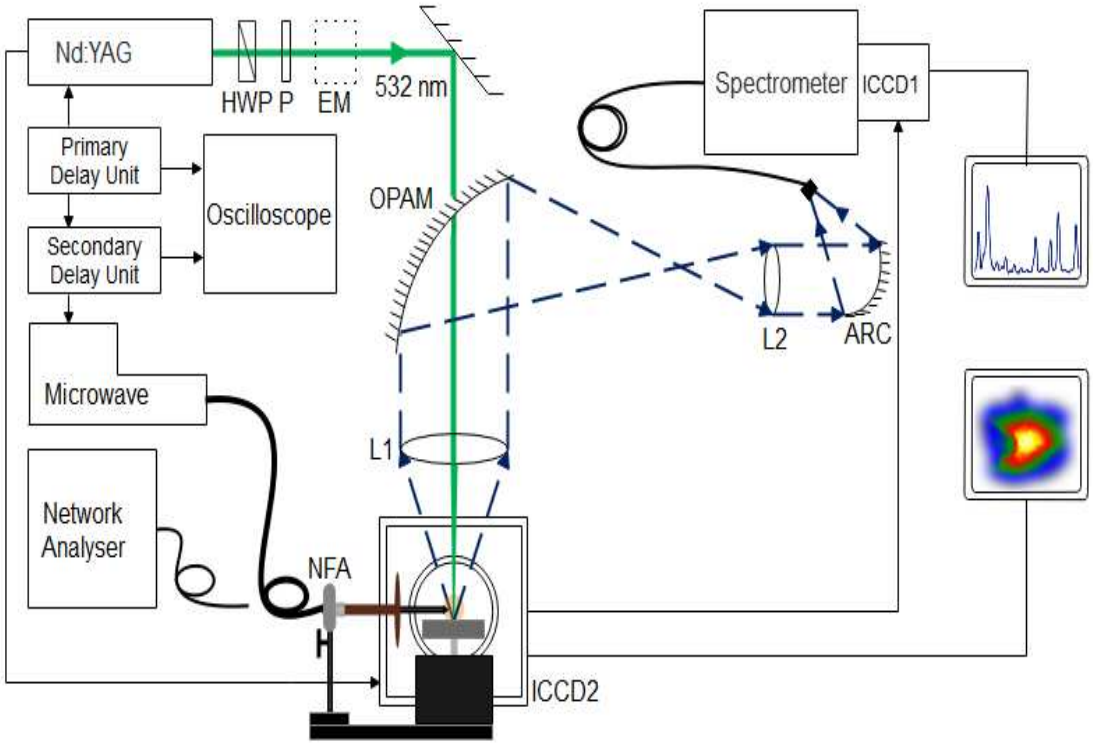

Figure 19 (a): Schematic of the experimental setup. ARC, achromatic reflective coupler; OAPM, off-axis parabolic mirror; HWP, half-wave plate; P, polarizer; EM, energy meter; an additional imaging channel is facilitated by using a second intensifier camera (ICCD2).

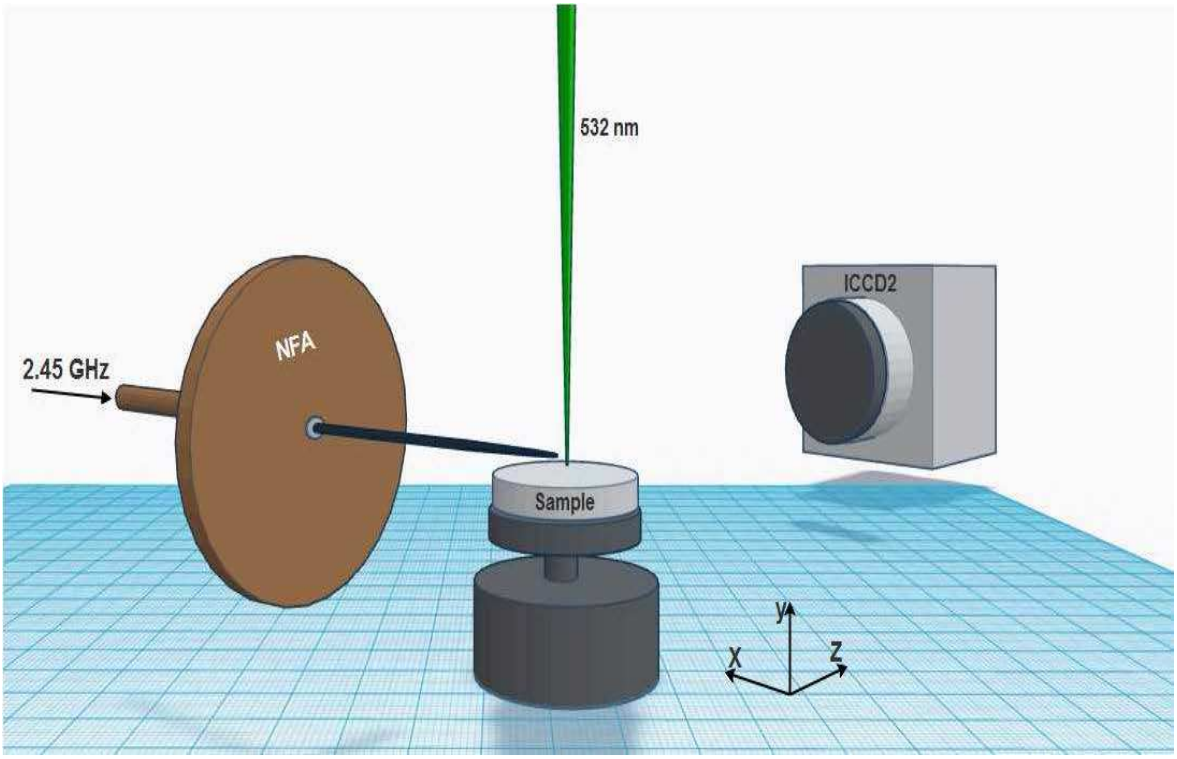

Figure 19 (b): Presentation of the relative position of the NFA, sample, the laser and imaging Camera (ICCD2)

4.3 Experimental

Experimental setup of MW-LIBS is demonstrated in the fig. 19 (a), which is almost the same as described in chapter 3, except a few minor experimental changes. Laser, microwave, spectrometric and imagining detections are same. However, in contrast to the chapter 3,

the imaging of whole plasma was carried out in conjunction with spectroscopy of copper. Imaging camera which is named as (ICCD2 Andor, iStar) was fixed with a macro lens (f = 90 mm, Tamron). A long pass filter was used instead of a narrow band filter to suppress the laser scattering at 532 nm. The filter has a transmission of 93.5% in the range from 600 to 800 nm. Relative position of NFA with respect to laser, solid sample and imaging camera is presented in fig. 19(b). Network analyzer shown in fig. 19 (a) was used to measure the reflection coefficient for all geometrical configurations of NFAs under various conditions, as explained in 4.4.1.1.

4.3.1 NFA Measurement

The reflection coefficient, denoted as |S11|, is one of the most important parameters for microwave devices, as it provides information on the accepted input power by the device in frequency domain [94] for example in the present case the NFA. Therefore, at the beginning of the experiment, the reflection coefficients of the five NFAs were measured using a network analyzer (Agilent FieldFox N9916A). The measurements were performed in situ in the LIBS test system, both with and without a sample in proximity. Then the measured reflection coefficients in the frequency range of interest can be compared with the simulated one.

4.4 Result and Discussion

4.4.1 NFA Characteristics

4.4.1.1 Reflection Coefficient

For efficient microwave coupling, it is critical to minimize the microwave reflected power. The reflection coefficient |S11| resulting from electromagnetic simulations in all five NFA geometries are displayed in Fig. 20 and are compared with the measurement results. A reasonable agreement in terms of resonance frequency (indicated by the minimum of |S11|) is observed between simulations and the measurements. To define the NFA

operational bandwidth, we consider the frequency ranges where the reflection coefficient |S11| remains below -10 dB, indicating that more than 90% input power is accepted by the NFA [94]. According to the results of measurements without LIBS samples, NFAs B, C, D and E have an operational bandwidth of 2.38 to 2.52, 2.35 to 2.65, 2.26 to 2.72, and 2.33 to 2.52 GHz, respectively. All of these frequency ranges contain the targeted microwave power source frequency of 2.45 GHz. In contrast, design A exhibits a -5.6 dB simulated reflection coefficient which indicates that its input power acceptance is only around 72.5%. In this case additionally, the rather poor qualitative agreement with simulation can be ascribed to the unpredictable coupling of return currents on the coaxial cable. For all cases, the best overall matching, i.e. the lowest reflection coefficient at the desired resonance frequency of 2.45 GHz, is achieved with NFA C. However, the bandwidth of operation, i.e. the range of acceptable frequency variations due to environmental changes, will be reduced in this case.

The oscillations observed in the measured data are due to reflections from the walls of the LIBS system enclosure, which provide shielding from the environment and are moderately absorbing. Considering now the more practical case where a sample is introduced at a distance of only approximately 0.2 mm from the NFA, a noticeable shift towards lower frequencies is observed in the measured resonance frequencies, with variations from tens to a few hundred MHz for all NFAs. The frequency shift is attributed to the NFA impedance variation induced by the samples in proximity. This demonstrates the importance of considering at design time the impact on the NFA due to the proximity of objects such as LIBS samples.

This critical factor can be taken into account by including these objects in the simulation and testing the robustness of the design across a realistic range of material electrical properties. For the case at hand with a copper sample, the reflection coefficients at 2.45 GHz, are -3.5, -6.7, -7.7, -8.7 and -7.9 dB, which correspond to an accepted input power level of 55.3, 78.6, 83.0, 86.5 and 83.8% for NFA A to E, respectively. As a result, these NFAs are still expected to operate as efficient applicators. However, this will be confirmed

through experiments, although it is noted that the overall NFA performance can be further improved if specifically designed for predefined test configurations.

4.4.1.2 Electrical Field Strength

Another indicator of the coupling power level of a NFA to the laser-induced plasma is the electric field strength around the conductor tip of NFA. This information can be computed and exported from the simulation tool. The distributions of simulated electrical field strength (V m^{-1}) around all NFA tips are displayed in the five plots on the first row of Fig. 21, with the x- and y-axes showing total spatial dimensions of 3mm x 3 mm. As illustrated by these simulation results, the highest electrical field strength is observed the closest to the tip, which suggests that the distance between the NFA and sample should be kept as small as possible to permit high microwave power coupling. However, this is usually limited by the system setup and the sample surface roughness.

The NFAs C, D and E exhibit a comparatively high electrical field strength compared to designs A and B. Which means that, in free space, these three designs are expected to produce high microwave coupling performance to the laser-induced plasma. The minor advantage of design E under ideal conditions is due to the large ground plane (compared to D) and operation at fundamental resonance (compared to C).

Nevertheless, the experimental results shown in the following indicate a slightly better performance of D, as compared to E for the available LIBS system, which might be explained by small experimental uncertainties (e.g. sharpness of the tip and/or distance between the sample and the NFA) and minor differences in spatial field distribution, which may affect the matching of the local field strength to electron density in the plasma and demonstrates the significance of considering the environmental impacts on the design of a particular NFA.

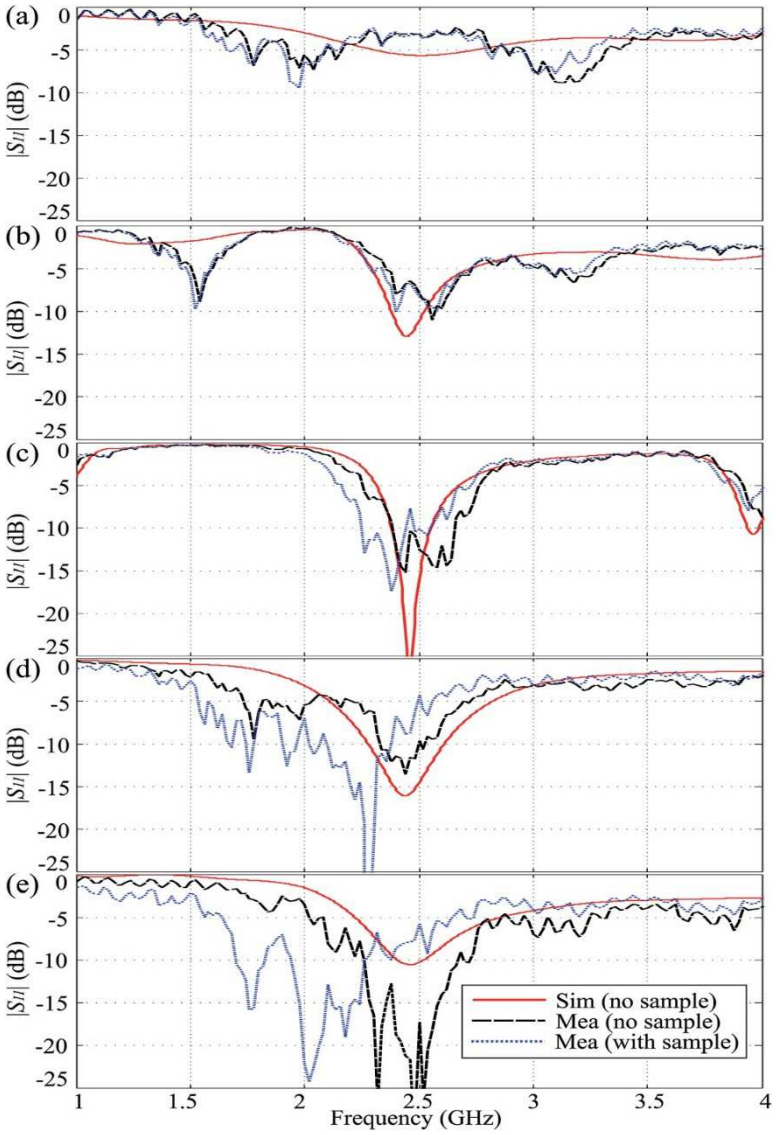

Figure 20: Simulated and measured reflection coefficients |S11| of: (a)design A, (b) design B, (c) design C, (d) design D and (e) design E.

4.4.2 NFA Performance

4.4.2.1 Plasma Dimensions

To investigate the LIBS signal quality with and without the microwave coupling, it is essential to use a sample with low concentration of analyte. However, the concentration cannot be too low as it is also necessary to detect LIBS signals before using microwave power to establish a reference point. It was found that when using an unspecified mineral ore sample from a lead processing plant, a small amount of copper was detectable without any microwave injection.

Therefore, copper was selected as the analyte for this investigation. The mineral ore solid sample was mixed with a binder and placed into a plastic disc having depth of 3.4 mm and diameter of 21 mm. It is worth mentioning that since the laser beam is not focused onto the NFA tip, there will be no induced plasma from the NFA surface.

The dependence of the MW-LIBS signal on copper concentration in solid samples using NFA, having same rod material has also been studied previously[86]. A linear dependence was observed confirming that the interference from the copper in the NFA tip is negligible. The performance of the five NFA designs was investigated firstly using four microwave powers ranging from 0 to 1.2 kW, while laser pulse energy, gate delay and gate width were kept constant. The plasma emission was recorded by ICCD 2 (imaging camera) and the spectrometer concurrently. The averaged plasma images obtained from 100 single shots at the microwave power of 0 kW (laser plasma only) and 1.2 kW are displayed in the second row of plots in Fig. 21. The laser focusing point is positioned at the origin of the scale. The laser energy per pulse and microwave power were fixed at 2.6 mJ/pulse and 1.2 kW, respectively. These plots clearly demonstrate that for a given microwave power, variations in spectral and image intensities can be observed for different geometrical designs of NFA.

The leftmost plot in Fig. 21 also shows the laser-induced plasma recorded when the microwave was off; hence the recorded signal intensity is multiplied by a factor of 100 in this case so that all the recorded images can be visualized using a single-color map. The length and the width of laser-generated plasma is approximately 1.7 and 1 mm, respectively. The dotted red ellipse shown in Fig. 21(a1)–(e1) illustrates the relative location and size of the laser-generated plasma with respect to the tip of the NFA.

It is noted that in these images, a part of the imaged microwave assisted plasma is overlapped with the tip where the strongest electrical field is formed. As the laser induced plasma electron density must be below the threshold of approximately 7 x10^{10} (cm^{-3})[80], to interact with the injected microwave power. As a result, the strength of the electrical field at the overlap location is critical in the microwave-assisted LIBS operation. Hence a matching of the electrical field strength with the local plasma electron density must be established for an efficient microwave injection. Fig. 21(a2) shows that the microwave-enhanced plasma is sustained near the reference NFA tip, at (0, 1.2) location.

Fig. 21 (b2) and (c2) show an increase in the plasma volume and intensity, indicating a more efficient microwave injection than the reference design in Fig. 21(a2). We note that it is still possible to see the tip of the NFA in Fig. 21 (b2) and (c2). The plasma shown in Fig. 21 (d2) and (e2) is further significantly enhanced in terms of intensity and volume, and as a result, in contrast to the previous cases, the NFA tip is no longer visible in these two plots: the plasma volume has grown large and appears to be covering the NFA.

The images outlined in Fig. 21 suggest that the biggest plasma volume was obtained with NFA designs D and E whereas the reference NFA delivers the smallest plasma enhancement even at the highest microwave power. To investigate the life-time of the microwave-enhanced plasma, time-resolved imaging was applied. Plasma images were recorded for the five NFA designs, at different gate-delay times such as 1, 250 and 500 μs, while keeping the gate-width and the microwave power fixed at 200 μs and 1.2 kW, respectively. The results are plotted in Fig. 28, and at the three gate-delay times, it is clear that the microwave-enhanced plasma is larger and stronger for designs C, D and E as compared to designs A and B. It is also clear that the plasma is sustained for a reasonably long time of

500 µs. It is interesting to note that although the intensity of microwave enhanced plasma decreases as the gate-delay increases, the recorded plasma cross section appears constant, for designs C to E. Based on the measured cross section, designs D and E produce a well-sustained plasma for a reasonably longer time.

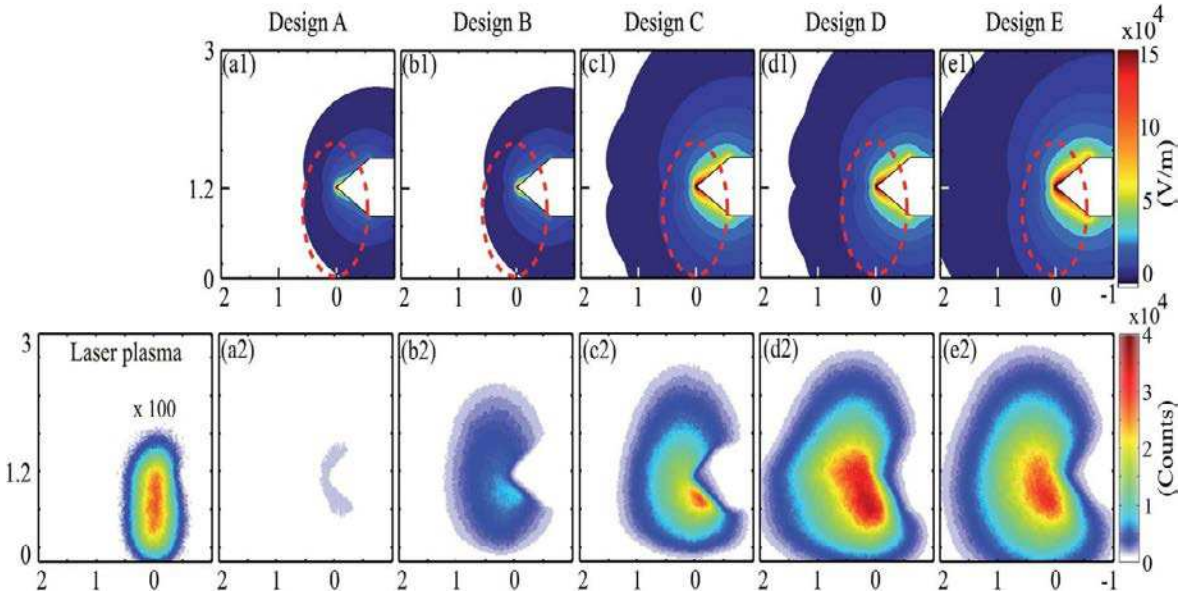

Figure 21: Electric field strength (the first row) and enhanced plasma images (the second row) of the five NFAs proposed, with the laser focusing point and the applicator tip located at the origin and (0, 1.2) in the map (3 mm x 3 mm), respectively. These are two-dimensional plasma images, averaged for 100 laser shots are recorded by ICCD2 for a copper bearing mineral ore solid sample. The laser energy was 2.6 mJ/pulse. The microwave power and pulse duration were 1.2 kW and 800 µs (after the laser pulse), respectively. The camera gate-width was 800 µs. Please note that the intensity of the laser-induced plasma image shown on the leftmost plot of the second row is multiplied by a factor of 100 for better visibility. The dotted red line in the first row indicates the spatial location of the laser-induced plasma.

4.4.2.2 **Spectroscopic Detection**

Spectral intensities of copper transitions in microwave-assisted laser-ablated plasma for the mentioned solid mineral sample have also been recorded to further describe the performance of the NFA in operation. Microwave-assisted LIBS spectra in the range from 324 to 328 nm were recorded at four microwave power levels, using the four designed NFAs. In all cases, the copper transitions at 324.754 and 327.395 nm are clearly resolved. Microwave power was controlled through secondary delay unit; the laser energy and gate-width were maintained at 2.6 mJ/pulse and 800 µs. Again, 100 single laser shots were recorded at each microwave power, which were then averaged and plotted separately for each NFA design, as shown in Fig. 23 as three assorted colors curves. The figure demonstrates that, as expected, for all the NFAs studied, the intensity of copper spectra is increasing with a rise in microwave power. While analyzing this figure vertically, it is found that for a given microwave power (i.e. a given color or curves), spectral intensities seem to increase from an order of A, B, C, E and D, which is consistent with the plasma intensity image shown in Fig. 21. From the clear qualitative interpretation of the spectral intensities in Fig. 23, it can be stated that designs D and E clearly performed better than the other 3 designs. This will be investigated quantitatively in the next paragraph.

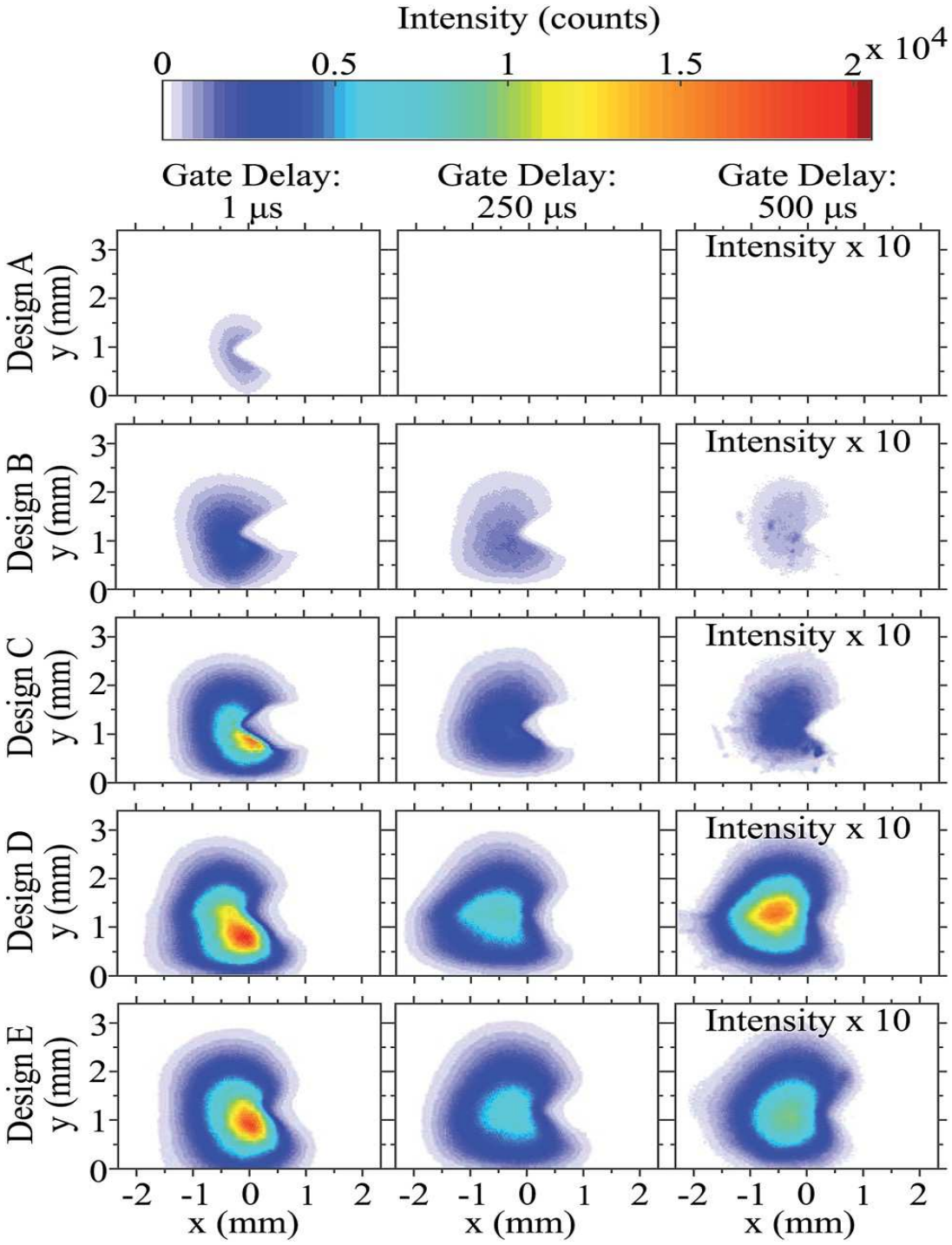

Figure 22: Microwave-enhanced plasma intensity of the five NFAs recorded with different gate delays of 1, 250 and 500 µs. The gate-width and the microwave power were fixed at 200 µs and 1.2 kW, respectively. The results for 500 µs gate delay have been multiplied by a factor of 10 to get a better visualization.

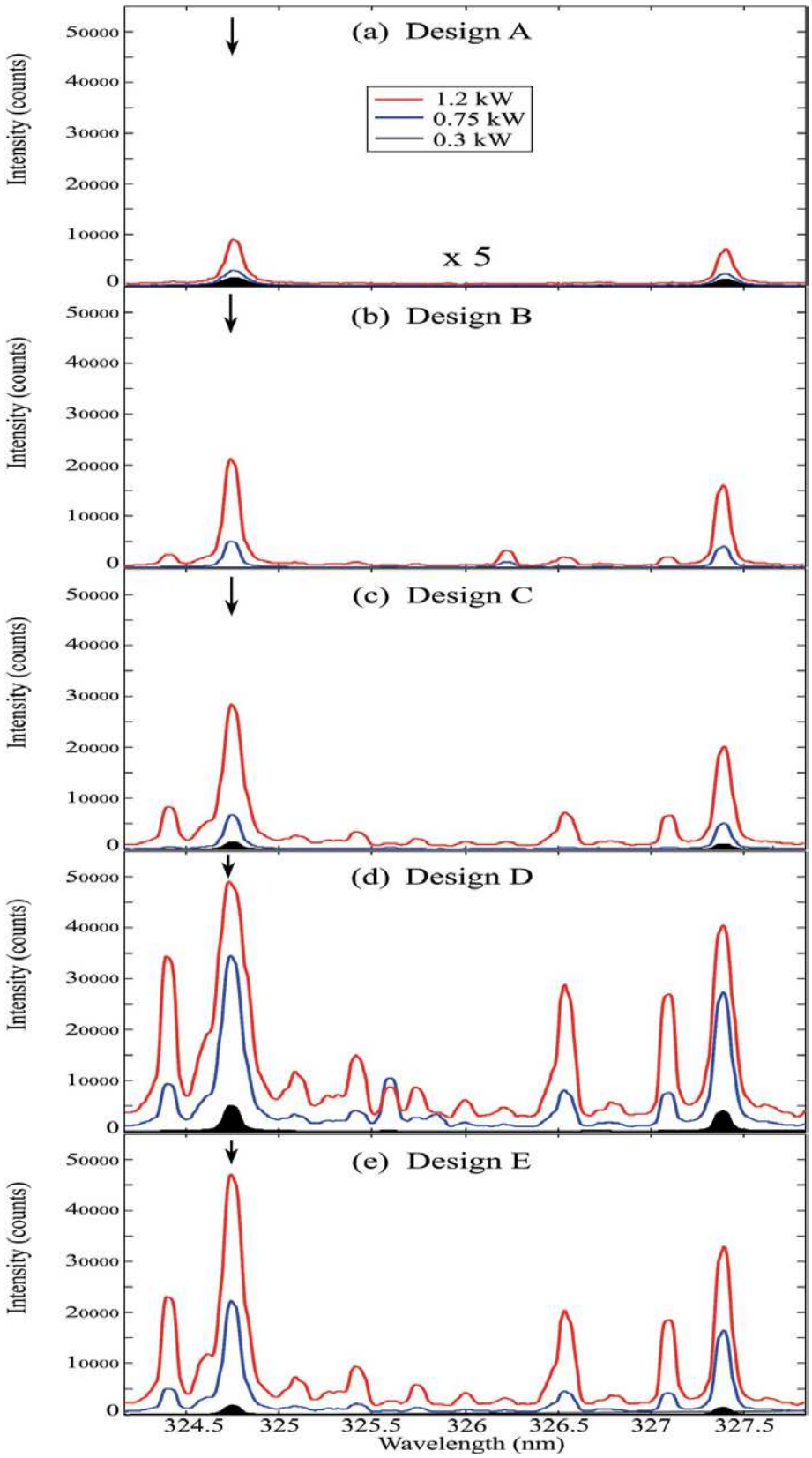

Figure 23: Microwave-assisted LIBS spectra of a copper bearing mineral ore solid sample, averaged for 100 laser shots and recorded using three microwave powers of 0.3, 0.75 and 1.2 kW. The laser energy, the gate-width were 2.6 mJ/pulse and 800 µs respectively. Two copper lines are clearly seen at 327.395 and 324.754 nm.

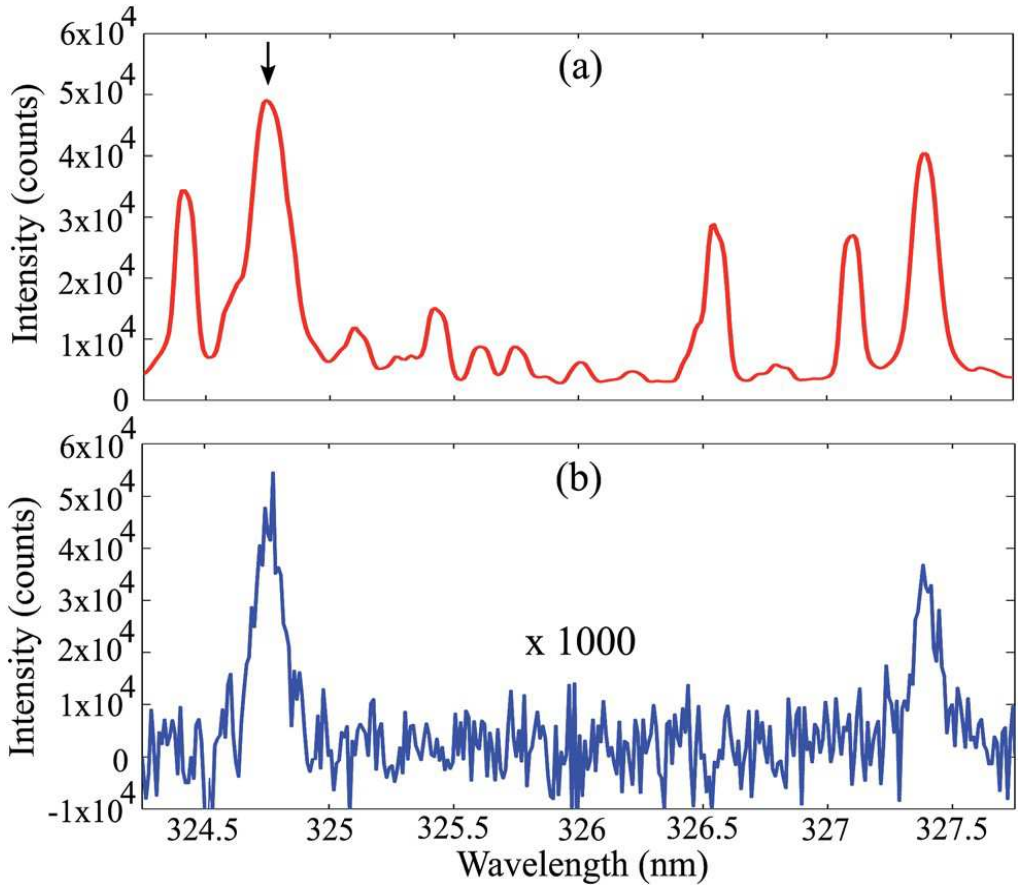

Figure 24: Spectra of (a) design D with 1.2 kW microwave power, (b) design D without microwave power (multiplied by a factor of 1000).

4.4.2.3 Signal Enhancement and SNR Improvement

Fig. 24 shows the LIBS spectra of the copper-bearing sample without and with assistance of 1.2 kW microwave power injected with the NFA design D. To interpret this figure quantitatively, we can define the signal strength for a particular line as the maximum intensity at the line center minus the baseline signal. In the present case, the signal at the 327.395 nm transition is specifically chosen as an indicator of the NFA performance. Using the obtained signal strengths in Fig. 24 for the considered transition, we can then define

the signal enhancement as the ratio between the signal with and without assistance of microwave power. This yields a critical measure to evaluate the absolute system sensitivity improvement with an injection of microwave power.

A complete characterization has been performed through measurement of all five NFAs. Design D has achieved the best performance (and is thus shown in Fig. 24), with the exceptionally high signal enhancement of 849 times. It was noted that, however, increasing the microwave power is accompanied by a simultaneous increase of noise floor, as illustrated in Fig. 25 (a) and (b), where the noise level (counts) and signal enhancement for design D are depicted as a function of microwave power.

The error bars indicate the standard deviations from 100 averaged shots. On that basis, we conclude that another relevant performance measure should be considered as well, namely the SNR improvement rising with microwave power assistance. From the plots of Fig. 25, we observe that the noise, signal enhancement and SNR improvement are clearly increasing with microwave power, and that the SNR can reach a maximum improvement by a factor of 76 when injecting 1.2 kW microwave power with the design D.

The signal enhancement and SNR improvement for all five NFAs with 1.2 kW microwave power is plotted in Fig. 26. As mentioned, the design D achieves the highest signal enhancement and SNR improvement of around 849 and 76, respectively, whereas the lowest ones are held by the reference NFA design A. It is worth mentioning that with a simple electromagnetic isolation technique such as added partial ground plane, design D can enhance the signal by more than 9 times, further than the previously reported very high signal enhancement of 93.27[86].

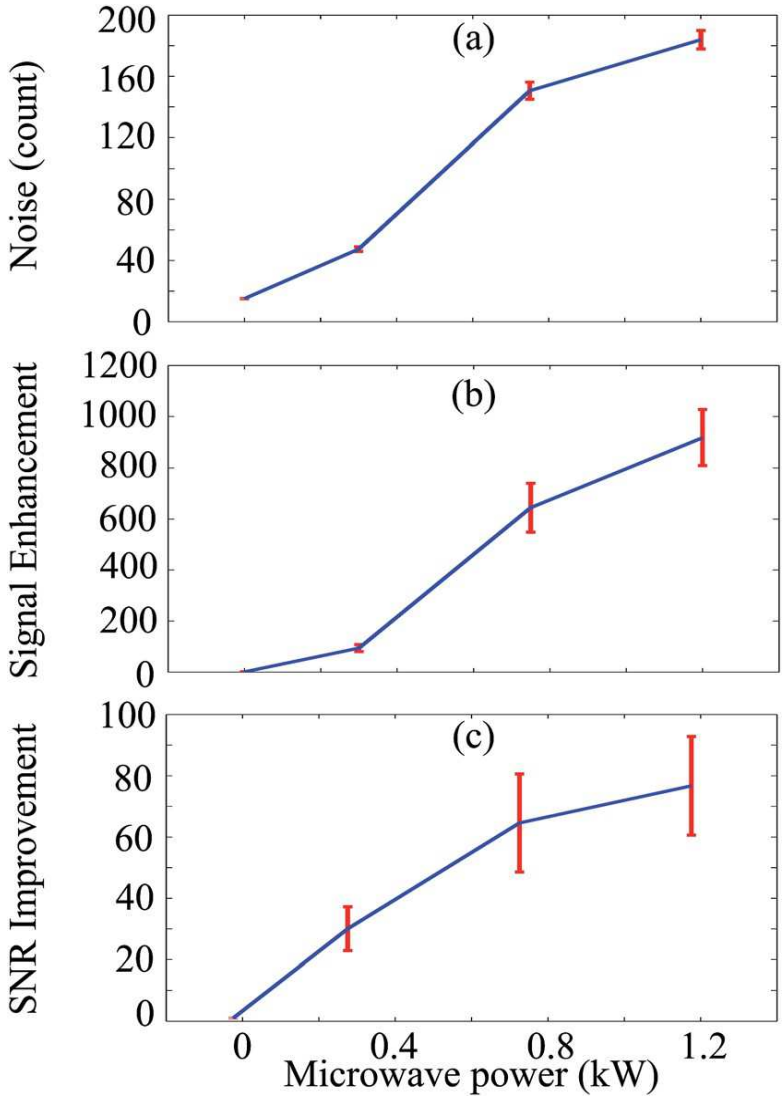

Figure 25:The (a) noise level (counts), (b) signal enhancement and (c) SNR improvement of design D at microwave power of 0, 0.3, 0.75 and 1.2 kW for copper line at 324.754 nm obtained from the spectra. Error bars are standard deviations from 100 shots.

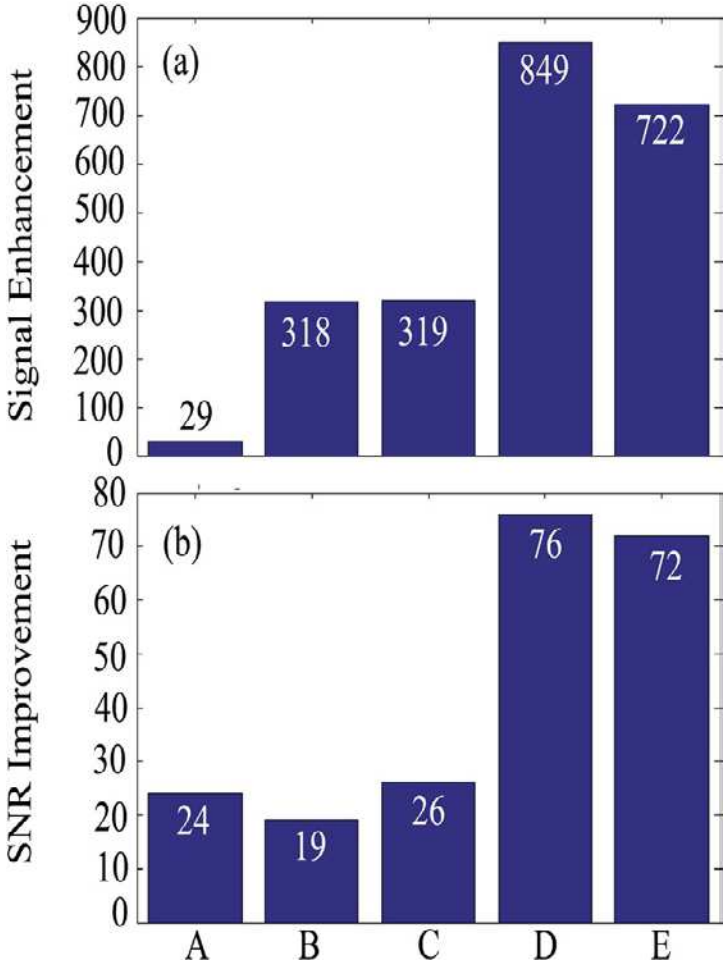

Figure 26: The signal enhancement (a) and SNR improvement (b) of the five NFAs at a microwave power of 1.2 kW for copper line at 324.754 nm obtained from the spectra.

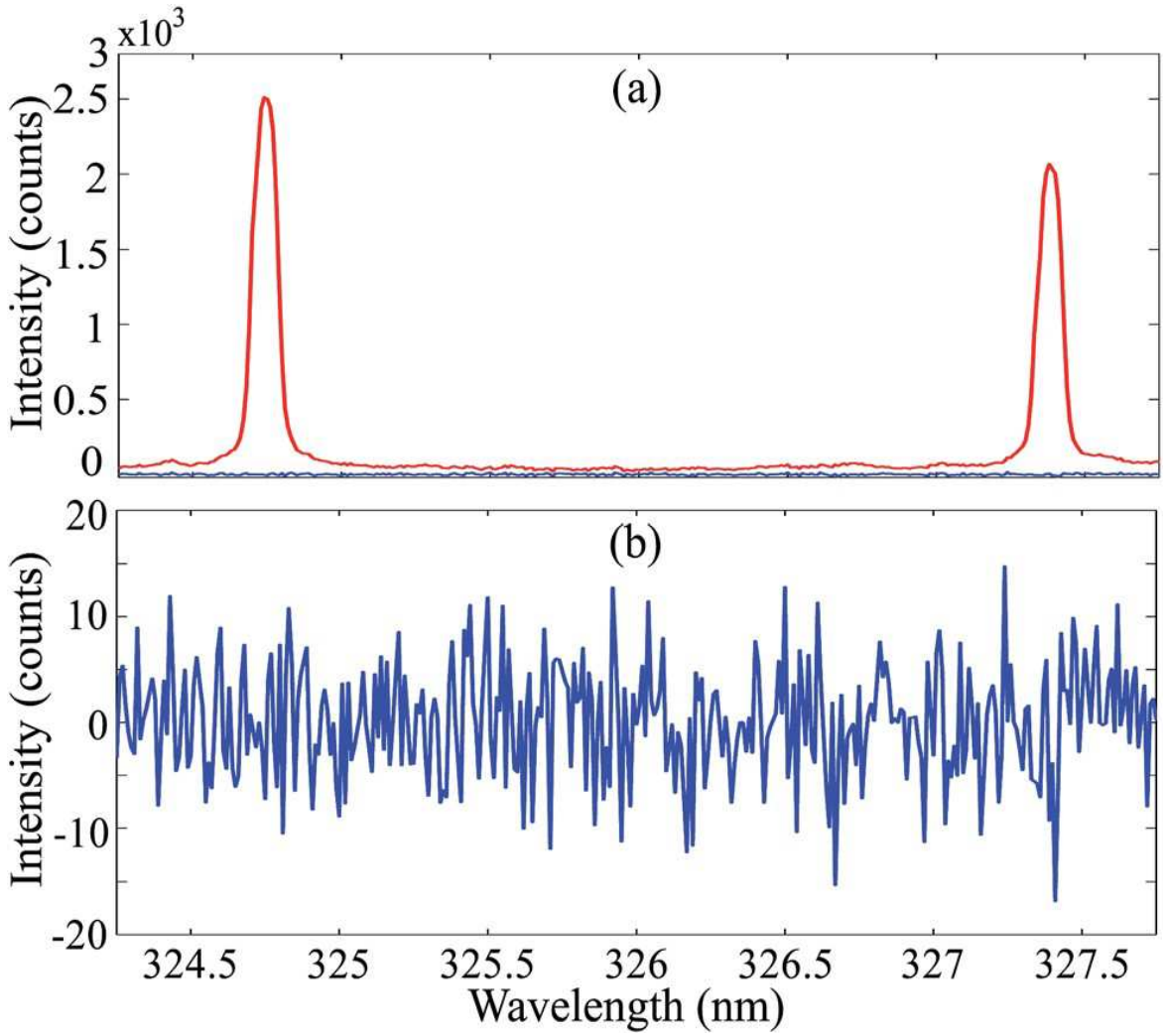

Figure 27: The LIBS spectra of a certified ore sample with copper element of 3.38 ppm without and with 0.57 kW microwave power. (a) Comparison of these two cases where the blue and the red curve correspond to the signal intensity with 0 kW and 1.2 kW microwave power, respectively. (b) Replotted signal intensity for 0 kW microwave power on a magnified scale.

4.4.2.4 Demonstration of the Detection Sensitivity

The ability of elemental detection at low concentration was tested using the best performing NFA, namely design D. A reference material OREAS 122 (Ore Research and Exploration) was used for this purpose[95]. OREAS 122 is a certified reference material containing uniform low-concentration of copper, among many other elements, at 3.38 parts per million (ppm). For the analytical detection, the powder sample was mixed with distilled water to produce a thick slurry, which was transferred into the cylindrical sample holder with a 21-mm diameter. A uniform solid surface was achieved by pressing these discs and drying them at 51^{o}C. Fig. 27 shows the LIBS spectra recorded near 324 nm with a laser pulse energy of 2 mJ, without and with microwave power. The LIBS spectra recorded without microwave power (Fig. 27b) shows no signal of copper at the signature wavelengths of 324.754 nm and 327.395 nm. In contrast, when the microwave power is switched on at 0.57 kW, a very strong signal at 324.754 nm and 327.395 nm are clearly observed. The SNR of the 324.754 nm copper line is calculated to be 166.

4.5 Summary

The enhancement in the performance of LIBS following microwave injection has been demonstrated by optimizing the microwave system for efficient transmission and radiation of supplied microwave power. An efficient microwave system can reduce the microwave power requirement without compromising the achieved improvement in LIBS. Hence low microwave power requirement in MW-LIBS along-with less laser power requirement can eventually take MW-LIBS system a step ahead towards development of the compact and portable commercial devices for the remote and field detections. Microwave antenna named as near field applicator (NFA) being one of the main components of the antenna coupled MW-LIBS system, can improve the performance of the entire system by efficiently transmitting and radiating the supplied microwave power. Considering the importance of

NFA to achieve better performance for same microwave power, four designs of NFAs were developed based on full-wave electromagnetic simulations and were experimentally investigated with respect to a reference design. Compared with the reference device, these four NFAs take into account critical factors such as the influence of the electromagnetic environment and the reflection coefficient, with the aim to maximize the electric field strength at the location of the plasma and predictably enhancing the results. The experimental results, including NFA reflection coefficients, plasma imaging and spectroscopy, show that NFAs designed in a systematic way leads to a significant improvement in the overall system performance, with very good stability and repeatability as observed during our measurement operation. The best SNR enhancement was achieved with the design having a 30-mm diameter ground plane located close to the rod conductor (design D), which leads to a 849-fold signal enhancement and a 76-fold SNR improvement at 1.2 kW microwave power, respectively, compared to measurements without microwave assistance. This is, to the author's best knowledge, the highest reported SNR in the literature. To illustrate the enhanced system performance, a very strong copper spectral line was recorded with a SNR of 166 for a microwave power of 0.57 kW on a certified ore sample with uniformly distributed copper elements of a very low concentration of 3.38 ppm. Such a high level of SNR suggests that a detection limit in the sub-ppb range can become a real possibility.

Chapter 5 Conclusion

This research was aimed to improve the analytical capabilities of LIBS for quick, in-situ, remote analytical measurements such as trace metal detection in many applications such as mining, agriculture and environmental monitoring. LIBS being the contactless, quick and multi-elemental detection technique has the potential to meet the desired analytical requirements in numerous applications, if signal quality, sensitivity, signal to noise ratio and limit of detection is improved. Inducing microwave radiation in the LIBS plasma can noticeably improve the mentioned analytical features of LIBS. However, further optimization of the microwave-assisted LIBS system is required to match the desired performance. In this research optimization of MW-LIBS system has been suggested by two separate approaches such as emission detection by narrow band-width elemental imaging for quantification and efficient injection of microwave radiation by well-designed NFA. It is believed that plasma emission is reduced when it travels through the spectroscopic components. While studies have shown that all emission from plasma cannot be captured by spectrometer due to increased plasma volume and dimensions, following the enhancement by microwave. Hence sensitivity and performance of MW-LIBS can further be increased by minimizing this signal loss. A custom made narrow bandpass filter coupled with an ICCD camera was used to present a simple yet sensitive, alternative detection channel which has the ability of capturing whole plasma emission, due to its large field of view. To study the quantitative nature of imaging technique, indium in the solid matrix was used for the experimental estimation. Spectroscopic detection was performed in conjunction with the indium elemental imaging to study the improvement in LIBS system. Experimental results demonstrated that an overall improvement of 14-fold as compared to conventional LIBS without microwave enhancement. While narrow band imaging detection technique was 3 times sensitive than spectroscopic detection in MW-LIBS. However, limit of detection of spectroscopic detection was better (16 ppm) than imaging technique

(50ppm) due to unresolved background interference, this issue can be resolved by using better narrowband pass filters or filtering system. As imaging technique cannot offer multi-elemental detection hence, a low resolution spectrometer would still be needed to identify the surrounding matrix. It was also observed that the microwave antenna/NFA based ambient MW-LIBS is highly dependent on the relative position of NFA with respect to solid sample and laser pulse, minor variation can generate highly unpredictable results therefore, sample preparation is required to achieve identical smooth sample surfaces. Extreme care and precise alignment would also be needed while switching between the samples.

The NFA being the vital component of the microwave injection system can influence the performance of the whole microwave system by several means. A well-designed NFA can generate predicable performance consistently by efficiently transmitting the supplied microwave power while reducing the reflection coefficient. It can further improve the enhancement through efficient radiation of the transmitted microwave power by developing localized concentrated electric field at the tip of the NFA conductor, in the close vicinity of laser ablated plasma. Considering the importance of this device, 4 designs of NFAs were simulated in CST studio, accounting the specialties of the available MW-LIBS system. These designs were fabricated and assessed in the MW-LIBS system for detection of Copper in mining sample using the 5^{th} design and reference, the broad plasma imaging was also carried out simultaneously to study the effect of improvement on the plasma dimensions and intensity. Experimental results revealed that Design D with finite ground plane of 30 mm diameter (used for isolation of return power), performed better than the rest and demonstrated a signal enhancement of 849-fold with 76-fold improvement in SNR.

These both optimization techniques have not yet been applied in-conjunction to investigate a collective improvement in analytical capabilities of MW-LIBS. However, it is logical to believe that these improvement techniques can collectively offer considerable improvement in LIBS system following microwave injection, the demonstrated enhancement presents a good possibility of the detections in parts per billion but the

enhancement can be different for various elements due to the different transitions energies.

These novel improvement approaches open many prospects of vital future research involving MW-LIBS. One aspect may involve the collective implementation of these techniques to investigate the improvement in analytical capabilities of MW-LIBS. New design of NFA presents the possibility of detections in sub part per million therefore detection of heavy metals in soil for pollution control or monitoring of nutrients in agriculture lands, can also be investigated by MW-LIBS using new design of NFA. As MW-LIBS offers different enhancement for various elements due to different transition state energies hence future work may also involve the investigation of enhancement for various important elements using these novel improvement techniques. One important inherent limitation of LIBS i.e. matrix effect has not yet been studied using MW-LIBS, this could be an interesting topic for future work as different matrices are believed to influence LIBS signals at the plasma generation stage, due to different ablation threshold energies and laser-material interactions. Enhancement by microwave being a post plasma generation phenomenon, can minimize or eliminate matrix effect specially when these new improvement approaches can impart such a considerable enhancement in MW-LIBS signal. Analytical capabilities of MW-LIBS for aqueous solution has already been demonstrate, hence further investigation of MW-LIBS performance using these detection and enhancement approaches can also be a vital topic for future work, as because real time analysis of water bodies for pollution control and of drinking water for quality control, can also become a very important field for LIBS application. Furthermore, investigation of single element plasma in aqueous samples by narrow bandwidth imaging for temporal elaboration, following microwave enhancement can also be an interesting future work. In addition, use of a cheap low-resolution spectrometer and simple camera without fast gating function for the analytical detection can become an important branch of future research in MW-LIBS, for the development of cost effective portable devices. Implementation of improved narrow bandpass filters to suppress the background

interference for better limit of detection and use of multi-element filtering system for minimizing the need of spectrometer may also be a focus of future work in MW-LIBEI. The good point about the MW-LIBS is that it needs less laser energy such as a few times higher than the ablation threshold which makes MW-LIBS convenient for the portable application as small robust laser source can be used. In addition, this research can contribute to suppress the need of high microwave power without compromising the enhancement. A compact cheap microwave source ~ 0.7 kWatt would be sufficient for many applications. Hence compact laser and microwave source coupled with simple and robust plasma detection based on single elemental imaging, can make a perfect combination for a robust, light weight commercial analytical device based on MW-LIBS.

Chapter 6 Reference

[1] D. DI´AZ, D.W. HAHN, A. MOLINA, Evaluation of Laser-Induced Breakdown Spectroscopy (LIBS) as a Measurement Technique for Evaluation of Total Elemental
Concentration in Soils, APPLIED SPECTROSCOPY, 66 (2012).
[2] N. Khajehzadeh, T.K. Kauppinen, Fast mineral identification using elemental LIBS technique., ScienceDirect-IFAC-PapersOnLine, (2015) 119–124.
[3] A.P.M. Michel, F. Sonnichsen, Laser induced breakdown spectroscopy for heavy metal detection in a sand matrix, Spectrochimica Acta Part B, 125 (2016) 177–183.
[4] Y. Ruilian, Y. Xing, ZHAO Yuanhui , H. Gongren2, T. Xianglin3, Heavy metal pollution in intertidal sediments from Quanzhou Bay, China, Journal of Environmental Sciences, 20 (2008) 664–669.
[5] P.B. Tchounwou, C.G. Yedjou, A.K. Patlolla, D.J. Sutton, Heavy Metal Toxicity and the Environment, Molecular, Clinical and Environmental Toxicology Springer., (2012).
[6] D.W. HAHN, N. OMENETTO, Laser-InducedmBreakdown Spectroscopy (LIBS), Part I:Review of Basic Diagnostics and Plasma–
Particle Interactions:Still-Challenging Issues Within the Analytical Plasma Community, APPLIED SPECTROSCOPY, (2010).
[7] G. Galbács1, A critical review of recent progress in analytical laser-induced
breakdown spectroscopy, Springer-Verlag Berlin Heidelberg, (31 July 2015).
[8] B. Kearton, Y. Mattley, Laser-induced breakdown spectroscopy: Sparking new applications, Nat Photon, 2 (2008) 537-540.
[9] Atomic Spectra Database | NIST, https://www.nist.gov/pml/atomic-spectra-database.
[10] A.W. Miziolek, V. Palleschi, I. Schechter, Laser Induced Breakdown Spectroscopy Fundamentals and Applications, Cambridge University Press, (2006).
[11] D.W. HAHN, N. OMENETTO, Laser-Induced Breakdown Spectroscopy (LIBS), Part II: Review of Instrumental and Methodological
Approaches to Material Analysis and Applications to Different Fields, APPLIED SPECTROSCOPY, (2012).
[12] J.J.L. L.M. Cabalin, Experimental determination of laser induced breakdown thresholds of metals under nanosecond Q-switched laser operation, Spectrochimica Acta Part B 53 (1998) 723-730
[13] L.C. R. Fantoni, F. Colao, L. Fornarini,, a.V.S. V. Lazic, Induced Breadown Spectroscopy (LIBS).The process, applications to artwork and
environment,, Springer, B. Di Bartolo and O. Forte,Eds., Advances in Spectroscopy for Lasers and Sensing (2006) 229-254.
[14] B.C. Windom, D.W. Hahn, Laser ablation—laser induced breakdown spectroscopy (LA-LIBS): A means for overcoming matrix effects leading to improved analyte response, 24 (2009) 1665-1675.
[15] C. Chaleard, P. Mauchien, N. Andre, J. Uebbing, J.L. Lacour, C. Geertsen, Correction of matrix effects in quantitative elemental analysis with laser ablation optical emission spectrometry, Journal of Analytical Atomic Spectrometry, 12 (1997) 183–188.
[16] U. Panne, C. Haisch, M. Clara, R. Niessner, Analysis of glass and glass melts during the vitrification process of fly and bottom ashes by laser-induced plasma spectroscopy. Part I:

Normalization and plasma diagnostics, Spectrochimica Acta Part B, 53 (1998) 1957–1968.
[17] Z. Hou, ZheWang, S.-l. Lui, T. Yuan, L. Li, Z. Li, W. Ni, Improving data stability and prediction accuracy in laser-induced breakdown spectroscopy by utilizing a
combined atomic and ionic line algorithm, Journal of Analytical Atomic Spectrometry, 28 (2013) 107–113.
[18] S.I. Gornushkin, I.B. Gornushkin, J.M. Anzano, B.W. Smith, J.D.Winefordener, Effective normalization technique for correction of matrix effects in laser induced breakdown
spectroscopy detection of magnesium in powdered samples, APPLIED SPECTROSCOPY, 56 (2002) 433–436.
[19] E. D'Andrea, S. Pagnotta, E. Grifoni, G. Lorenzetti, S. Legnaioli, V. Palleschi, B. Lazzerini, An artificial neural network approach to laser-induced breakdown spectroscopy quantitative analysis, Spectrochimica Acta Part B, 99 (2014) 52–58.
[20] T.B. Yuan, Z. Wang, Z. Li, W.D. Ni, J.M. Liu, A partial least squares and wavelet-transform hybrid model to analyze carbon content in coal using laser-induced breakdown spectroscopy, Analytica Chimica Acta, 807 (2014) 29-35.
[21] S.M. Clegg, E. Sklute, M.D. Dyar, J.E. Barefield, R.C. Wiens, Multivariate analysis of remote laser-induced breakdown spectroscopy spectra using partial least squares, principal component analysis, and related techniques, Spectrochimica Acta Part B 64 (2009) 79-88.
[22] E. Tognoni, G. Cristoforetti, S. Legnaioli, V. Palleschi, Calibration-Free Laser-Induced Breakdown Spectroscopy: State of the art, Spectrochimica Acta Part B 65 (2010) 1-14.
[23] M. Boudhib, J. Hermann, C. Dutouquet, Compositional Analysis of Aerosols Using Calibration-Free Laser-Induced Breakdown Spectroscopy, Analytical chemistry, 88 (2016) 4029-4035.
[24] L. Zheng, S. Niu, A. QayyumKhan, S. Yuan, J. Yu, H. Zeng, Comparative study of the matrix effect in Cl analysis with laser-induced breakdown spectroscopy in a pellet or in a dried solution layer on a metallic target, Spectrochimica Acta Part B 118 (2016) 66-71.
[25] M.S.A.-A. Abdallah A. Shaltout, N. Y. Mostafa THE VALIDITY OF COMMERCIAL LIBS FOR QUANTITATIVE ANALYSIS
OF BRASS ALLOY — COMPARISON OF WDXRF AND AAS, Journal of Applied Spectroscopy, 78 (2011) 633–640.
[26] M.M. Ctvrtnickova T, Yañez A, Nicolas G, Laser induced breakdown spectroscopy application for ash characterisation
for a coal fired power plant., Spectrochim Acta B, 65 (2010) 734–737.
[27] N.e.M. Arafat A, Kantarelou V, Haddad N, Giakoumaki A,, A.D. Argyropoulos V, Karydas A-G, Combined in
situ micro-XRF, LIBS and SEM-EDS analysis of base metal and corrosion products for Islamic copper alloyed
artefacts from Umm Qais museum, Jordan., J Cult Herit 1, 4 (2013) 261–269.
[28] B.R. Alberghina MF, Brai M, Schillaci T, Tranchina L, Comparison of LIBS and μ-XRF measurements on bronze alloys for monitoring plasma effects., J Phys Conf Ser (2011).
[29] G.M. Khalil AA, Shemis M, Khan IS, Detection of carcinogenic metals in kidney stones using ultraviolet laser induced
breakdown spectroscopy., Applied Optics 5, 4 (2015) 2123–2131.
[30] H.M. Grolmusova Z, Plavcan J, Kopani M, Babal P,, V. P, Laser induced breakdown spectroscopy of human liver samples with Wilson's disease, European Physical Journal-Applied Physics, (2013).
[31] R.S. McMillan NJ, Kochelek K, McManus C, Geological applications of laser-induced breakdown spectroscopy, Geostand Geoanal Res 38 (2014) 329–343.
[32] K.P. Diwakar K, Birch ME, New approach for near real-time measurement of elemental composition of aerosols using

laser induced breakdown spectroscopy, Aerosol Sci Technol, 46 (2012).
[33] B.M. Asgill ME, Frische K, Roquemore WM, Hahn DW, Double-pulse and single-pulse laser-induced breakdown spectroscopy for distinguishing between gaseous and particulate
phase analytes., Applied Optics (2010).
[34] K.G. Kwak J, Kim YJ, Park K, Determination of heavy metal distribution in PM10 during Asian dust and local pollution
events using laser induced breakdown spectroscopy (LIBS), Aerosol Science and Technology, 46 (2012) 1079–1089.
[35] J.S. Lazic V, Laser induced breakdown spectroscopy inside liquids: processes and analytical aspects, Spectrochimica Acta Part B
101 (2014) 288–311.
[36] D. Yoshihiro, W. Zhenzhen, Industrial Applications of Laser-Induced Breakdown Spectroscopy,Industrial Applications of Laser-Induced Breakdown Spectroscopy, Intecopen (www.intechopen.com), 14 (2016).
[37] R. S, A. G, B. B, H. R, M. J, P. T, Z. A, Development of a method for automated quantitative analysis of ores using LIBS, Spectrochimica Acta Part B, 56 (2001) 707-714.
[38] M. MP, N. G, Y. A, Characterization of inorganic species in coal by laserinduced breakdown spectroscopy using UV and IR radiations, Applied Surface Science, 254 (2007) 868-872.
[39] C. T, M. MP, Y. A, N. G, Characterization of coal fly ash components by laser-induced breakdown spectroscopy, Spectrochimica Acta Part B, 64 (2009) 1093-1097.
[40] F. J, W. Z, L. L, L. Z, N. WD, A nonlinearized multivariate dominant factorbased partial least squares (PLS) model for coal analysis by using laser-induced Industrial Applications of Laser-Induced Breakdown Spectroscopy, APPLIED SPECTROSCOPY, 67 (
2013) 291-300.
[41] Y. W, Z. L, D. L, M. WG, J. ST, Design of a laser-induced breakdown spectroscopy system for on-line quality analysis of pulverized coal in power plants, APPLIED SPECTROSCOPY, 63 (2009) 865-872.
[42] K. M, I. K, I. Y, D. Y, T. H., Optimal boiler control through real-time monitoring of unburned carbon in fly ash by laser-induced breakdown
spectroscopy, Appl. Opt., 42 (2003) 6159-6165.
[43] P. Z, D. Z, D. S, Significant radioactive contamination of soil around a coal-fired thermal power plant, Journal of Environmental Radioactivity, 59 (2009) 191-205.
[44] H. C, P. S, S. JR, Temperature effect on laser-induced breakdown spectroscopy spectra of molten and solid salts, Spectrochimica Acta Part B, 97 (2014) 79-85.
[45] G. M, S.-S. I, H.Modiano, R.Stana, Laser induced breakdown spectroscopy for bulk minerals online analyses, Spectrochimica Acta Part B, 62 (2007) 1496-1503.
[46] H. Olli, T. Kauppinen, H. Heikki, Laser-Induced Breakdown Spectroscopy for Rapid Elemental Analysis of Drillcore, IFAC Proceedings Volumes, 46 (2013) 87-91.
[47] A. T, D. C, T. F, G. B, M. H, L.B. O, F. E, On-line monitoring of composite nanoparticles synthesized in a pre-industrial laser pyrolysis reactor
using laser-induced breakdown spectroscopy, Spectrochimica Acta Part B, 63 (2008) 1183–1190.
[48] L. C, Kaegi R, F. M, R. M, G. D, B. M, Development of a mobile fast-screening laser-induced breakdown detection (LIBD) system for field-based measurements
of nanometre sized particles in aqueous solutions, Journal of environmental monitoring, 12 (2010) 1422–1429.
[49] D.G. A, G. R, K. C, D.A. M, D.P. O, Nanoparticle-enhanced laser-induced breakdown spectroscopy of metallic samples, Analytical chemistry, 85 (2013) 10180–10187.
[50] H.V.M. E.H. Piepmeier, Q-switched laser energy absorption in the plume of an aluminium alloy., Analytical Chemistry 41 (1969) 700–707.

[51] A.S. R.H. Scott, Laser-induced plasmas for analytical spectroscopy. , Spectrochimica Acta Part B, 25 (1970) 311–332.
[52] L.J.R. D.A. Cremers, T.R. Loree, Spectrochemical analysis of liquids using the laser spark., Applied Spectroscopy, 38 (1984) 721–729.
[53] V.I. Babushok, F.C. DeLucia Jr, J.L. Gottfried, C.A. Munson, A.W. Miziolek, Double pulse laser ablation and plasma: Laser induced breakdown spectroscopy signal enhancement, Spectrochimica Acta Part B: Atomic Spectroscopy, 61 (2006) 999-1014.
[54] J.P. J. S caffidi, W. Pearman, S.R. Goode, B.W. Colston Jr., J.C. Varter, S.M. Angel, Dual- pulse laser-induced breakdown spectroscopy with combinations of femtosecond and nanosecond laser pulses., Applied Optics 42 (2003) 6099–6106.
[55] W.P. J. Scaffidi, J.C. Carter, B.W. Colston Jr., S.M. Angel, Temporal dependence of the enhancement of material removal in femtosecond–nanosecond dual-pulse laser-induced breakdown spectroscopy Applied Optics, 43 (2004) 6492–6499
[56] Ran Hai, Xingwei Wu, Yu Xin, Ping Liu, Ding Wu, Hongbin Ding, Yan Zhou, Laizhong Cai, L. Yan, Use of dual-pulse laser-induced breakdown spectroscopy for characterization of the laser cleaning of a first mirror exposed in HL-2A, Journal of Nuclear Materials, 447 (2014) 9-14.
[57] Masaki Oba, Yoichiro Maruyama, Katsuaki Akaoka, Masabumi Miyabe, I. Wakaida, Double-pulse LIBS of gadolinium oxide ablated by femto- and nano-second laser pulses., Applied Physics 101 (2010) 545–549.
[58] Timur A.Labutin, Andrey M.Popov, Sergey M.Zaytsev, Nikita B.Zorov, Mikhail V.Belkov, Vasilii V.Kiris, S. N.Raikov, Determination of chlorine, sulfur and carbon in reinforced concrete structures by double-pulse laser-induced breakdown spectroscopy, Spectrochimica Acta Part B, 99 (2014) 94-100.
[59] V.S.Burakov, N.V.Tarasenko, M.I.Nedelko, V.A.Kononov, N.N.Vasilev, S.N.Isakov, Analysis of lead and sulfur in environmental samples by double pulse laser induced breakdown spectroscopy, Spectrochimica Acta Part B, 64 (2008) 141-146.
[60] F.C.D. LuciaJr., J. L.Gottfried, C. A.Munson, A. W.Miziolek, Double pulse laser-induced breakdown spectroscopy of explosives: Initial study towards improved discrimination, Spectrochimica Acta Part B, 62 (2007) 1399-1404.
[61] J. Mo, Y. Chen, R. Li, Silver jewelry microanalysis with dual-pulse laser-induced breakdown spectroscopy: 266 + 1064 nm wavelength combination, Optical Society of America, 53 (2014) 7516-7522
[62] H.Sobral, A.Robledo-Martinez, Signal enhancement in laser-induced breakdown spectroscopy using fast square-pulse discharges, Spectrochimica Acta Part B, 124 (2016) 67-73.
[63] O.A. Nassef, H.E. Elsayed-Ali, Spark discharge assisted laser induced breakdown spectroscopy, Spectrochimica Acta Part B, (2015).
[64] A. A, B. Shakov, X. Maob, R.E. Russo, Spectral emission enhancement by an electric pulse for LIBS and LAMIS, Journal of Analytical Atomic Spectrometry, 32 (2017) 657–670.
[65] K. LI, W. Zhou, Q. Shen, Z. Ren, B. Peng, Laser ablation assisted spark induced breakdown spectroscopy on soil samples, Journal of Analytical Atomic Spectrometry, 25 1475–1481.
[66] W. Zhou, K. Li, H. Qian, Z. Ren, Y. Yu, Effect of voltage and capacitance in nanosecond pulse discharge enhanced laser-induced breakdown spectroscopy, Optical Society of America, 51 (2012).
[67] Y. Li, D. Tian, Y. Ding, G. Yang, K. Liu, C. Wang, X. Han, A review of laser-induced breakdown spectroscopy signal enhancement, APPLIED SPECTROSCOPY REVIEWS, (2017).
[68] S. Eschlböck-Fuchs, P.J. Kolmhofer , M.A. Bodea, J.G. Hechenberger, N. Huber, R. Rössler, J.D. Pedarnig, Boosting persistence time of laser-induced plasma by electric arc discharge for optical emission spectroscopy, Spectrochimica Acta Part B, 109 (2015) 31-38.

[69] L. Liu, X. Huang, S. Li, Y. Lu, K. Chen, L. Jiang, J.F. Silvain, Y.F. Lu, Laser-induced breakdown spectroscopy enhanced by a micro torch, Optics Express, 23 (2015) 15047-15056.
[70] L. Liu, S. Li, X.N. He, X. Huang, C.F. Zhang, L.S. Fan, M.X. Wang, Y.S. Zhou, K. Chen, L. Jiang, J.F. Silvain, Y.F. Lu, Flame-enhanced laser-induced breakdown spectroscopy, Optics Express, 22 (2014) 7686-7693.
[71] X. Li, Z. Yang, J. Wu, W. Wei, Y. Qiu, S. Jia, A. Qiu, Spatial confinement in laser-induced breakdown spectroscopy, Journal of Physics D: Applied Physics, 50 (2016).
[72] Y. Wang, A. Chen, L. Sui, S. Li, D. Liu, X. Wang, Y. Jiang, X. Huang, M. Jin, Persistence of atomic spectral line on laser-induced Cu plasma with spatial confinement, Physics of Plasmas, 23 (2016).
[73] P. Yeates, E.T. Kennedy, Spectroscopic, imaging, and probe diagnostics of laser plasma plumes expanding
between confining surfaces, JOURNAL OF APPLIED PHYSICS, (2010).
[74] S.S. Mao, X. Zeng, X. Mao, R.E. Russo, Laser-induced breakdown spectroscopy: flat surface vs. cavity structures, Journal of Analytical Atomic Spectrometry, 4 (2004) 495–498.
[75] V. Rai, A. Rai, F. Yueh, J. Singh, Optical emission from laser-induced breakdown plasma of solid and liquid samples in the presence of a magnetic field., Appl. Opt., 42(12) (2003) 2085–2093.
[76] L. Cheng, G. Xun, L. Qi, S. Chao, L. Jingquan, Spectral Enhancement of Laser-Induced Breakdown Spectroscopy in External Magnetic Field, Plasma Science and Technology, 17 (11) (2015) 919–922.
[77] S.S. Harilal, M. Tillack, B. O'Shay, C. Bindhu, F. Najmabadi, Confinement and dynamics of laser-produced plasma expanding across a transverse magnetic field, PHYSICAL REVIEW E, 69 (2004).
[78] G.L. Hao ZQ, LiCM, Shen M, Zhou XH, LiXY, Lu YF, Zeng XY, Sensitivity improvement in the detection of Vand Mn elements in steel using laser-induced breakdown spectroscopy with ring-magnet confinement. , Journal of Analytical Atomic Spectrometry, 29 (2014) 2309–2314.
[79] Y. Liu, B. Bousquet, M. Baudelet, M. Richardson, Improvement of the sensitivity for the measurement of copper concentrations in soil by microwave-assisted laser-induced breakdown spectroscopy, Spectrochimica Acta Part B: Atomic Spectroscopy, 73 (2012) 89-92.
[80] Y. Liu, M. Baudelet, M. Richardson, Elemental analysis by microwave-assisted laser-induced breakdown spectroscopy: Evaluation on ceramics, Journal of Analytical Atomic Spectrometry, 25 (2010) 1316-1323.
[81] I. Yuji, T. Ryoji, Characteristics of microwave plasma induced by lasers and sparks, Appl. Opt., 51 (2012) B183-B191.
[82] Ali Khumaeni, Tampo Motonobu, Akaoka Katsuaki, Miyabe Masabumi, W. Ikuo, Enhancement of LIBS emission using antenna-coupled microwave, Optical Society of America, (2013).
[83] Ali Khumaeni, Katsuaki Akaoka, Masabumi Miyabe, I. Wakaida, The role of microwaves in the enhancement of laser-induced plasma emission, Frontiers of Physcis (2015).
[84] M. Tampo, M. Miyabe, K. Akaoka, M. Oba, H. Ohba, Y. Maruyama, I. Wakaida, Enhancement of intensity in microwave-assisted laser-induced breakdown spectroscopy for remote analysis of nuclear fuel recycling, The Royal Society of Chemistry 2014, (2014).
[85] T.A. Zeyad, S. Zhiwei, W. Matthew, Laser Induced Breakdown Spectroscopy: Detection of High and Low Concentrations, 7th Australian Conference on Laser Diagnostics in Fluid Mechanics and Combustion Melbourne, Australia
(2015).
[86] J. Viljanen, Z. Sun, Z.T. Alwahabi, Microwave assisted laser-induced breakdown spectroscopy at
ambient conditions, Spectrochimica Acta Part B, (2016).
[87] M. Wall, Z. Sun, Z. Alwahabi, Quantitative detection of metallic traces in water-based liquids by microwave-assisted laser-induced breakdown spectroscopy, Optics Express, 24 (2016) 1507-1517.

[88] H.H.H. Hui-qin), X.X.X. Xue-hong), H.L.H. Lin), Y.M.Y. Ming-yin), C.C. Tian-bing), L.M.L. Mu-hua), W.C.W. Cai-hong), Study on the Enhancement Intensity of Cd in Rice with Microwave-Assisted Laser-Induced Breakdown Spectroscopy, SPECTROSCOPY AND SPECTRAL ANALYSIS, 36 (2016) 1180-1185.
[89] Alluxa, in.
[90] V.B.G. Alankar Shrivastava, Methods for the determination of limit of detection and limit of quantitation of the analytical methods, Chronicles of Young Scientists, Vol. 2 (| Jan-Mar 2011).
[91] V.M.J. Henriques, Three-dimensional temperature mapping of solar photospheric fine structure using Ca II H filtergrams, Astronomy & Astrophysics, 548 (2012) A114.
[92] CST http://www.cst.com, Online accessed (December 2016).
[93] D.M. Pozar, Microwave Engineering, 4th Edition, Wiley, (2011).
[94] C.A. Balanis, ANTENNA THEORY ANALYSIS AND DESIGN, A JOHN WILEY & SONS, INC., PUBLICATION, (2005).
[95] Ore Research & Exploration, http://oreas.com.au/.

Appendix A

Publications Outcome

Journal Publication outcome from this thesis are:

1. Adeel Iqbal, Zhiwei Sun, Matthew Wall, Z. Alwahab, Sensitive elemental detection using microwave-assisted laser-induced breakdown imaging, Spectrochimica Acta Part B, 136 (2017) 16-22.

   Note: This publication is included in print copy of the thesis and is available in the Library of The University of Adelaide.

   It is also available to authorized users at:

   http://www.sciencedirect.com/science/article/pii/S0584854717300988

2. Shengjian Jammy Chen, Adeel Iqbal†, Matthew Wall, Christophe Fumeauxa, Z.T. Alwahabi, Design and application of near-field applicators for efficient microwave-assisted laser-induced breakdown spectroscopy, Journal of Analytical Atomic Spectrometry, 32 (2017) 508–1518.

   † Both Authors contributed equally

   Note This publication is included in print copy of the thesis and is available in the Library of The University of Adelaide.

   It is also available to authorized users at:

   http://pubs.rsc.org/en/content/articlelanding/2017/ja/c7ja00046d

Spectrochimica Acta Part B 136 (2017) 16–22

Contents lists available at ScienceDirect

Spectrochimica Acta Part B

journal homepage: www.elsevier.com/locate/sab

Sensitive elemental detection using microwave-assisted laser-induced breakdown imaging☆

Adeel Iqbal [a], Zhiwei Sun [b], Matthew Wall [a], Zeyad T. Alwahabi [a,*]

[a] School of Chemical Engineering, The University of Adelaide, S.A. 5005, Australia
[b] School of Mechanical Engineering, The University of Adelaide, S.A. 5005, Australia

ARTICLE INFO

Article history:
Received 21 February 2017
Received in revised form 22 June 2017
Accepted 30 July 2017
Available online 9 August 2017

Keywords:
Laser-induced breakdown spectroscopy (LIBS)
Signal enhancement
Microwave assisted
Imaging

ABSTRACT

This study reports a sensitive spectroscopic method for quantitative elemental detection by manipulating the temporal and spatial parameters of laser-induced plasma. The method was tested for indium detection in solid samples, in which laser ablation was used to generate a tiny plasma. The lifetime of the laser-induced plasma can be extended to hundreds of microseconds using microwave injection to remobilize the electrons. In this novel method, temporal integrated signal of indium emission was significantly enhanced. Meanwhile, the projected detectable area of the excited indium atoms was also significantly improved using an interference-, instead of diffraction-, based technique, achieved by directly imaging microwave-enhanced plasma through a novel narrow-bandpass filter, exactly centered at the indium emission line. Quantitative laser-induce breakdown spectroscopy was also recorded simultaneously with the new imaging method. The intensities recorded from both methods exhibit very good mutual linear relationship. The detection intensity was improved to 14-folds because of the combined improvements in the plasma lifetime and the area of detection.

1. Introduction

Laser induced breakdown spectroscopy (LIBS) is an analytical technique, which has great capabilities of quick response, multi-detection, no sample pre-treatment and analyzing solid, liquid and gaseous samples [1,2]. LIBS can effectively be applied to many fields such as heavy metal detection, space and underwater explorations and ore identification in mining [3–5]. Despite being equipped with excellent features, LIBS has a few limitations such as low sensitivity, poor limit of detection (LoD), weak signal-to-noise ratio (SNR) and surface dependence, which limit its application as a reliable detection method. Significant research has been carried out to overcome these limitations by developing various improved techniques that mainly relay on the concept of aiding LIBS by another energy source. For example, second longer laser pulse [6–8], spark discharge [9], stable flame [10], torch [11], steady magnetic field [12] and microwave (MW) [13–17], are well known secondary sources that induce additional energy into the conventional LIBS to retain and/or re-excite the laser ablated plasma, hence imparting essential improvement in sensitivity, LoD and SNR of LIBS.

As one of these signal enhancement techniques, microwave-assisted LIBS is based on the concept of coupling MW radiations to the plasma regimes with low electron density. For a typical 2.45 GHz MW source, electron density of plasma should be less than the critical density of 7×10^{10} (cm^{-3}) to achieve efficient coupling [14]. The initial laser-induced plasma has a high electron density on the order of 10^{17}–10^{19} cm^3, but during its relaxation and at its periphery, the electron density decreases to be lower than the critical density. At this stage, MW radiations can be coupled into the plasma for re-excitation and signal enhancement [14]. MW radiations can retain and re-excite laser-induced plasma for the whole duration of the MW source by creating localised electric field near to the plasma and delivering kinetic energy to free electrons. These free electrons keep exciting the plasma through atoms, ions and electrons collisions within plasma till the MW remains coupled. MW radiations prevent further decay of plasma density, while the volume and emission intensity of plasma can increase substantially, resulting in stronger emission signals and an improved detection sensitivity.

Several works of MW-LIBS have been reported previously, laser assisted microwave plasma spectroscopy (LAMPS) was initially developed by Ocean Optics and its partner company Envimetrics [3]. A MW cavity was used in the LAMPS setup and an improvement in detection sensitivity by a factor of 10 to 1000, depending on the sample type, was demonstrated [3]. Liu et al. applied a MW cavity for copper detection in soil sample [16] and elemental analysis of ceramic samples [14] in these works, 23 and 33 times enhancement in detection sensitivity was achieved respectively. In gaseous samples, Ikeda and Tsuruoka studied the characteristics of laser- and spark-induced plasmas with

☆ Selected paper from the 9th International Conference on Laser-Induced Breakdown Spectroscopy (LIBS), Chamonix-Mont-Blanc, France, September 12–September 16 2016.

* Corresponding author.
E-mail address: zeyad.alwahabi@adelaide.edu.au (Z.T. Alwahabi).

http://dx.doi.org/10.1016/j.sab.2017.07.008
0584-8547/

an external antenna-coupled MW power, where a 15 times enhancement in lead (Pb) spectra was reported [13]. Khumaeni et al. demonstrated antenna-coupled MW enhanced LIBS using solid samples at lower pressure in enclosed cavity environment [15], where a loop antenna was used to deliver MW radiation close to laser ignited plasma and the authors observed a loss of signal intensity with the increase in surrounding pressure. Viljanen et al. applied MW-LIBS in ambient conditions by using a near field applicator (NFA), which was placed at 0.5 mm from laser beam and 1 mm from sample surface. They achieved 93 folds signal improvement and LoD of 8.1 ppm, for copper detection in Cu/Al_2O_3 solid samples [18]. Wall et al. demonstrated LoD of 10.1 ppm for indium detection in aqueous solution by using a NFA for MW injection at ambient conditions [19]. Furthermore, Eschlbock-Fuchs et al. [20] re-excite the laser induced plasma by a pulsed electric discharge. This results in the extension of the plasma life-time to several millisecond. In these previous studies, it was noticed that the plasma volumes were also enlarged with the presence of MW sources. Therefore, it was highly possible that not all emission signals had been captured using the detection systems which are usually fiber-coupled spectrometers. Equally, it is also possible to further enhance the emission signals in MW-LIBS if the whole plasma volume can be captured. Besides, it is also believed that LIBS signal is being lost significantly as it travels from the plasma to the detector through all the spectrometer components, resulting in a relatively low collection efficiency. To our best knowledge, no alternative detection method has yet been proposed to improve detection efficiency by minimizing the signal loss. So far, all the work has been done to retain and enhance plasma. In addition, the long persisting time of MW-LIBS signal also mitigates the requirement of a fast gating function for the detector used in LIBS to temporally suppress the strong continuum emissions with and shortly after the laser pulse.

While simultaneous analysis of dominant composition is beneficial in LIBS measurements, detection of a single target element is also necessary in many practical application, such as selection of ore in mining industry where reliable, quick and sensitive detections are required. Meanwhile, owing to the advancement in manufacturing of novel filters, it has become possible to achieve signal imaging, i.e. replacing the spectrometer with a filter (or a filter system) in LIBS. Novel filters with an ultra-narrow band pass (BP) up to 0.1 nm are commercially accessible now, e.g. filters manufactured by Alluxa [21]. This level of spectral resolution is comparable to small compact spectrometers typically used in compact LIBS. Besides, both high transmission throughout (T_s) and high optical density (OD) are unique for these new narrow bandpass filters. Therefore, it is attractive to replace the spectrometer in LIBS with a simple filter, leading to a more compact and efficient setup, but potentially also of lower cost.

In the present work, we report a novel concept of elemental detection in MW-LIBS based on imaging. Two narrow band filters are combined to spectrally select the target element emission, which is then recorded using a camera. The demonstrated technique, namely microwave-assisted laser-induced breakdown elemental imaging (MW-LIBEI), possesses several advantages, such as high sensitivity and large field of view (FoV), as will be outlined in detailed in this work.

2. Experimental setup

Fig. 1 shows the schematic diagram of MW-LIBEI. The harmonic output (532 nm, 6 ns pulse duration) from an Nd:YAG laser (Brilliant B) was used as light source to generate initial plasma as does in conventional LIBS. The laser pulse was fired at 200 μs after the starting time of MW. The pulsed MW radiation, operated at 2.45 GHz, was delivered and coupled into the laser-induced plasma. The MW pulse duration was set to 1 millisecond (ms) and was generated with a water-cooled 3 kW Sairem MW system which is available commercially. The adjustable MW power was typically set to 1.2 kW, of which ~50% was finally coupling into the plasma. The MW radiation was delivered with a 1 m flexible coaxial cable (50 Ω NN cable) with 0.14 dB@2.45 GHz, connected with semi rigid cable (RG402/U) at the end. The other end of the semi rigid cable was stripped off to expose the inner silver-plated copper steel core by ~25 mm to form a NFA. The end of NFA was tapered with a double included angle of ~45° to form a pointed tip which was located ~0.5 mm horizontally and vertically away from the interaction point of the focused laser beam (~100 μm in diameter) and the solid sample surface.

The plasma emission was simultaneously recorded through two detection channels. The first is a backward collection scheme that is often used in conventional LIBS set-ups. As shown in Fig. 1, after the first focusing/collimating lens (f = 100 mm) the emission was focused by a perforated parabolic mirror and directed by a combination of a focusing lens into another parabolic and then into a fiber bundle (Thorlabs, BFL200HS02). The emitted radiation was then channeled into a spectrometer (f = 500 mm) installed with a 2400 lines/mm grating and an ICCD camera (iStar, Andor).

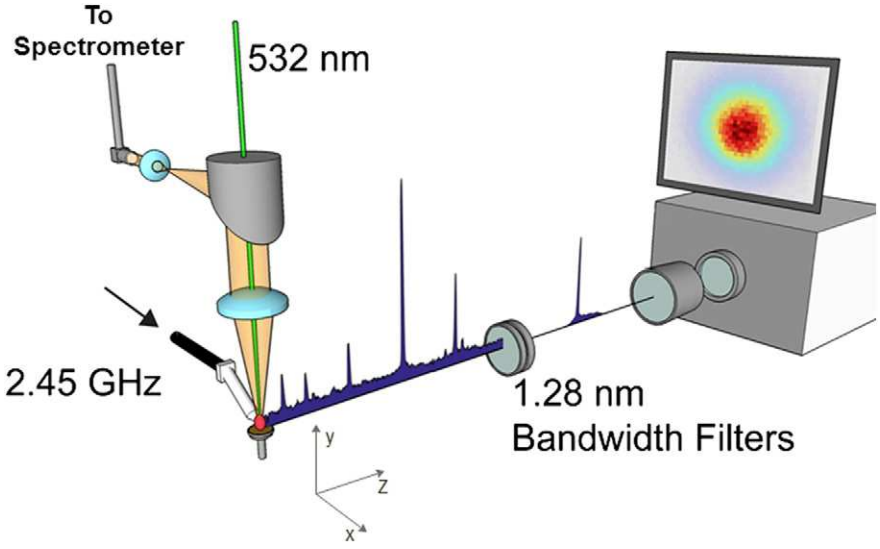

Fig. 1. Outline of the microwave-assisted, laser-induced breakdown elemental imaging, i.e. MW-LIBEI. The two filters are attached in front end of the camera lens in the actual set-up. Also shown is a second detection channel, representing the spectrometer based detection used in microwave-assisted laser-induced breakdown spectroscopy (MW-LIBS). The spectrometer and the intensified camera used in MW-LIBS are not shown.

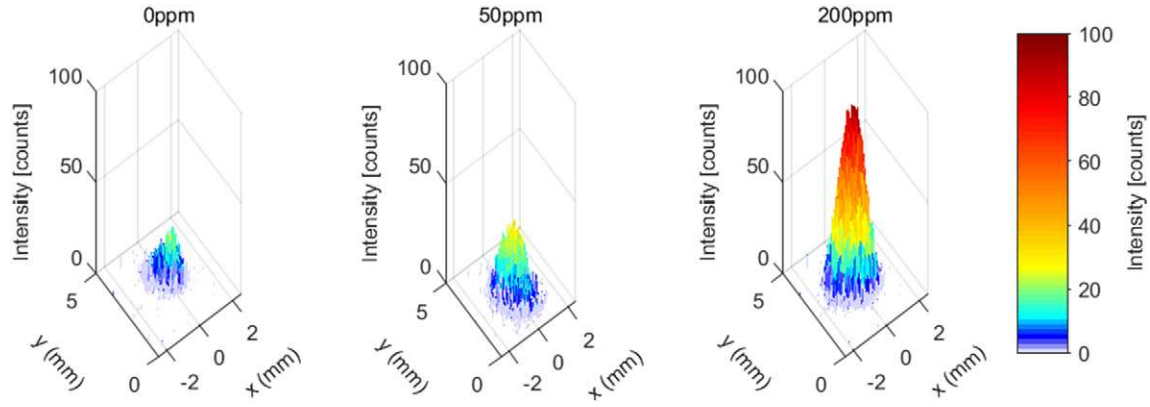

Fig. 2. MW-LIBEI emission imaging plotted in three dimensions for samples with indium concentration of 0, 50 and 200 ppm while laser and MW was 2 mJ/pulse and 900 W.

The second detection channel is used for demonstrating the proof-of-concept of the MW-LIBEI technique. The plasma emission was directly filtered by a combination of two BP filters, both 50.8 mm in diameter. This is to select only the 451.13 nm Indium emission line following the transmission from the second (24,372.957 cm^{-1}) to the first excited levels (2212.599 cm^{-1}). The first filter is a standard filter with a full-width at half-maximum (FWHM) of 10 nm (450FS10-50, Andover), while the second is a custom-made filter with a narrower BP (FWHM = 1.28 nm, Alluxa) [21], centered exactly at 451.4 nm. The two filters have transmission of 54% and 95%, respectively, resulting in a combined transmission of 51% at 451.13 nm. The combined Optical Density (OD) is ~5.6 out of the range of 450.12–452.68 nm and is ~8 below 440 and above 460 nm. These high OD values are critical in (MW-) LIBEI to block not only strong emissions from other elements, e.g. excited atomic N and O from buffering air, but also the background emission integrated over the full spectral region. The combined filters were installed in front of a Nikon camera lens (f = 50 mm and f-number = 1.8), located at about 300 mm away from the detection volume. The emission signals passing the filters were recorded by a second ICCD camera (iStar, Andor), whose gating time and width were synchronized with those of the ICCD used in the spectroscopic detection channel. While it is possible to use a normal camera with a basic gate function to capture emission, an ICCD was used in this work to facilitate comparisons of the MW-LIBEI signals with those from the spectrometer-based MW-LIBS. The intensifier gain was set at 20 and 200, respectively, for the MW-LIBEI and MW-LIBS cameras. These values correspond to ~8% and 78% of the full available gain (255), respectively.

To test the quantitative nature and the response linearity of the MW-LIBEI technique, solid samples containing a range of indium concentration from 50 to 1400 ppm (by weight) were in-house prepared by mixing 1% solution of indium chloride ($InCl_3$) with 14.25% solution of sodium chloride with various stoichiometric ratios. The additional water was then evaporated at 250 °C. Solid mixtures were transformed into uniform surface discs of 3.5 mm in thickness and 21 mm in diameter, which were then dried at 51 °C for 15 min.

3. Results and discussion

In developing LIBEI, several following concerns must be assessed. The first is to evaluate the blocking ability of the filtering system. This is because in LIBS the emission is spectrally resolved; hence the background interference, if presented, can often be satisfactorily evaluated and then subtracted from the spectrally resolved signal. However, this approach may not be applicable in MW-LIBEI. All photons at multiple wavelengths, transmitting through the filters and detectable by the camera, can contribute to the image intensity, e.g. atomic N and O emission, when the sample is in air. Fig. 2 shows the MW-LIBEI signals for indium at three concentrations of 0, 50 and 200 ppm, respectively, averaged from 200 laser shots. The gate width of the camera was 800 μs and delayed 10 μs from the laser pulse of 2 mJ/pulse. As shown in Fig. 2, the image intensity for the non indium (0 ppm) sample is still detectable, but already too weak, <20 counts. The image peak intensity significantly increases to 30 and 100 counts in the 50 and 200 ppm samples. While the leaking background influences the LoD of MW-LIBEI, Fig. 2 evidently shows the good sensitivity of MW-LIBEI, for which a further discussion is given below. It is also worth noting that in MW-LIBEI the image is integrated over the plasma image to present the signal intensity that corresponds to elemental concentration, leading high SNR (also see Fig. 4).

The second concern to be assessed in developing MW-LIBEI is the corresponding relationship between MW-LIBEI and MW-LIBS signal intensities, given that the latter holds quite good linear relations with the elemental concentrations [18,19]. Fig. 3 shows simultaneous results of the MW-LIBEI and MW-LIBS intensities measured in samples with different indium concentration (0–1400 ppm). In this measurement, all experimental settings were kept same as stated in Fig. 2. The intensities of the MW-LIBEI are calculated by integrating area over the plasma image, while those of the MW-LIBS are spectrally integrated over the indium line at 451 nm, both with background subtractions. Fig. 3a shows an excellent linear relationship between MW-LIBEI and MW-LIBS with a square correlation coefficient (R^2) value better than 98%. Furthermore, the linearity holds in a large dynamical range, indicating the feasibility of using MW-LIBEI for element quantifications, as quantitative element measurements using MW-LIBS has already been demonstrated [19].

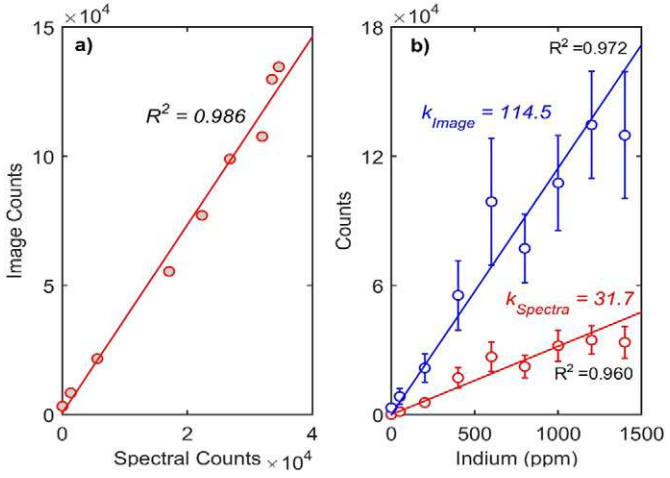

Fig. 3. (a) Represents the relationship between spectral counts (MW-LIBS) and image intensities (MW-LIBEI) simultaneously recorded by spectrometer and imaging camera. (b) The intensities of MW-LIBS and MW-LIBEI signals as a function of indium concentration. The first three data in the MW-LIBEI signal curve correspond to the three images shown in Fig. 2. Laser and MW was 2 mJ/pulse and 900 W in these measurements.

Fig. 3b shows MW-LIBEI and MW-LIBS signals against the indium concentration. General good linear relationships exist in both measurements, noting that there are also potential uncertainties of concentrations of the samples. The relatively large standard deviations, for both type of signals in Fig. 3b, are attributed to the fluctuation of the coupling efficiency of MW to plasma. An important finding is that the slope of the MW-LIBEI signal curve is approximately 3 times larger than that of MW-LIBS, indicating an improvement of 3 folds in signal intensity for the present setup. The signal intensity of MW-LIBS may be improved using a low-resolution grating with higher reflection efficiency, such as that of 300 lines/mm. However, noting the gains used for both cameras, the present work clearly demonstrates that the simple MW-LIBEI based on a low-cost camera can achieve higher signals than the MW-LIBS. This enhancement is particularly attractive because MW-LIBS is already more sensitive than conventional LIBS by a factor of ~1–100 [18, 19].

The LoDs of MW-LIBS and MW-LIBEI are estimated to be 16 ppm and 50 ppm, respectively. The LoD of MW-LIBS was estimated based on the signal-to-noise method. The LoD of MW-LIBEI was estimated from Fig. 2 using visual evaluation method [22].Considering the leakage through the filter in the absence of the indium (0 ppm) as shown in Fig. 2, for a safe detection the acceptable signal value was assumed three times of this leakage, in terms of intensity counts. MW-LIBEI demonstrates poor LoD because even in sample without presence of indium there was still emission intensity acting as background interference, as shown in Fig. 2. This leakage through filter limits the quantitative detections beyond 50 ppm, however, Fig. 3b demonstrates that MW-LIBEI offers higher sensitivity for the smaller variation in concentration as compared to MW-LIBS. The background interference can potentially be reduced to improve LoD of MW-LIBEI. In principle, a filter with a narrower BP (i.e. that is <1.28 nm) and a higher OD can be employed since atomic emission is typically much narrower in spectra. Such a filter, e.g. which has a FWHM of 0.12 nm around 396 nm, indeed had already applied in astronomy study [23]. Another potential method is to introduce a second narrow BP filter that is slightly off-resonant to the target spectral line, installed with the resonant filter in a stereoscopic lens configuration, allowing the recording of the background signal simultaneously.

The third concern in developing MW-LIBEI may be the neighboring spectral interference from other elements. Fig. 4 shows a typical MW-LIBS and MW-LIBEI recorded in a feedstock sample from an industrial lead processing plant. The sample contains many other elements including indium and, therefore, several spectral lines appear within this 10 nm spectral range in the MW-LIBS. However, it is still feasible to select indium signals in the MW-LIBEI with a quite good SNR. Also, the cross section along one pixel array of the MW-LIBEI image demonstrates both high intensity and great SNR ratio in the MW-LIBEI. The limited capability of detecting multiple elements of MW-LIBS can potentially be resolved by applying a cheap low-resolution spectrometer for multi-elemental identifications.

We also emphasize the necessary role of the MW source in MW-LIBEI. Fig. 5 presents the imaging signals recorded with and without the assistance of external MW source, as well as the corresponding MW-LIBS intensities as comparison. Fig. 5a and b presents single shot image intensities without and with MW. Fig. 5c and d presents averaged image intensities without and with MW respectively. While Fig. 5e and f presents a comparison of spectral and image intensities captured by both detection channels, i.e. LIBS and LIBEI without and with MW, while operated simultaneously. All measurement settings were held the same as shown in Figs. 2 and 3, while without MW the camera gate-width was only delayed 200 ns from the laser pulse to capture more indium signal. Also, a higher laser power (3 mJ/pulse) than in Figs. 2 and 3 was applied to ensure detectable signal in the MW-off testing. Firstly, it can be seen that the signals have been significantly enhanced following the MW injection, both in spectra and in imaging, revealing the crucial role of MW. Secondly, the enhancement on LIBEI signal is clearly larger than that of LIBS (see Fig. 5e and f). This is another advantage of MW-LIBEI, i.e. its large FoV ensures that all emission signals are being captured and makes MW-LIBS more tolerant to the fluctuation of the plasma volume. This tolerance against the change of plasma volume is difficult to achieve in both MW assisted and conventional LIBS. Comparison of the signal in MW-LIBEI (in Fig. 5f) with that

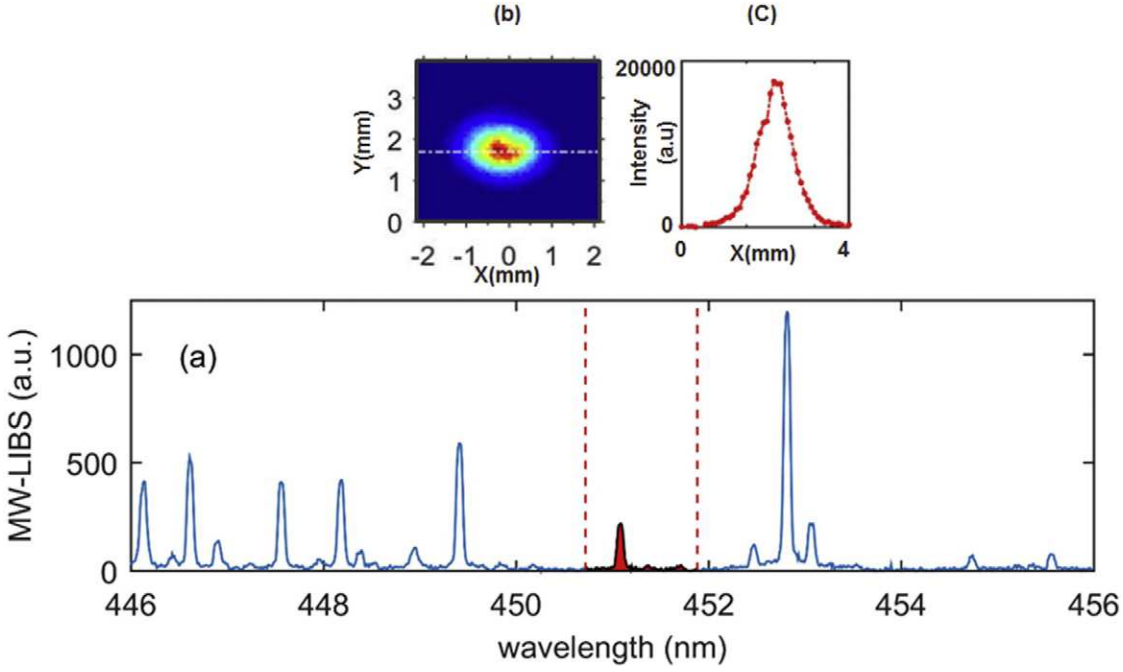

Fig. 4. (a) Typical spectrum of MW-LIBS and (b) emission imaging of MW-LIBEI recorded simultaneously in a feedstock sample from a lead processing plant plate using 2.5 mJ/pulse laser and 900 W MW. In (a) the transmission band of the filters is indicted by the two red dash lines. The cross section of the MW-LIBEI image (b) along the dash-dot line is shown in (c).

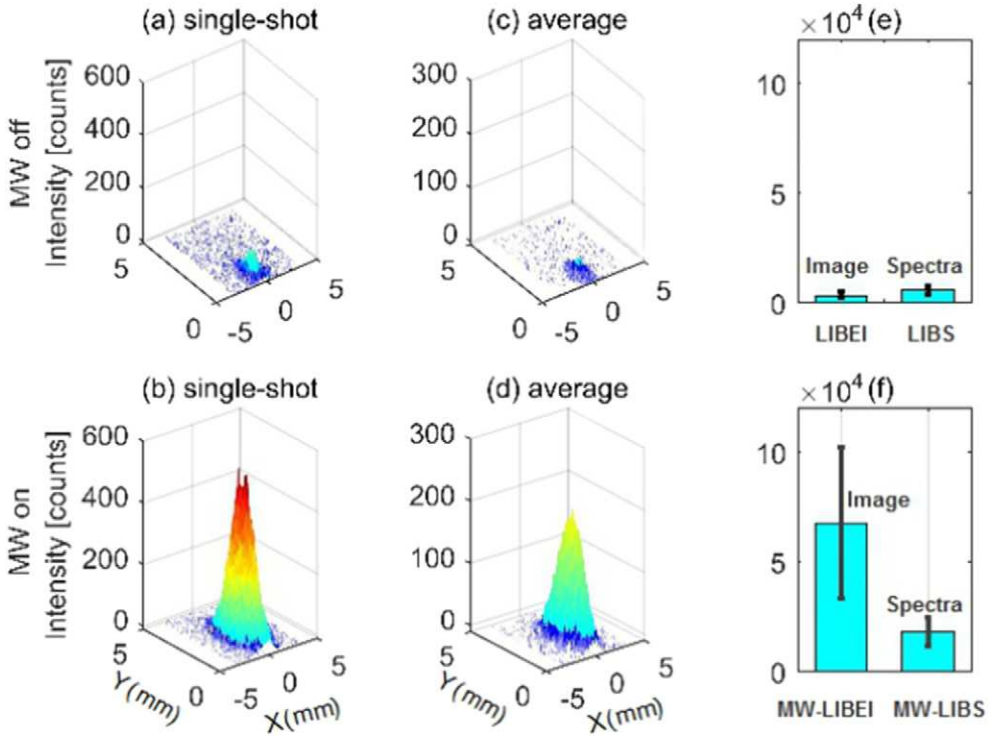

Fig. 5. Indium emission imaging plotted in three dimensions for snapshot signals (a) without and (b) with MW assistance, and signals averaged over 100 laser shots (c) without and (d) with MW assistance. The corresponding image and spectral intensities of MW-LIBEI and MW-LIBS are shown in (e) and (f). Solid samples containing 400 ppm indium were used with a laser energy of 3 mJ/pulse laser and microwave power of 0 and 900 W.

in conventional LIBS (in Fig. 5e), reveals a total signal enhancement of ~ 14-fold for the present MW-LIBEI setup.

Additionally, MW-LIBEI signal can be further enhanced by increasing the MW power. In Fig. 6a, both normalized MW-LIBS and MW-LIBEI signals are shown against the MW power. A linear relationship is found in the MW-LIBEI curve for the MW power up to 1.6 kW, which potentially holds for higher MW power. Contrastively, the MW-LIBS signal responses nonlinearly to the MW power above ~1.0 kW and appears to be saturated. This non-linear response is attributed to the increase of the plasma volume, as illustrated in Fig. 6b showing that the plasma volume increases linearly with the MW power when it is effective (>0.4 kW) on the plasma. In MW-LIBEI, the enlargement of the plasma volume and the enhancement in signals are well detectable because of its large FoV. However, the volume enlargement is not detectable in MW-LIBS beyond 1.2 kW MW power, since the plasma volume becomes too large to be effectively coupled into the fiber optical cable, as clearly illustrated in Fig. 6a. It should be noted that the plasma volume was calculated based on an effective radius. A process of image binary was applied firstly to the recorded image based on the $1/e^2$ value of the maximum intensity to get the projected area of the plasma, from which an effective radius was calculated by assuming that the plasma is spherical in shape. This process was acceptable because that, as shown in Fig. 4b, the plasma images are reasonable approximated as round in the present work.

In addition, it is also significant to demonstrate the change in physical appearance of the plasma following the MW injection at various powers, to strengthen the claim of MW-LIBEI benefiting from FoV. Fig. 7 presents the change in the appearance and intensity of indium plasma images, captured at various MW powers keeping the laser power constant. 200 single shots have been recorded at each MW power and plotted as an average image. X-axis in these figures represents the position of the sample holder. NFA is placed 1 mm from sample and 0.5 mm from

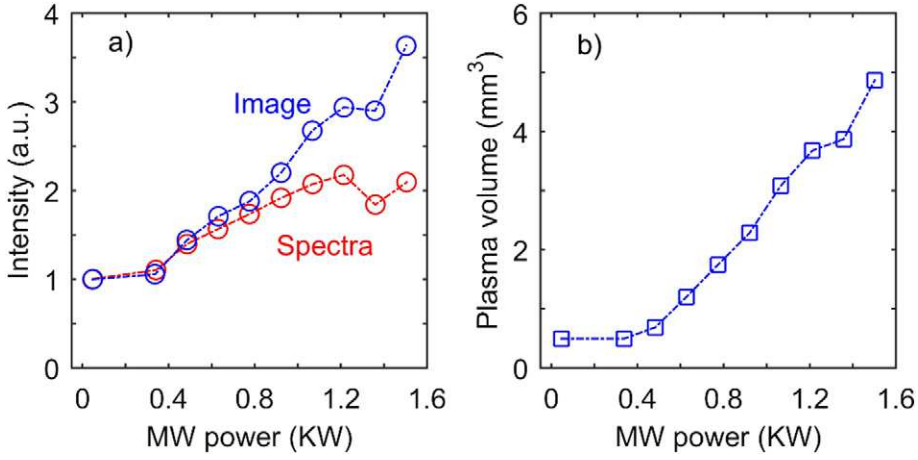

Fig. 6. (a) Normalized intensities of MW-LIBEI and MW-LIBS, as a function of the MW power, and (b) the corresponding plasma volume recorded in MW-LIBEI using 2.5 mJ/pulse of laser.

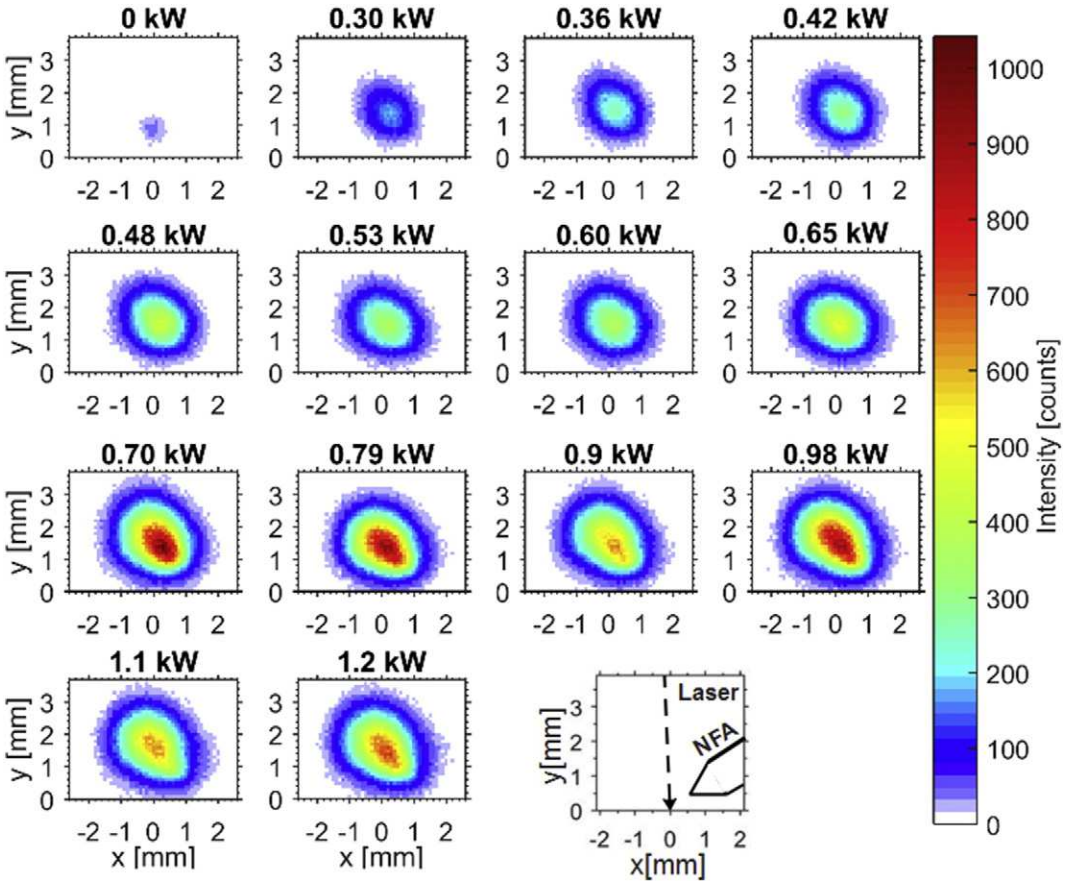

Fig. 7. Wavelength- and specially-resolved microwave-enhanced plasma images, recorded with a narrow-bandpass filter exactly centered at 451.13 nm capering the indium emission line. The images were recorded using solid sample containing 1200 ppm indium and laser energy of 2.5 mJ/pulse with various microwave powers as indicated. The axes are presented in mm with the point (0,0) approximating the incident location of the laser beam on the sample. The inserted figure at the lower-right illustrates the location and orientation of the near field applicator with respect to the laser propagating axis.

laser beam, while laser beam is propagating at 10° towards solid sample. Y-axis represents vertical distance from the sample holder and is at right angle to the axis of imaging camera (*Z*-axis) as shown in Fig. 1. Axis values have been presented in millimeter (mm) by calculating the pixels/mm from recorded image of a sample, having known length and width. Zero mm on the X-axis is the approximate position of the laser beam while NFA applicator is located on the right as shown in Fig. 7. From this figure it can be seen that with the increase of MW power, physical appearance and intensity of plasmas tend to increase substantially, which proves the concept of FoV in MW-LIBEI. While a few exceptions can also be observed at 0.9, 1.1 and 1.2 kW which are assumed to be, because of damaged surface of solid sample, resulted as irregular MW coupling.

In contrast to LIBS, MW-LIBEI is suitable for a single elemental detection. It is worth noting that a stereoscope in front of the camera lens can offer a second elemental detection channel, if needed. A low-cost spectrometer can also be used for elemental identification and or, for larger scans to identify the whole matrix, whereas major species of interest can be analyzed by elemental imagining

4. Conclusions

Microwave-assisted laser-induced breakdown elemental imaging as a new elemental detection method has been demonstrated. MW-LIBEI offers a desirable high-level of intensity because of the large FoV and a negligible flight-out-of-view. An improvement of 14 folds in the detection intensity was demonstrated for indium in solid samples. The demonstrated improvement in the intensity is because of the large FoV of the MW-LIBEI technique, which is not available in MW-LIBS. The detection intensity can be further improved by increasing the power and the pulse-duration of the MW radiation. The limit of detection of the MW-LIBEI technique is higher than that of the MW-LIBS, 16 ppm versus 50 ppm, but it can be potentially improved by using a filter (or a filtering system) with a narrower BP or higher OD. Furthermore, the MW-LIBEI is a spectrometer-free technique, in which only a relatively simple camera, with neither fast gating nor an intensifier, can be used to achieve similar detection capability as that of conventional MW-LIBS. The spectrometer-free MW-LIBEI technique responds well to the demand for cost-effective, reliable, sensitive and real-time detection in remote and harsh environments including, space, defense, chemical processing and mining industries.

Acknowledgement

The authors would like to thank Mr. Jeffrey Hiorns, from the mechanical workshop at the School of Chemical Engineering, for his outstanding technical support. The financial support from the Institute or Mineral and Energy Resource (IMER) and the Faculty of Engineering, Computer & Mathematical Science (ECMS) at The University of Adelaide is acknowledged.

References

[1] D.W. Hahn, N. Omenetto, Laser-induced breakdown spectroscopy (LIBS), part I: review of basic diagnostics and plasma–particle interactions: still-challenging issues within the analytical plasma community, Appl. Spectrosc. 64 (2010) 335A–336A.
[2] D.W. Hahn, N. Omenetto, Laser-induced breakdown spectroscopy (LIBS), part II: review of instrumental and methodological approaches to material analysis and applications to different fields, Appl. Spectrosc. 66 (2012) 347–419.

[3] B. Kearton, Y. Mattley, Laser-induced breakdown spectroscopy: sparking new applications, Nat. Photonics 2 (2008) 537–540.
[4] D.A. Cremers, L.J. Radziemski, Handbook of Laser-Induced Breakdown Spectroscopy, 2nd ed Wiley, Hoboken, 2013.
[5] R. Noll, Laser-Induced Breakdown Spectroscopy Fundamentals and Applications, Springer, Berlin, Heidelberg, 2012.
[6] V.I. Babushok, F.C. DeLucia Jr., J.L. Gottfried, C.A. Munson, A.W. Miziolek, Double pulse laser ablation and plasma: laser induced breakdown spectroscopy signal enhancement, Spectrochim. Acta B At. Spectrosc. 61 (2006) 999–1014.
[7] F. Colao, V. Lazic, R. Fantoni, S. Pershin, A comparison of single and double pulse laser-induced breakdown spectroscopy of aluminum samples, Spectrochim. Acta B At. Spectrosc. 57 (2002) 1167–1179.
[8] C. Gautier, P. Fichet, D. Menut, J. Dubessy, Applications of the double-pulse laser-induced breakdown spectroscopy (LIBS) in the collinear beam geometry to the elemental analysis of different materials, Spectrochim. Acta B At. Spectrosc. 61 (2006) 210–219.
[9] O.A. Nassef, H.E. Elsayed-Ali, Spark discharge assisted laser induced breakdown spectroscopy, Spectrochim. Acta B At. Spectrosc. 60 (2005) 1564–1572.
[10] L. Liu, S. Li, X.N. He, X. Huang, C.F. Zhang, L.S. Fan, M.X. Wang, Y.S. Zhou, K. Chen, L. Jiang, J.F. Silvain, Y.F. Lu, Flame-enhanced laser-induced breakdown spectroscopy, Opt. Express 22 (2014) 7686–7693.
[11] L. Liu, X. Huang, S. Li, Y. Lu, K. Chen, L. Jiang, J.F. Silvain, Y.F. Lu, Laser-induced breakdown spectroscopy enhanced by a micro torch, Opt. Express 23 (2015) 15047–15056.
[12] Y. Li, C. Hu, H. Zhang, Z. Jiang, Z. Li, Optical emission enhancement of laser-produced copper plasma under a steady magnetic field, Appl. Opt. 48 (2009) B105–B110.
[13] Y. Ikeda, R. Tsuruoka, Characteristics of microwave plasma induced by lasers and sparks, Appl. Opt. 51 (2012) B183–B191.
[14] Y. Liu, M. Baudelet, M. Richardson, Elemental analysis by microwave-assisted laser-induced breakdown spectroscopy: evaluation on ceramics, J. Anal. At. Spectrom. 25 (2010) 1316–1323.
[15] A. Khumaeni, T. Motonobu, A. Katsuaki, M. Masabumi, W. Ikuo, Enhancement of LIBS emission using antenna-coupled microwave, Opt. Express 21 (2013) 29755–29768.
[16] Y. Liu, B. Bousquet, M. Baudelet, M. Richardson, Improvement of the sensitivity for the measurement of copper concentrations in soil by microwave-assisted laser-induced breakdown spectroscopy, Spectrochim. Acta B At. Spectrosc. 73 (2012) 89–92.
[17] A. Khumaeni, K. Akaoka, M. Miyabe, I. Wakaida, The role of microwaves in the enhancement of laser-induced plasma emission, Front. Phys. 11 (2016) 114209.
[18] J. Viljanen, Z. Sun, Z.T. Alwahabi, Microwave assisted laser-induced breakdown spectroscopy at ambient conditions, Spectrochim. Acta B At. Spectrosc. 118 (2016) 29–36.
[19] M. Wall, Z. Sun, Z. Alwahabi, Quantitative detection of metallic traces in water-based liquids by microwave-assisted laser-induced breakdown spectroscopy, Opt. Express 24 (2016) 1507–1517.
[20] S. Eschlböck-Fuchs, P.J. Kolmhofer, M.A. Bodea, J.G. Hechenberger, N. Huber, R. Rössler, J.D. Pedarnig, Boosting persistence time of laser-induced plasma by electric arc discharge for optical emission spectroscopy, Spectrochim. Acta B 109 (2015) 31–38.
[21] Alluxa, Alluxa filters, http://www.alluxa.com.
[22] V.B.G. Alankar Shrivastava, Methods for the determination of limit of detection and limit of quantitation of the analytical methods, Chronicles of Young Scientists 2 (2011) 21–25.
[23] V.M.J. Henriques, Three-dimensional temperature mapping of solar photospheric fine structure using CaII H filtergrams, Astron. Astrophys. 548 (2012) A114.

JAAS

PAPER

Cite this: *J. Anal. At. Spectrom.*, 2017, **32**, 1508

Design and application of near-field applicators for efficient microwave-assisted laser-induced breakdown spectroscopy

Shengjian Jammy Chen, †[a] Adeel Iqbal,†[b] Matthew Wall,[b] Christophe Fumeaux[a] and Zeyad T. Alwahabi *[b]

Received 1st February 2017
Accepted 8th June 2017

DOI: 10.1039/c7ja00046d

rsc.li/jaas

Laser-induced breakdown spectroscopy (LIBS) can benefit from sustaining laser generated plasma with microwaves to enhance elemental detection sensitivity. To achieve efficient microwave coupling, critical factors, such as the electromagnetic environment and reflection coefficient of the coupling device, need to be considered to quantitatively predict the electric-field strength in the plasma location. 3D full-wave electromagnetic simulations were used to design near-field microwave applicators suitable to maximize microwave coupling into the short-lived laser-induced plasmas. The simulations pointed out to four effective and practical designs containing varieties of isolation techniques. The four developed microwave applicators were then used to improve the detection of copper present in a mineral ore solid sample, using LIBS and imaging techniques simultaneously. It was found that, with 1.2 kW microwave power, an applicator design with a 30 mm diameter ground plane can significantly boost the signal of copper line 324.754 nm with a factor of 849, which is, to the authors' best knowledge, the highest reported value. Furthermore, an outstanding signal to noise ratio of 166 was recorded in a solid sample containing a certified 3.38 μg g^{-1} copper concentration.

1 Introduction

Laser-induced breakdown spectroscopy (LIBS) is a relatively simple and powerful technique for spectrochemical analysis.[1–3] Since the signal strength and signal to noise ratio (SNR) are crucial for achieving high sensitivity in LIBS, several methods including nano-particle deposition,[4] double-pulsed excitation,[1,5,6] spatial confinement,[7–9] resonance enhancement,[10–12] and coupling to external energy sources[13–27] have been developed. For this last method in particular, microwave is one of the most popular external energy sources[14,18–20,23–27] leading to techniques generally referred as microwave-assisted LIBS. Additionally, microwave technologies have been also exploited to launch or generate plasma in various applications.[28–30] Compared with the other mentioned techniques such as double-pulsed excitation and spatial confinement, microwave-assisted methods can be less intrusive to the sample and can conveniently create localized plasma enhancement. The external energy supplied *via* the microwave sustains the free electrons present within the short-lived laser-induced plasma. These energized free electrons will then act as an excitation source leading to a significant extension of the life-time of the laser-induced plasma.

The life-time of the microwave assisted laser-induced plasma can reach ms time scale and it is usually determined by the pulse-length of the microwave source. The life-time extended plasma will provide higher signal counts by allowing the use of a longer detection window gate. The challenge, however, is the ability to supply the microwave power into the laser-induced plasma at an appropriate time and precise spatial location. This is because if the plasma electron density of the laser-induced plasma is above a critical value of approximately 7×10^{10} (cm^{-3}),[15,20] the microwave will not interact with the laser-induced plasma. Therefore, to efficiently and effectively improve the sensitivity and detectability of LIBS systems, well-designed near-field applicators (NFAs) which have a predictable microwave radiation performance and are optimized based on the specificities of LIBS systems are critical. Firstly, a well-designed NFA should provide an efficient microwave localized application obtained by minimizing the reflection in the microwave power transmission path, which needs to take the NFA and the surrounding environment into account during the design process. Secondly, it should have predictable microwave radiation characteristics such electric field distribution and strength, which can be obtained and optimized from electromagnetic simulation software. As a result, a well-designed NFA can lead to an efficient and effective microwave-assisted LIBS,

[a]*The University of Adelaide, School of Electrical and Electronic Engineering, SA 5005, Australia*

[b]*The University of Adelaide, School of Chemical Engineering, SA 5005, Australia. E-mail: zeyad.alwahabi@adelaide.edu.au*

† These authors contributed equally to this work.

by increasing the interaction of the plasma with concentrated microwave power.

Most recently, Wall *et al.*[26] and Viljanen *et al.*[27] reported that a NFA can be used for LIBS signal enhancement at atmospheric pressure in ambient air. The signal enhancement factors for copper in a solid matrix and for indium in aqua solution were found to be 100 and 60, respectively. In these studies, the NFA was designed and empirically tuned to produce satisfactory microwave injection without systematically optimizing the coupling, which thus did not necessarily lead to the most efficient NFA. However, NFAs with high efficiency are strongly desired as they are extremely important for LIBS system sensitivity and operation at lower microwave power. Therefore, designing NFAs in a more systematic way can lead to a better performance.

In this paper, we demonstrate how relatively small changes in the geometry of the NFA can lead to significant improvement of the microwave-assisted LIBS overall system performance. To this end, four NFAs are designed based on full-wave electromagnetic simulations (performed with CST Microwave Studio,[31] referred to as CST in this paper), taking into account critical factors, such as the influence of the electromagnetic environment and the reflection coefficient, to maximize the electric field strength at the location of the laser-induced plasma. The coupling efficiency of the resulting designs was assessed by experimental comparison with a reference design, involving simultaneous imaging of the enhanced plasma and spectroscopic detection of copper in the solid sample. This allowed us to evaluate the entire system sensitivity by monitoring the plasma spatial and temporal dimensions and by measuring the microwave-assisted signal enhancement for copper lines.

2 NFA designs

The NFAs in a typical microwave-assisted LIBS setup for ambient conditions, such as demonstrated in ref. 26 and 27 are affixed with adjustable posts and connected to the microwave generator through a series of equipment and coaxial cables in a relatively open space. Therefore, these NFAs are more sensitive to the exterior environment compared with the microwave launching devices in a relatively confined environment,[15,18,20,24] since the objects electrically connected or in proximity to them can have an impact on their performance and repeatability owing to electromagnetic coupling. This is especially critical for metallic objects such as the NFA holder and the adjustable posts, whose positions might change for different measurements. In order to develop NFAs with a predictable performance, this type of impact must be mitigated through appropriate electromagnetic design. Hence, different applicator designs involving some well-known techniques such as a quarter-wave choke or a finite ground plane[32] are proposed here to strongly limit the return currents along the outside of the coaxial cable feeding the NFA. This will consequently limit the direct coupling to the outside objects in the system. Such undesired coupling can drastically alter the behaviour of a NFA, and in the presence of a typically complicated environment, can render the performance prediction unreliable.

Four designs variations of NFAs, namely designs B, C, D and E, are designed, fabricated and investigated in this paper by comparing them to a reference design A. The general schematic diagrams of the NFA designs are shown in Fig. 1, where (a) refers to the reference design A, while (b) shows the design B and (c) the generic geometry of designs C, D and E. Their dimensions are given in Table 1, as designed for operation at a microwave frequency of 2.45 GHz. All considered NFAs consist of a rod-shaped conductor fed by a standard SMA (Subminiature version A) connector for radio-frequency (RF) connection. The rod of the applicator conductor is made of silver plated copper clad steel and has a radius of 0.45 mm, and is formed by stripping the inner conductor of a 50 Ω rigid coaxial cable, and sharpening its tip to an angle of α. In this study, design A is considered as a reference NFA and does not have any electromagnetic isolation to the environment. In contrast, the other four NFAs employ some simple but effective isolation techniques such as choke and ground plane to render their performance more robust and predictable. The main aim of those techniques is to suppress the return RF currents on the outside of the coaxial cable. To this end, a quarter-wave choke is soldered on the outer conductor for design B whereas for the other three NFAs a finite-size circular ground plane is added to the design. The SMA connector at the other end of the cable is connected to the waveguide output from the microwave generation apparatus. When excited with microwave power at the system frequency of 2.45 GHz, designs D and E are working at

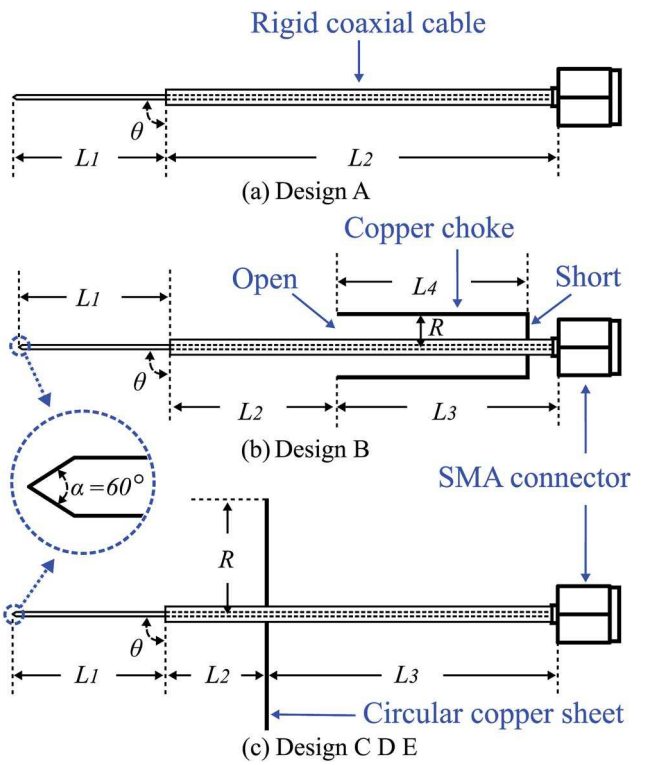

Fig. 1 NFA configurations: (a) reference NFA design A (b) NFA with quarter-wave choke (design B) and (c) NFAs with ground plane (designs C, D and E).

Table 1 Dimensions of the NFA designs under investigation. The configuration of reference A is shown in Fig. 1(a), whereas design B refers to Fig. 1(b), and the parametrized geometry of designs C, D and E is shown in Fig. 1(c)

Parameters (mm)	L_1	L_2	L_3	L_4	R
Design A	28	68.5	N/A	N/A	N/A
Design B	27.5	30.5	38	30	1.6
Design C	28	61	7.5	N/A	42.5
Design D	33	0	68.5	N/A	15
Design E	28	0	68.5	N/A	42.5

their fundamental resonant mode while designs B and C operate at higher-order modes, as shown in Fig. 2. In principle, the resulting NFAs are variations of monopole antennas but the main difference is that they are designed for operation in the near-field through maximization of field strength in the vicinity of the tip. Compared with an NFA such as design A without an added choke or ground structure, these devices offer higher predictability in design as well as enhanced system performance and stability, as it will be seen in the later sections. On the one hand, the choke and ground plane enhance performance predictability as they act as an electrical isolation between the antenna and the physical objects behind it, thus suppressing return RF currents on the outside of the coaxial cable. More importantly, on the other hand, the electric field strength near the tip of the applicator increases owing to the ground plane, according to the image theory.[33] Due to the importance of the ground plane size, NFAs D and E are designed to have different ground plane sizes while varying the position of the ground plane between NFAs C and E provides additional information in the investigation.

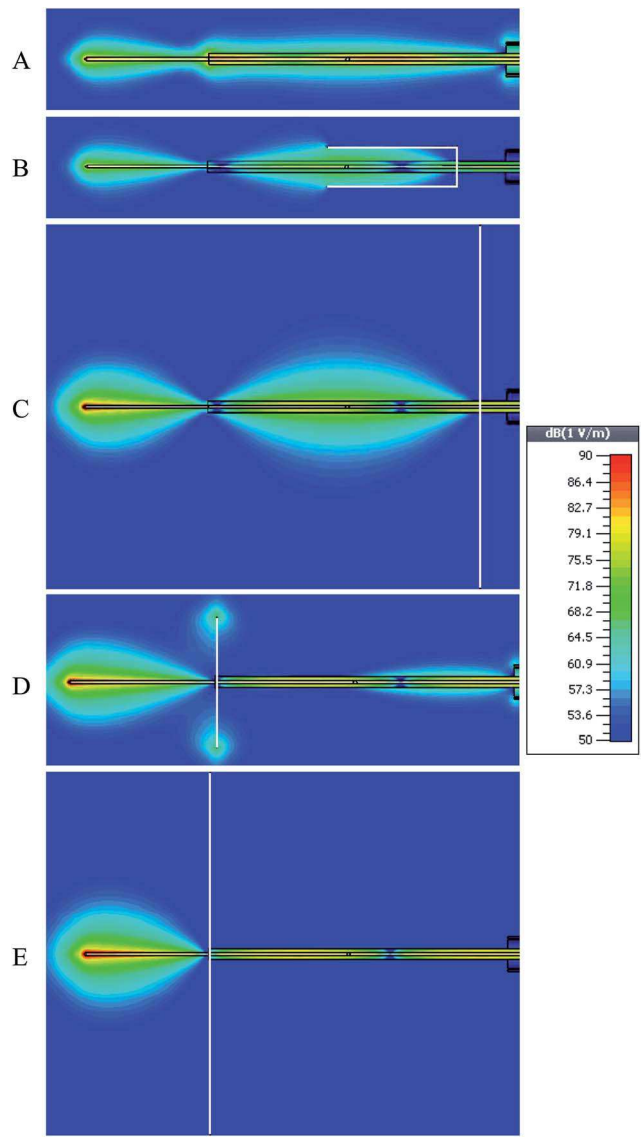

Fig. 2 NFA electric field magnitude distribution at 2.45 GHz: (A) reference NFA A, (B) NFA B with a quarter-wave choke, (C) NFA C with a large ground plane (R = 42.5 mm) close to the SMA connector, (D) NFA D with a small ground plane (R = 15 mm) and (E) NFA E with a large ground plane (R = 42.5 mm) close to the start of the rod conductor.

The proposed NFAs are designed and simulated using CST where the time-domain full-wave solver based on a finite-integration of Maxwell's equations is used.[31] A 3D NFA model with realistic electrical characteristics for the materials involved was constructed, and a finite free-space computational domain truncated by perfectly-matched absorbers was considered. The behavior of the structure under microwave excitation of the coaxial cable was then calculated, and the device characteristics including a reflection coefficient, electric field strength, efficiency and radiation patterns can be obtained from the simulation results. For the present application, the critical parameters under investigation are the surface current density on the coaxial outside conductor behind the ground plane, reflection coefficient and electric field strength around the NFA tip.

The length of the NFA conductor L_1, as shown in Fig. 1, determines the resonance/operation frequency and is approximately a quarter of the wavelength at the operation frequency of the microwave source. For design B, L_4 and L_2 are also nearly a quarter of the wavelength which forms a very high impedance on the coaxial outer conductor near the choke open end, thus suppressing return RF currents. The longitudinal position L_2 of the circular ground plane for designs D and E is zero since both of them resonate at the fundamental mode. For C, L_2 is approximately twice the length L_1, as it operates in its third-order resonant mode in which its stripped conductor and coaxial cable outer shell act together as an additional radiator. The length L_3 is not a critical parameter, since it is behind the ground plane and thus does not affect markedly the NFA performance. In all cases, the conductor tip was tapered with an angle $\alpha = 60^\circ$ which offers a compromise between high electric field strength and acceptable durability of the tip during operation. The conductor bending angle θ in all the NFAs is set to be 90° as this allows simple design and an easier comparison. However, it is noted that the designs can be adapted to other angles to fit specific system configurations and requirements. From theoretical expectations, to minimize return currents and radiation towards the back of the ground plane, the ground plane radius R should be made as large as possible. This is confirmed by a parametric study of applicators with different

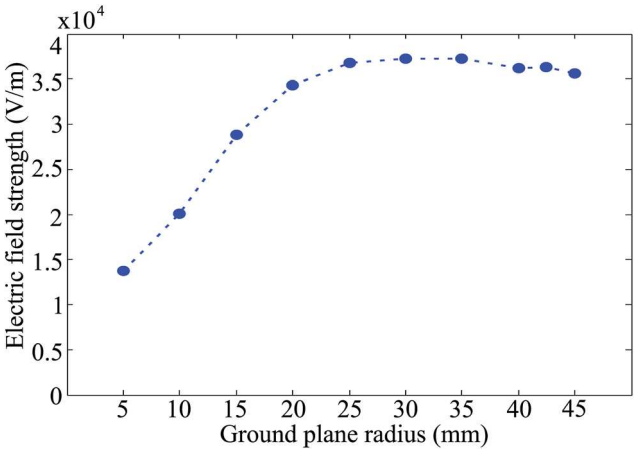

Fig. 3 Simulated electric field strength near the tip of the NFA as a function of the ground plane radius.

ground plane sizes. As shown in Fig. 3, the simulated electrical field strength at a point 0.2 mm away from the NFA tip rises when the ground plane size increases, and it stabilizes (with minor variations) with a ground plane radius of around 30 mm. Nevertheless, the feasible size is limited by the available system space. For our system, $R = 42.5$ mm is the maximum feasible ground plane radius.

From the simulation results, as expected, it is found that the surface current density on the coaxial outer conductor behind the choke or the ground plane is very small for NFAs B to E. This indicates that exterior electromagnetic coupling to objects in this region will not be insignificantly altering the operation of the devices. This also confirms that in these cases, removing the objects behind the ground plane, even if electrically connected or close to the coaxial cable, is a valid modeling simplification. In contrast, to attain a more accurate simulation result, influence of the objects in proximity to the NFA tip such as the sample under test, should be included in the simulation. This issue will be discussed in the following section in conjunction with the considerations on the reflection coefficient.

3 Experimental arrangement

3.1 Optical and microwave setup

An experiment verifying the performance of the NFAs has been conducted with a setup consisting of four sections: (I) laser ablation, (II) microwave injection, (III) emissions recording by spectrometer and (IV) imaging of plasma. Fig. 4 shows the schematic diagram of the entire setup. A Q-switch Nd:YAG laser (Quantel, Brilliant B), operated at 532 nm wavelength with 10 Hz repetition rate and 5–6 ns pulse duration was used as the ablation source. The energy of the laser was controlled by using a half-wave plate and a Glan-laser polarizer, and measured by using a pyroelectric sensor (Thorlabs, ES220C). The laser beam was focused on the solid sample by using a plano-convex UV fused silica lens Lens1 ($f_1 = 100$ mm, $D_1 = 50.8$ mm) to generate a tiny plasma on the solid target. The spectral resolution of the spectrometer with the 2400 lines per mm grating is 0.031 nm at

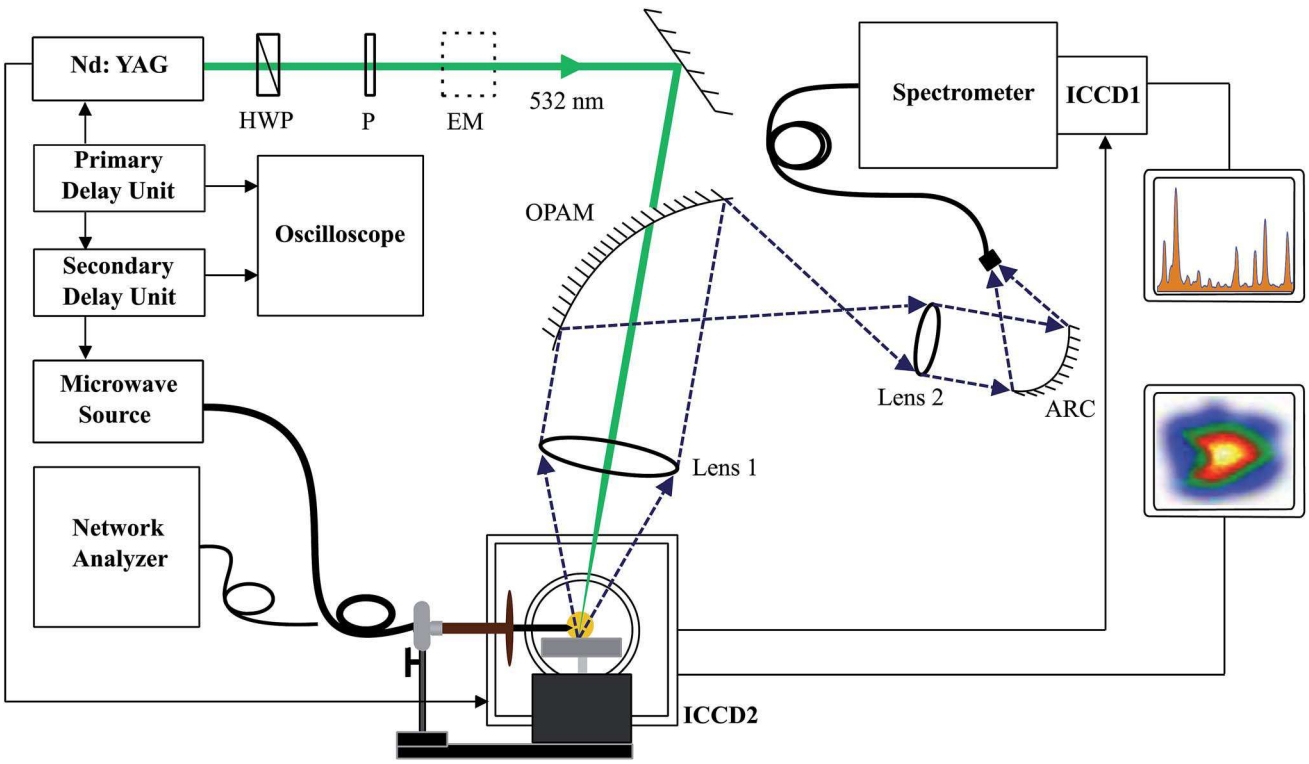

Fig. 4 Schematic of the experimental setup. ARC, achromatic reflective coupler; OAPM, off-axis parabolic mirror; HWP, half-wave plate; P, polarizer; EM, energy meter; an additional imaging channel is facilitated by using a second intensifier camera (ICCD2).

320–332 nm, with a resolving power of 10 000. A water cooled 3 kW Sairem Microwave system was used as the source of pulsed microwave power at 2.4 GHz. A WR340 waveguide directed the microwave power through a 3-stub impedance tuner to a waveguide-to-coaxial adapter (WR340RN), after passing through a quartz window. A 1 m flexible coaxial cable (50 Ω cable) with 0.14 dB insertion loss at 2.45 GHz was attached to this waveguide-to-coaxial adapter. Each NFAs was individually and sequentially attached to the end of this coaxial cable and fixed to a 3-stages positioner. The position of the NFA was adjusted with respect to the laser beam and solid samples in order to achieve maximum coupling of microwave power. A microscope connected to a computer was used to align the location of all five NFA designs exactly at an identical position. This alignment procedure minimizes the risk of experimental variations in coupling due to inaccurate positions of the NFA tip. For safety reasons, the system is enclosed in an aluminum microwave shielding box with a door at the front for LIBS sample loading. It is still very simple and easy to load and upload samples, even when compared to an open LIBS setup.

3.2 NFA measurement

The reflection coefficient, denoted as $|S_{11}|$, is one of the most important parameters for microwave devices, as it provides information on the accepted input power by the device in frequency domain,[33] for example in the present case the NFA. Therefore, at the beginning of the experiment, the reflection coefficients of the five NFAs were measured using a network analyzer (Agilent FieldFox N9916A). The measurements were performed *in situ* in the LIBS test system, both with and without a sample in proximity. Then the measured reflection coefficients in the frequency range of interest can be compared with the simulated ones.

3.3 Spectroscopic detection and plasma imaging

For the spectroscopic detection, the plasma emission was captured by the focusing/collimating lens Lens1, focused by the off-axis parabolic mirror on to a second lens Lens2 ($f_2 = 20$ mm, $D_2 = 12.54$ mm). Lens2 directed emission to a second parabolic mirror, which finally coupled the emission into a round-to-linear 7 fiber bundle (Thorlabs, BFL200HS02). The emission was then channeled into the slit of the spectrometer (Andor, Shamrock using 2400 lines per mm diffraction gratings) equipped with an ICCD (ICCD1) camera (Andor, iStar). The enhanced plasma images were simultaneously recorded by a second ICCD camera (ICCD2) (Andor, iStar) using a macro lens ($f = 90$ mm, Tamron), as shown in Fig. 5. A long pass filter was used to suppress the laser scattering at 532 nm. The filter has a transmission of 93.5% in the range from 600 to 800 nm. Both cameras were synchronized with the pulsed laser and the pulsed microwave source through primary and secondary external delay units to carry out spectra recording and plasma imaging simultaneously.

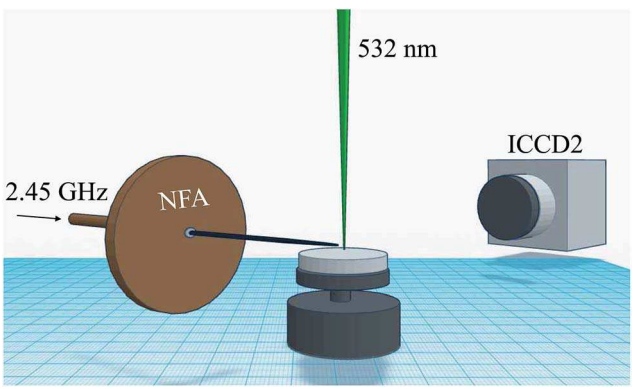

Fig. 5 A close look showing the setup of NFA, sample and ICCD2.

4 Results and discussion

4.1 NFA characteristics

4.1.1 Reflection coefficient. For efficient microwave coupling, it is critical to minimize the microwave reflected power. The reflection coefficient $|S_{11}|$ resulting from electromagnetic simulations in all five NFA geometries are displayed in Fig. 6 and they are compared with the measurement results. A reasonable agreement in terms of resonance frequency (indicated by the minimum of $|S_{11}|$) is observed between simulations and the measurements. To define the NFA operational bandwidth, we consider the frequency ranges where the reflection coefficient $|S_{11}|$ remains below −10 dB, indicating that more than 90% input power is accepted by the NFA.[33] According to the measurement results without LIBS samples, NFAs B, C, D and E have an operational bandwidth of 2.38 to 2.52, 2.35 to 2.65, 2.26 to 2.72, and 2.33 to 2.52 GHz, respectively. These frequency ranges all contain the targeted microwave power source frequency of 2.45 GHz. In contrast, design A exhibits a −5.6 dB simulated reflection coefficient which indicates that its input power acceptance is only around 72.5%. In this case additionally, the rather poor qualitative agreement with simulation can be ascribed to the unpredictable coupling of return currents on the coaxial cable. For all cases, the best overall matching, *i.e.* the lowest reflection coefficient at the desired resonance frequency of 2.45 GHz, is achieved with NFA C. However, the bandwidth of operation, *i.e.* the range of acceptable frequency variations due to environmental changes, will be reduced in this case. The oscillations observed in the measured data are due to reflections from the walls of the LIBS system enclosure, which provide shielding from the environment and are moderately absorbing. Considering now the more practical case where a sample is introduced at a distance of only approximately 0.2 mm from the NFA, a noticeable shift towards lower frequencies is observed in the measured resonance frequencies, with variations from tens to a few hundred MHz for all NFAs. The frequency shift is attributed to the NFA impedance variation induced by the samples in proximity. This demonstrates the importance of considering at design time the impact on the NFA due to the proximity of objects such as LIBS samples. This critical factor can be taken into account by including these objects in the simulation and testing the robustness of the design across a realistic range of material electrical properties.

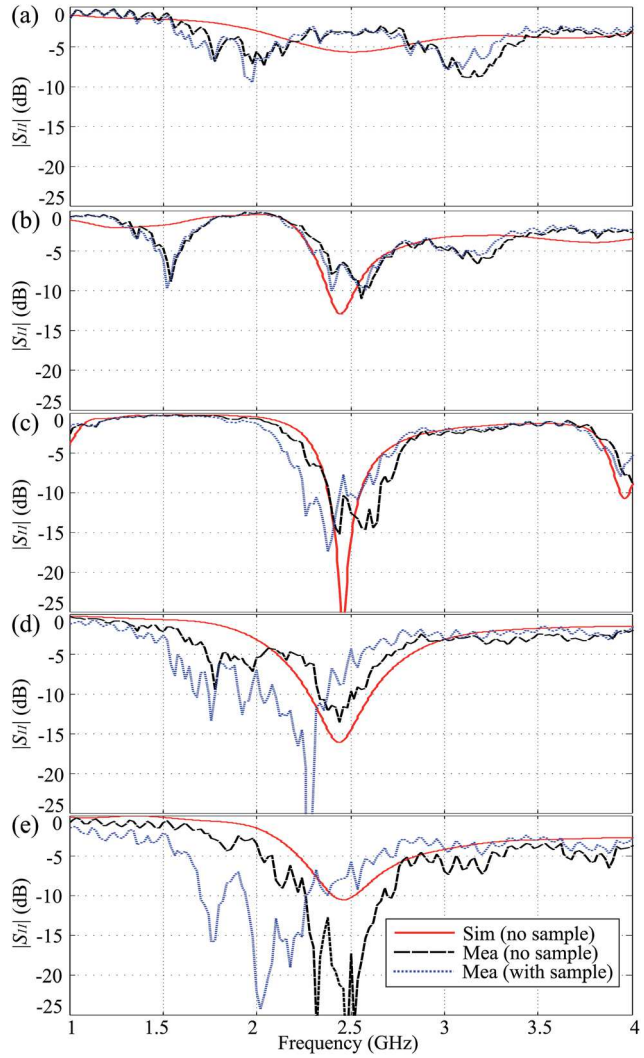

Fig. 6 Simulated and measured reflection coefficients $|S_{11}|$ of: (a) design A, (b) design B, (c) design C, (d) design D and (e) design E.

In future work, this important aspect will be more specifically investigated. For the case at hand with a copper sample, the reflection coefficients at 2.45 GHz, are −3.5, −6.7, −7.7, −8.7 and −7.9 dB which correspond to an accepted input power level of 55.3, 78.6, 83.0, 86.5 and 83.8% for NFA A to E, respectively. As a result, these NFAs are still anticipated to operate as efficient applicators. This will be confirmed through experiments, although it is noted that the overall NFA performance can be further improved if specifically designed for predefined test configurations.

4.1.2 Electrical field strength. Another indicator of the coupling power level of a NFA to the laser-induced plasma is the electric field strength around the conductor tip. This information can be computed and exported from the simulation tool. The distributions of simulated electrical field strength (V m^{-1}) around all NFA tips are displayed in the five plots on the first row of Fig. 7, with the *x*- and *y*-axes showing total spatial dimensions of 3 mm × 3 mm. As illustrated by these simulation results, the highest electrical field strength is observed the closest to the tip, which suggests that the distance between the NFA and sample should be kept as small as possible to permit high microwave power coupling. However, this is usually limited by the system setup and the sample surface roughness. The NFAs C, D and E exhibit a relatively high electrical field strength compared to designs A and B. That is, in free space, these three designs are expected to yield high microwave coupling performance to the laser-induced plasma. The slight advantage of design E under ideal conditions is due to the large ground plane (compared to D) and operation at fundamental resonance (compared to C). Nevertheless, the experimental results shown in the following indicate a marginally better performance of D over E for our LIBS system, which might be explained by small experimental uncertainties (*e.g.* sharpness of the tip and/or distance between the sample and the NFA) and fine differences in spatial field distribution, which may affect the matching of the local field strength to electron density in the plasma. This is indicative of the significance of considering the environmental impacts in the NFA design.

4.2 NFA performance

4.2.1 Plasma dimensions. To investigate the LIBS signal quality with and without the microwave coupling, it is essential to use a sample with low concentration of analyte. However, the concentration cannot be too low as it is also necessary to detect LIBS signals before using microwave power to establish a reference point. It was found that when using an unspecified mineral ore sample from a lead processing plant, a small amount of copper was detectable without any microwave injection. Therefore copper was selected as the analyte for this investigation. The mineral ore solid sample was mixed with a binder and placed into a plastic disc 3.4 mm thick and 21 mm in diameter. It is worth mentioning that since the laser beam is not focused onto the NFA tip, there will be no induced plasma from the NFA surface. The dependence of the MW-LIBS signal on copper concentration in solid samples using NFA with the same rod material was studied previously.[27] A linear dependence was observed confirming that the interference from the copper in the NFA tip is negligible. The performance of the five NFA designs was investigated firstly using four microwave powers ranging from 0 to 1.2 kW, while laser pulse energy, gate delay and gate width were kept constant. The plasma emission was recorded by ICCD 2 (imaging camera) and the spectrometer concurrently.

The averaged plasma images obtained from 100 single shots at the microwave power of 0 kW (laser plasma only) and 1.2 kW are displayed in the second row of plots in Fig. 7. The laser focusing point is positioned at the origin of the scale. The laser energy per pulse and microwave power were fixed at 2.6 mJ and 1.2 kW, respectively. The microwave pulse duration, the gate-delay and the gate-width were identical for all the recorded images, namely at 800 μs, 1 μs and 800 μs, respectively. These plots clearly demonstrate that for a given microwave power, variations in spectral and image intensities can be observed for different geometrical designs of NFA. The leftmost plot in Fig. 7 also shows the laser-induced plasma recorded when the

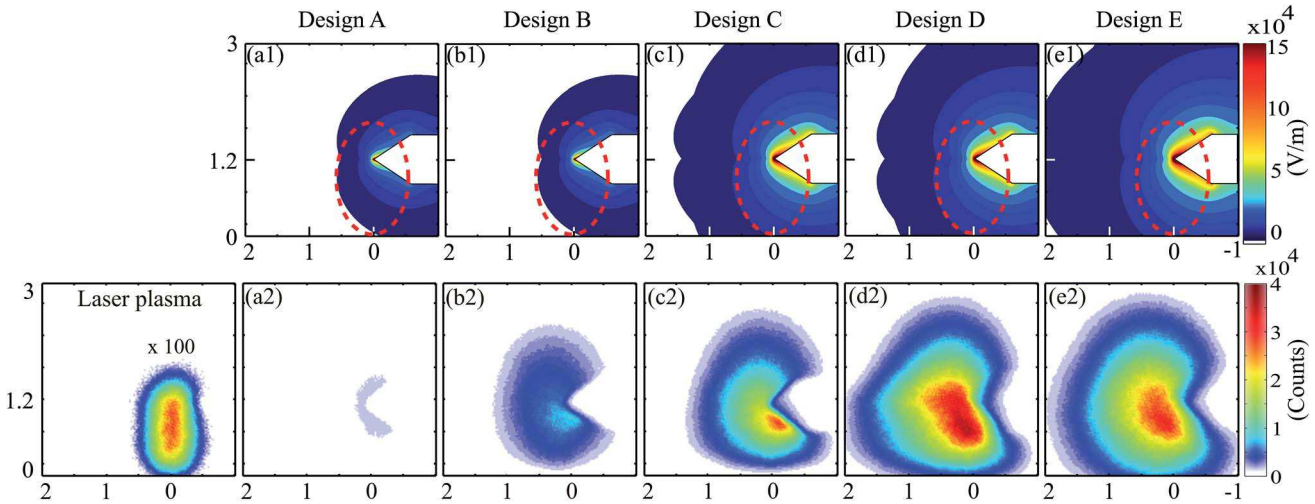

Fig. 7 Electric field strength (the first row) and enhanced plasma images (the second row) of the five NFAs proposed, with the laser focusing point and the applicator tip located at the origin and (0, 1.2) in the map (3 mm x 3 mm), respectively. These are two-dimensional plasma images, averaged for 100 laser shots, recorder using a 633 nm long pass filter by microwave-assisted LIBS in a copper bearing mineral ore solid sample. The laser energy was 2.6 mJ. The microwave power and pulse duration were 1.2 kW and 800 μs, respectively. The camera gate-width and the gate-delay were 800 μs and 1 μs, respectively. Please note that the intensity of the laser-induced plasma image shown on the leftmost plot of the second row is multiplied by a factor of 100 for better visibility. The dotted red line indicates the spatial location of the laser-induced plasma.

microwave was off; hence the recorded signal intensity is multiplied by a factor of 100 in this case so that all the recorded images can be visualized using a single color map. The length and the width of laser-generated plasma is approximately 1.7 and 1 mm, respectively. The dotted red ellipse shown in Fig. 7(a1)–(e1) illustrates the relative location and size of the laser-generated plasma with respect to the tip of the NFA. We note that in these images, a part of the imaged microwave-assisted plasma is overlapped with the tip where the strongest electrical field is formed. As mentioned before, the laser-induced plasma electron density must be below the threshold of approximately 7×10^{10} (cm^{-3}), to interact with the injected microwave power. As a result, the strength of the electrical field at the overlap location is critical in the microwave-assisted LIBS operation. Hence a matching of the electrical field strength with the local plasma electron density must be established for an efficient microwave injection.

Fig. 7(a2) shows that the microwave-enhanced plasma is sustained near the reference NFA tip, at (0, 1.2) location. Fig. 7(b2) and (c2) show an increase in the plasma volume and intensity, indicating a more efficient microwave injection than the reference design in Fig. 7(a2). We note that it is still possible to see the tip of the NFA in Fig. 7(b2) and (c2). The plasma depicted in Fig. 7(d2) and (e2) is further significantly enhanced in terms of intensity and volume, and as a result, in contrast to the previous cases, the NFA tip is no longer visible in these two plots: the plasma volume has grown large and appears to be engulfing the NFA. The images outlined in Fig. 7 suggest that the biggest plasma volume was obtained with NFA designs D and E whereas the reference NFA delivers the smallest plasma enhancement even at the highest microwave power.

To investigate the life-time of the microwave-enhanced plasma, time-resolved imaging was applied. Plasma images were recorded for the five NFA designs, at different gate-delay times, namely 1, 250 and 500 μs, while maintaining the gate-width and the microwave power fixed at 200 μs and 1.2 kW, respectively. The results are plotted in Fig. 8, and at the three gate-delay times, it is clear that the microwave-enhanced plasma is larger and stronger for designs C, D and E compared to designs A and B. It is also clear that the plasma is sustained for a reasonably long time, approaching 500 μs. It is interesting to note that although the intensity of microwave-enhanced plasma decreases as the gate-delay increases, the recorded plasma cross section appears constant, for designs C to E. Based on the measured cross section, designs D and E produce a well-sustained plasma with a volume of 87 mm^{-3} approximately.

4.2.2 Spectroscopic detection. Spectral intensities of copper transitions in microwave-assisted laser-ablated plasma for the mentioned solid mineral sample have also been recorded to further characterize the performance of the NFA in operation. Microwave-assisted LIBS spectra in the range from 324 to 328 nm were recorded at four microwave power levels, using the four designed NFAs. In all cases, the copper transitions at 324.754 and 327.395 nm are clearly resolved. Microwave power was controlled through secondary delay unit; the laser energy and gate delay were maintained at 2.6 mJ and 800 μs. Again, 100 single laser shots were recorded at each microwave power, which were then averaged and plotted separately for each NFA design, as shown in Fig. 9 as three different colors curves. The figure demonstrates that, as expected, for all the NFAs studied, the intensity of copper spectra is increasing with a rise in microwave power. While analyzing this figure vertically, it is found that for a given microwave power (*i.e.* a given color or curves), spectral intensities seem to increase from an order of A, B, C, E and D, which is consistent with the plasma intensity

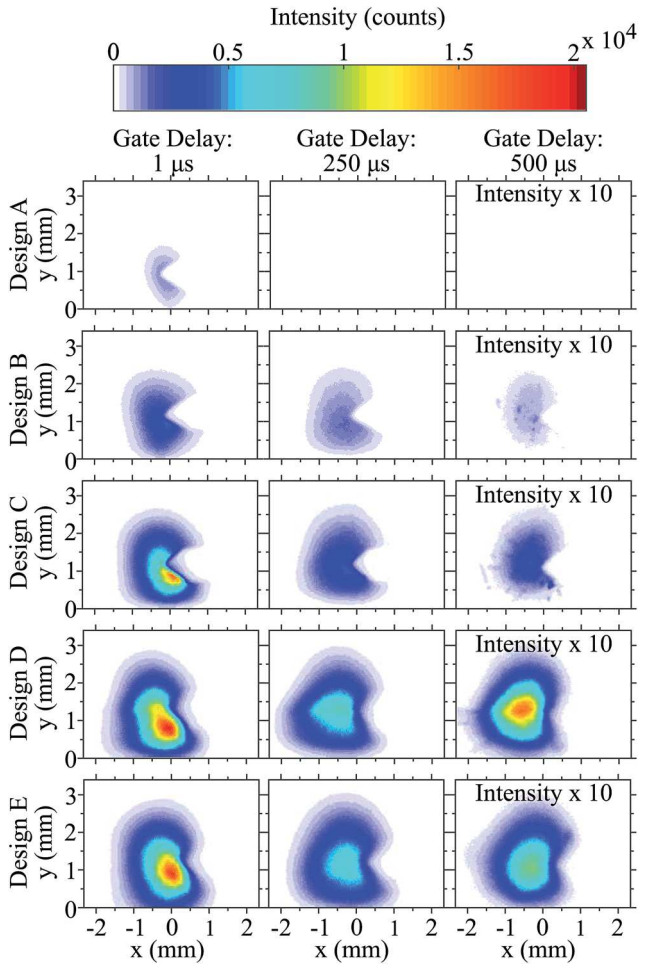

Fig. 8 Microwave-enhanced plasma intensity of the five NFAs recorded with different gate delays of 1, 250 and 500 µs. The gate-width and the microwave power were fixed at 200 µs and 1.2 kW, respectively. The results for 500 µs gate delay have been multiplied by a factor of 10 to get a better visualization.

image shown in Fig. 7. From the clear qualitative interpretation of the spectral intensities in Fig. 9, it can be stated that designs D and E clearly performed better than the other 3 designs. This will be investigated quantitatively in the next paragraph.

4.2.3 Signal enhancement and SNR improvement. Fig. 10 shows the LIBS spectra of the copper-bearing sample without and with assistance of 1.2 kW microwave power injected with the NFA design D. To interpret this figure quantitatively, we can define the signal strength for a particular line as the maximum intensity at the line center minus the baseline signal. In the present case, the signal at the 327.395 nm transition is specifically chosen as an indicator of the NFA performance. Using the obtained signal strengths in Fig. 10 for the considered transition, we can then define the signal enhancement as the ratio between the signal with and without assistance of microwave power. This yields a critical measure to evaluate the absolute system sensitivity improvement with an injection of microwave power. A complete characterization has been performed through measurement of all five NFAs. Design D has achieved

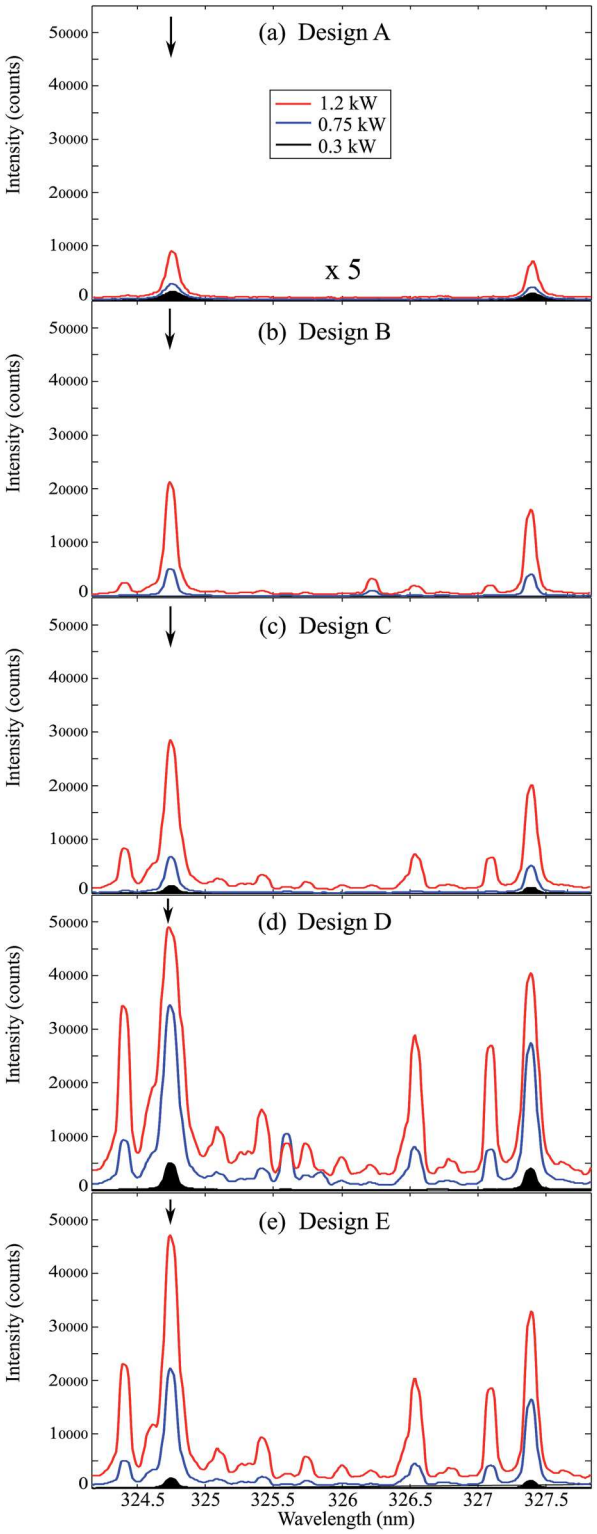

Fig. 9 Microwave-assisted LIBS spectra of a copper bearing mineral ore solid sample, averaged for 100 laser shots and recorded using three microwave power of 0.3, 0.75 and 1.2 kW. The laser energy, the gate-width and the gate-delay were 2.6 mJ, 800 µs, and 1 µs, respectively. Two copper lines are clearly seen at 327.395 and 324.754 nm.

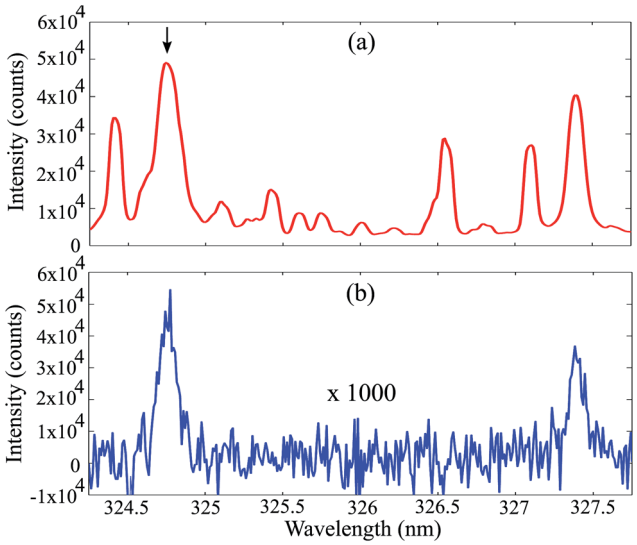

Fig. 10 Spectra of (a) design D with 1.2 kW microwave power, (b) design D without microwave power (multiplied by a factor of 1000).

the best performance (and is thus shown in Fig. 10), with the exceptionally high signal enhancement of 849 times, which we believe is the highest value to date.

It was noted that, however, increasing the microwave power is accompanied by a simultaneous increase of noise floor, as illustrated in Fig. 11(a) and (b), where the noise level (counts) and signal enhancement for design D are depicted as a function of microwave power. The error bars indicate the standard deviations from 100 averaged shots. On that basis, we conclude that another relevant performance measure should be considered as well, namely the SNR improvement arising with microwave power assistance. From the plots of Fig. 11, we observe that the noise, signal enhancement and SNR improvement are monotonously increasing with microwave power, and that the SNR can reach a maximum improvement by a factor of 76 when injecting 1.2 kW microwave power with the design D.

The signal enhancement and SNR improvement for all five NFAs with 1.2 kW microwave power is plotted in Fig. 12. As mentioned, the design D achieves the highest signal enhancement and SNR improvement of around 849 and 76, respectively, whereas the lowest ones are held by the reference NFA design A. It is worth mentioning that with a simple electromagnetic isolation technique, namely an added partial ground plane, design D can enhance the signal by more than 9 times, further than the previously reported very high signal enhancement of 93.[27]

4.2.4 Demonstration of the detection sensitivity. The ability of elemental detection at low concentration was tested using the best performing NFA, namely design D. A reference material OREAS 122 (Ore Research and Exploration) was used for this purpose. OREAS 122 is a certified reference material containing uniform low-concentration of copper, among many other elements, at 3.38 parts per million (ppm), equivalent to 3.38 μg g^{-1}. The powder sample was mixed with distilled water to produce a thick slurry, which was transferred into the

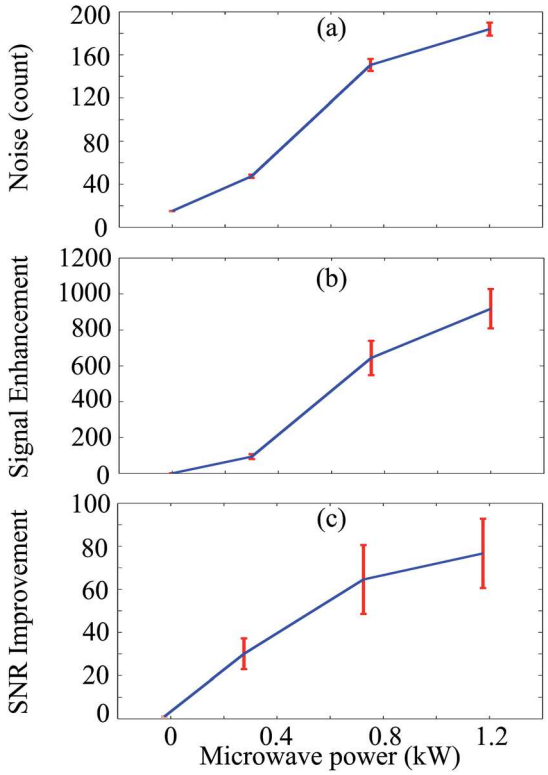

Fig. 11 The (a) noise level (counts), (b) signal enhancement and (c) SNR improvement of design D at microwave power of 0, 0.3, 0.75 and 1.2 kW for copper line at 324.754 nm obtained from the spectra. Error bars are standard deviations from 100 shots.

cylindrical sample holder with a 21 mm diameter. A uniform solid surface was achieved by pressing these discs and drying them at 51 °C. Fig. 13 shows the LIBS spectra recorded near

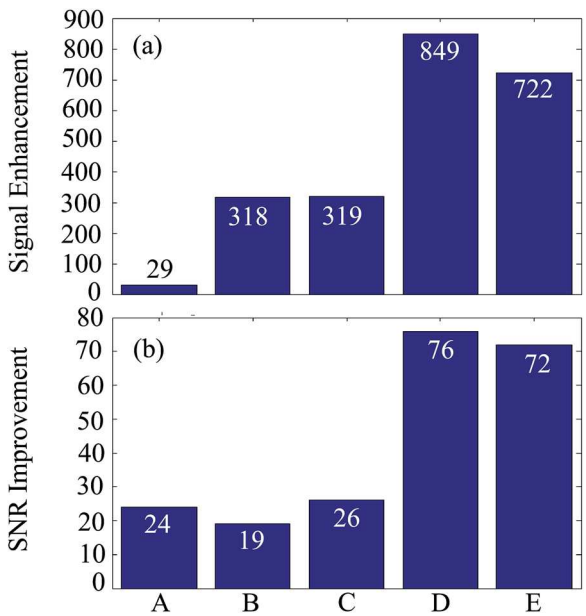

Fig. 12 The signal enhancement (a) and SNR improvement (b) of the five NFAs at a microwave power of 1.2 kW for copper line at 324.754 nm obtained from the spectra.

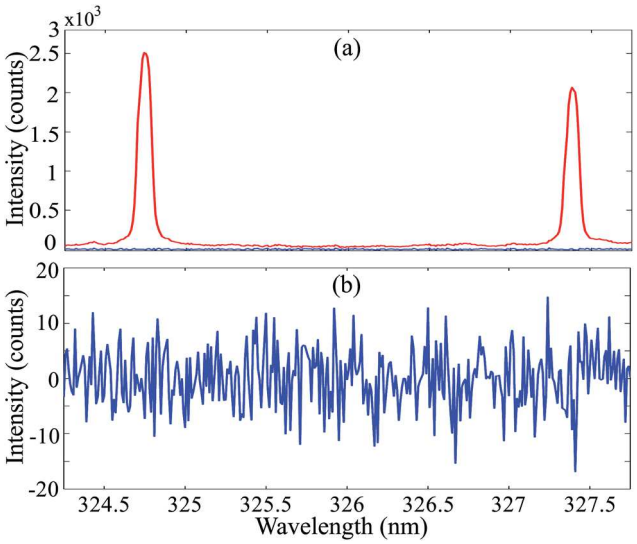

Fig. 13 The LIBS spectra of a certified ore sample with copper element of 3.38 part per million without and with 0.57 kW microwave power. (a) Comparison of these two cases where the blue and the red curve correspond to the signal intensity with 0 kW and 1.2 kW microwave power, respectively. (b) Replotted signal intensity for 0 kW microwave power on a magnified scale.

324 nm with a laser pulse energy of 2 mJ, without and with microwave power. The LIBS spectra recorded without microwave power (Fig. 13(b)) shows no signal of copper at the signature wavelengths of 324.754 nm and 327.395 nm. In contrast, when the microwave power is switched on at 0.57 kW, a very strong signal at 324.754 nm and 327.395 nm are clearly observed. The SNR of the 324.754 nm copper line is calculated to be 166.

5 Conclusion

Four NFA designs developed based on full-wave electromagnetic simulations have been experimentally investigated with respect to a reference design. Compared with the reference device, these four NFAs take into account critical factors such as the influence of the electromagnetic environment and the reflection coefficient, with the aim to maximize the electric field strength at the location of the plasma and predictably enhance the results. The experimental results, including NFA reflection coefficients, plasma imaging and spectroscopy, show that NFAs designed in a systematic way leads to a significant improvement in the overall system performance, with very good stability and repeatability as observed during our measurement campaign. The best SNR enhancement was achieved with the design having a 30 mm diameter ground plane located close to the rod conductor (design D), which leads to a 849-fold signal enhancement and a 76-fold SNR improvement at 1.2 kW microwave power, respectively, compared to measurements without microwave assistance. This is, to the authors' best knowledge, the highest reported SNR in the literature. To illustrate the enhanced system performance, a very strong copper spectral line was recorded with an SNR of 166 for a microwave power of 0.57 kW on a certified ore sample with uniformly distributed copper elements of a very low concentration of 3.38 ppm. Such a high level of SNR suggests that a detection limit in the sub-ppb range can become a real possibility in the near future.

Acknowledgements

The authors would like to thank Mr. Jeffrey Hiorns, form the mechanical workshop at the School of Chemical Engineering, for his outstanding technical support. The financial support from the Institute for Mineral and Energy Resource (IMER) and the Faculty of Engineering, Computer & Mathematical Science (ECMS) at The University of Adelaide is acknowledged.

References

1 D. W. Hahn and N. Omenetto, *Appl. Spectrosc.*, 2010, **64**, 335–366.
2 D. W. Hahn and N. Omenetto, *Appl. Spectrosc.*, 2012, **66**, 347–419.
3 J. D. Winefordner, I. B. Gornushkin, T. Correll, E. Gibb, B. W. Smith and N. Omenetto, *J. Anal. At. Spectrom.*, 2004, **19**, 1061–1083.
4 A. De Giacomo, M. Dell'Aglio, R. Gaudiuso, C. Koral and G. Valenza, *J. Anal. At. Spectrom.*, 2016, **31**, 1566–1573.
5 K. Rifai, S. Laville, F. Vidal, M. Sabsabi and M. Chaker, *J. Anal. At. Spectrom.*, 2012, **27**, 276–283.
6 E. Tognoni and G. Cristoforetti, *J. Anal. At. Spectrom.*, 2014, **29**, 1318–1338.
7 Z. Wang, Z. Hou, S.-l. Lui, D. Jiang, J. Liu and Z. Li, *Opt. Express*, 2012, **20**, A1011.
8 Z. Hao, L. Guo, C. Li, M. Shen, X. Zou, X. Li, Y. Lu and X. Zeng, *J. Anal. At. Spectrom.*, 2014, **29**, 2309–2314.
9 H. Yin, Z. Hou, T. Yuan, Z. Wang, W. Ni and Z. Li, *J. Anal. At. Spectrom.*, 2015, **30**, 922–928.
10 S. L. Lui and N. H. Cheung, *Appl. Phys. Lett.*, 2002, **81**, 5114.
11 C. Goueguel, S. Laville, F. Vidal, M. Sabsabi and M. Chaker, *J. Anal. At. Spectrom.*, 2010, **25**, 635–644.
12 K. Rifai, F. Vidal, M. Chaker and M. Sabsabi, *J. Anal. At. Spectrom.*, 2013, **28**, 388–395.
13 Z. Zakrzewski and M. Moisan, *Plasma Sources Sci. Technol.*, 1995, **4**, 379.
14 Y. Ikeda and M. Kaneko, *14th Int. Symp. on Appl. Laser Techniques to Fluid Mechanics*, 2008, pp. 1–9.
15 Y. Ikeda and R. Tsuruoka, *50th AIAA Aerosp. Sci. Meet. Incl. New Horizons Forum Aerosp. Expo*, Reston, Virigina, 2012, pp. 1–8.
16 Y. Ikeda and R. Tsuruoka, *Appl. Opt.*, 2012, **51**, B183.
17 D. K. Killinger, S. D. Allen, R. D. Waterbury, C. Stefano and E. L. Dottery, *Opt. Express*, 2007, **15**, 12905.
18 Y. Liu, B. Bousquet, M. Baudelet and M. Richardson, *Spectrochim. Acta, Part B*, 2012, **73**, 89–92.
19 A. Khumaeni, T. Motonobu, A. Katsuaki, M. Masabumi and W. Ikuo, *Opt. Express*, 2013, **21**, 29755–29768.
20 M. Tampo, M. Miyabe, K. Akaoka, M. Oba, H. Ohba, Y. Maruyama and I. Wakaida, *J. Anal. At. Spectrom.*, 2014, **29**, 886–892.

21 L. Liu, S. Li, X. N. He, X. Huang, C. F. Zhang, L. S. Fan, M. X. Wang, Y. S. Zhou, K. Chen, L. Jiang, J. F. Silvain and Y. F. Lu, *Opt. Express*, 2014, **22**, 7686.
22 L. Liu, X. Huang, S. Li, Y. Lu, K. Chen, L. Jiang, J. Silvain and Y. Lu, *Opt. Express*, 2015, **23**, 15047.
23 E. Surducan, V. Surducan, C. Neamtu and C. D. Tudoran, *2010 IEEE Int. Conf. Autom. Qual. Testing, Robot*, 2010, pp. 1–4.
24 Y. Liu, M. Baudelet and M. Richardson, *J. Anal. At. Spectrom.*, 2010, **25**, 1316.
25 A. Khumaeni, K. Akaoka, M. Miyabe and I. Wakaida, *Front. Phys.*, 2016, **11**, 114209.
26 M. Wall, Z. Sun and Z. T. Alwahabi, *Opt. Express*, 2016, **24**, 1507.
27 J. Viljanen, Z. Sun and Z. T. Alwahabi, *Spectrochim. Acta, Part B*, 2016, **118**, 29–36.
28 J. Pollak, M. Moisan and Z. Zakrzewski, *Plasma Sources Sci. Technol.*, 2007, **16**, 310.
29 E. Tatarova, F. M. Dias, E. Felizardo, J. Henriques, M. J. Pinheiro, C. M. Ferreira and B. Gordiets, *J. Appl. Phys.*, 2010, **108**, 123305.
30 H. Suzuki, S. Nakano, H. Itoh, M. Sekine, M. Hori and H. Toyoda, *Appl. Phys. Express*, 2015, **8**, 036001.
31 CST, http://www.cst.com, 2016, Online, accessed 19-Dec-2016.
32 D. Pozar, *Microwave Engineering*, Wiley, 4th edn, 2011.
33 C. Balanis, *Antenna Theory: Analysis and Design*, 2005.